

**EXPERIMENTAL AND NUMERICAL INVESTIGATION OF THE TOP PLATE
INFLUENCE ON THE PERFORMANCE OF SOLAR VORTEX ENGINE**

by

YEW JIA-WEI

15994

Dissertation submitted in partial fulfillment of

the requirements for the

BACHELOR OF ENGINEERING (HONS)

MECHANICAL ENGINEERING

JANUARY 2016

UNIVERSITI TEKNOLOGI PETRONAS

BANDAR SERI ISKANDAR

31750 TRONOH

PERAK DARUL RIDZUAN

CERTIFICATION OF APPROVAL

**EXPERIMENTAL AND NUMERICAL INVESTIGATION OF THE TOP PLATE
INFLUENCE ON THE PERFORMANCE OF SOLAR VORTEX ENGINE**

by

Yew Jia-Wei

15994

A project dissertation submitted to the
Mechanical Engineering Programme
UNIVERSITI TEKNOLOGI PETRONAS
in partial fulfillment of the requirement for the
BACHELOR OF ENGINEERING (Hons)
MECHANICAL ENGINEERING

Approved by,

(Prof. Dr. Hussain H. Jaafar Al-Kayiem)

UNIVERSITI TEKNOLOGI PETRONAS
TRONOH, PERAK

January 2016

CERTIFICATION OF ORIGINALITY

This is to certify that I am responsible for the work submitted in this project, that the original work is my own except as specified in the references and acknowledgments, and that the original work contained herein have not been undertaken or done by unspecified sources or persons.

YEW JIA-WEI

ABSTRACT

Solar energy – the clean and renewable energy has been receiving recognition and welcome from the society and authorities. Researches have been done all over the world to improve solar energy harvesting efficiency, and fully utilize solar energy to replace non-renewable energy resources in the future. Many solar technologies have been developed to capture solar thermal and light energy. Solar chimney or Solar Updraft Tower (UTP) is one of the inventions created and provide promising power generation. Solar Chimney Power Plant (SCPP) captures solar thermal energy and to be converted into mechanical energy using wind turbine before producing electricity. However, higher chimney tower is required to enable higher efficiency, inducing a higher construction cost. Thus, the Solar Vortex Engine (SVE) was proposed to utilize artificially developed vortexes as replacement on chimney tower.

This research mainly focused on the Solar Vortex Engine (SVE) and aimed to investigate on the influence of an annulus shaped top plate on the SVE's power generation performance and efficiency. The design parameters of top plate were considered as the controlling variable while the flow field within Solar Vortex Engine (SVE) was treated as the changing variable.

Numerical methodology applied computational fluid dynamics (CFD) for simulation with ANSYS Fluent 15 as the operational platform. Simulations were conducted on different top plate opening diameter ranging from 0.3m, 0.5m, 0.7m and 0.9m. The optimum opening diameter was then implemented to a canopy shaped top plate. Several slanting angles (8.53°, 10°, 20°, 30°, and 40°) were simulated to resolve air-cornering issue. Experiments were later conducted on pre-built prototype installed in solar research field within Universiti Teknologi PETRONAS to verify and validate the result findings. Aluminum and Perspex top plate with 0.3m opening diameter were applied for testing.

This research proved that increasing the transparency of the top plate did improved the solar updraft and airflow temperature. Increasing top plate opening diameter and slanting angle did enhanced outlet volume flow rate and resolved the air-cornering issue but failed to improve updraft velocity.

ACKNOWLEDGEMENT

I would like to acknowledge with gratitude to Professor Dr. Hussain H. Al-Kayiem, my respective supervisor, for giving me the opportunity to work on this research title under his intellectual guidance. Dr. Hussain has provided guidance and assistance along the way from title selection to submission of this research paper.

I am immensely grateful to Dr. Hussain who has always been sincere and helpful in assisting my understanding on the topic. His guidance helped me in all the time of research and writing of this research paper. I learned a lot from this research and the knowledges gained are beneficial to both my academic and future career path.

Besides, I would like to express my dearest appreciation to Mr. Ali. A. Ismaeel, a PhD Candidate who is also my co-supervisor who in-spite assisted me on both numerical simulation and experimental setup. Mr. Ali has been continuous monitored my progress and correct my mistake.

My sincere thanks to Mr. Mohammed A. Aurybi, a PhD Candidate who provided vast assistance on my numerical simulation. Thanks to Mr. Mohammed, solar radiation setup has been successfully considered within numerical simulation.

Last but not least, I would like to thank my family for supporting me spiritually throughout the writing of this research paper. This research paper is made possible through the helps and supports from everyone and I sincerely thank you for their insights and advises.

TABLE OF CONTENTS

ABSTRACT	IV
ACKNOWLEDGEMENT	V
ABBREVIATIONS AND NOMENCLATURES	5
CHAPTER 1 INTRODUCTION	6
1.1 – Prelude	6
1.2 – Problem Statement.....	9
1.3 – Objectives	9
1.4 – Scope of Study	10
CHAPTER 2 LITERATURE REVIEW	11
2.1 – Solar Vortex Engine	11
2.2 – Top Plate.....	12
2.3 – Airflow.....	15
CHAPTER 3 METHODOLOGY	16
3.1 – Project Approaches.....	16
3.2 – Modeling On Solar Vortex Engine.....	18
3.3 – Modelling of Top Plate.....	20
3.4 – Numerical Investigation	22
3.4.1 Mesh Generation	22
3.4.2 Numerical Simulations.....	23
3.4.3 Governing Equations.....	24
3.4.4 Numerical Simulation Setup	26
3.4.5 Boundary Conditions	28
3.5 – Experimental Approach.....	32
3.5.1 Experimental Setup for Solar Vortex Engine (SVE)	33
3.5.2 Components and Dimensions for Solar Vortex Engine	35
3.5.3 Experimental Positioning For Measurements	36
3.6 – Gantt Chart	39
3.6.1 FYP 1	39
3.6.2 FYP 2	40
3.7 – Project Key Milestone	41
3.8 – Summary.....	41
CHAPTER 4 RESULT AND DISCUSSION	42
4.1 Foreword.....	42
4.2 Numerical Simulation Results	42

4.2.1	Mesh Independency Test (MIT).....	43
4.2.2	Numerical Investigation on Top Plate Material	46
4.2.3	Numerical Investigation on Top Plate Opening Diameter...54	
4.2.4	Numerical Investigation on Slanting Angle for Canopy Shaped Top Plate	57
4.3	Experimental Results	60
4.3.1	Solar Collector	60
4.3.2	Vortex Engine Generator	62
4.4	Summary.....	71
CHAPTER 5	CONCLUSION AND RECOMMENDATIONS	73
REFERENCE	75
Appendix A	– Measuring Instruments	78
Appendix B	– Mesh Independency Test.....	87
B.1	Mesh Independency Test at 0.5m/s Inlet Velocity.....	87
B.2	Mesh Independency Test at 0.7m/s Inlet Velocity.....	88

List of Figures

Figure 1. 1	– Schematic of Solar Updraft Tower (SUT) [4]	7
Figure 1. 2	– Vortex Power Generator with Tangential Air Entry Duct-Side View [5]....	8
Figure 2. 1	- Concept of Solar Vortex Engine (SVE)	12
Figure 2. 2	- Concept of Greenhouse Effect Applied on Top Plate	12
Figure 3. 1	– Study Approach on SVE Top Plate	16
Figure 3. 2	- Flow Chart for Research Methodology	17
Figure 3. 3	- Sectioned view on Geometrical Modeling for VEG	18
Figure 3. 4	- Configuration for Vortex Engine Generator (VEG).....	19
Figure 3. 5	– Fluid Body Structure of Vortex Engine Generator (VEG).....	20
Figure 3. 6	– Annulus Shaped Top Plate	21
Figure 3. 7	– Canopy Shaped Top Plate.....	21
Figure 3. 8	- Proposed opening diameters for top plate	22
Figure 3. 9	- Proposed Modifications on Solar Top Plate.....	22
Figure 3. 10	– Mesh Generated on VEG model.....	23
Figure 3. 11	- ANSYS Fluent 15 Viscous Model Setup	26
Figure 3. 12	- Solar Vortex Engine Testing Unit installed at UTP Solar Research Site..	34
Figure 3. 13	– Top View of Solar Vortex Engine (SVE) with Aluminum Top Plate.....	34
Figure 3. 14	– Top View of Solar Vortex Engine (SVE) with Perspex Top Plate.....	35
Figure 3. 15	- Sectional Schematic for Experimental Measurements Positions	38
Figure 3. 16	– Key Milestone for FYP.....	41

Figure 4. 1 - Graph of Maximum Simulated Velocity and pressure vs Trials on MIT....	44
Figure 4. 2 - Graph of Aspect Ratio vs Trials on Mesh Independency Test.....	44
Figure 4. 3 - XY Plot for Top Plate Outlet Velocity on Trial 11	44
Figure 4. 4 - Graph on Flow Rates vs Trials	45
Figure 4. 5 – Case 1 Sectional Incident Radiation Contour (Aluminum).....	47
Figure 4. 6 – Case 2 Sectional Incident Radiation Contour (Perspex)	47
Figure 4. 7 – Case 1 Sectional Static Temperature Contour on (Aluminum).....	48
Figure 4. 8 – Case 2 Sectional Static Temperature Contour on (Perspex).....	48
Figure 4. 9 – Case 1 Sectional Velocity Magnitude Contour (Aluminum)	49
Figure 4. 10 – Case 2 Sectional Velocity magnitude Contour (Perspex)	50
Figure 4. 11 – Case 1 Sectional Pressure Contour (Aluminum).....	50
Figure 4. 12 – Case 2 Sectional Pressure Contour (Perspex).....	51
Figure 4. 13 – Illustration on Vortex Engine Generator	51
Figure 4. 14 – Case 1 Tangential Velocity at Convection Region (Aluminum).....	52
Figure 4. 15 – Case 1 Tangential Velocity at Convergence Region (Aluminum)	52
Figure 4. 16 – Case 2 Tangential Velocity at Convection Region (Perspex)	53
Figure 4. 17 – Case 2 Tangential Velocity at Convergence Region (Perspex).....	53
Figure 4. 18 – Case 1 Sectional Vorticity Contour (Aluminum).....	54
Figure 4. 19 – Case 2 Sectional Vorticity Contour (Perspex).....	54
Figure 4. 20 – Sectional Temperature Contour at Perspex opening diameter 0.3m	55
Figure 4. 21 – Sectional Temperature Contour at Perspex opening diameter 0.5m	55
Figure 4. 22 – Sectional Temperature Contour at Perspex opening diameter 0.7m	55
Figure 4. 23 – Sectional Temperature Contour at Perspex opening diameter 0.9m	55
Figure 4. 24 – Sectional Velocity Contour at Perspex opening diameter 0.3m.....	56
Figure 4. 25 – Sectional Velocity Contour at Perspex opening diameter 0.5m.....	56
Figure 4. 26 – Sectional Velocity Contour at Perspex opening diameter 0.7m.....	56
Figure 4. 27 – Sectional Velocity Contour at Perspex opening diameter 0.9m.....	56
Figure 4. 28 – Sectional Temperature Contour at Perspex 8.53° <i>slanting angle</i>	57
Figure 4. 29 - Sectional Temperature Contour at Perspex 10° <i>slanting angle</i>	57
Figure 4. 30 - Sectional Temperature Contour at Perspex 20° <i>slanting angle</i>	57
Figure 4. 31 - Sectional Temperature Contour at Perspex 30° <i>slanting angle</i>	57
Figure 4. 32 - Sectional Temperature Contour at Perspex 40° <i>slanting angle</i>	58
Figure 4. 33 – Sectional Velocity Contour at 8.53° <i>slanting angle</i>	58
Figure 4. 34 - Sectional Velocity Contour at 10° <i>slanting angle</i>	58
Figure 4. 35 - Sectional Velocity Contour at 20° <i>slanting angle</i>	58
Figure 4. 36 - Sectional Velocity Contour at 30° <i>slanting angle</i>	58
Figure 4. 37 - Sectional Velocity Contour at 40° <i>slanting angle</i>	59
Figure 4. 38 – Maximum Velocity Simulated on Various Top Plate Slanting Angle	59
Figure 4. 39 – Solar Intensity against Time	60
Figure 4. 40 – Temperatures within Solar Collector (SC)	61
Figure 4. 41 – Illustration on VEG Top Plate and TBS	62
Figure 4. 42 – Solar Intensity against Time	62

Figure 4. 43 – Measured Top Plate Temperature against Time	63
Figure 4. 44 – Temperature of Transparent Bounding Structure (TBS) against Time ...	64
Figure 4. 45 – Illustration on VEG Interior Wall and Base	65
Figure 4. 46 – Interior Wall Temperature of VEG against Time.....	65
Figure 4. 47 – Measured Base Temperature for VEG against Time.....	65
Figure 4. 48 – Illustration on VEG inflow and outflow.....	66
Figure 4. 49 – Measured Transient Behavior of Air Inflow Temperature	66
Figure 4. 50 – Measured Transient Behavior of Air Outflow Temperature	67
Figure 4. 51 – Air Outflow Humidity (RH %) against Time	67
Figure 4. 52 – Measured Transient Behavior of Air Inflow Velocity.....	69
Figure 4. 53 - Measured Transient Behavior of Air Outflow Velocity.....	69
Figure 4. 54 – Percentage Enhancement in Outflow Velocity against Time.....	70
Figure 4. 55 – Measured Transient Behavior of Tangential Velocity against Time.....	70
Figure 4. 56 – Measured Outlet Volume Flow rate against Time.....	71
Figure 5. 1 – Proposed Model of Vortex Engine Generator (VEG)	74

List of Tables

Table 3. 1 – Parameters for Vortex Engine Generator.....	19
Table 3. 2 – Dimensions for Vortex Engine Generator (VEG).....	19
Table 3. 3 – Material Properties for Top Plate.....	22
Table 3. 4 – Boundary Condition for Case 1	28
Table 3. 5 – Boundary Condition for Case 2	29
Table 3. 6 – Boundary Condition for Case 3	30
Table 3.7 – Boundary Condition for Case 4	31
Table 3. 8 – Components and Dimensions for Solar Vortex Engine	35
Table 3. 9 – Experimental Measuring Positions with Instruments	38
Table 3. 10 – Gantt Chart for FYP 1	39
Table 3. 11 – Gantt Chart for FYP 2.....	40
Table 4. 1 - Inlet and Outlet Flow rate for 11 trials	45
Table 4. 2 – Comparison on Experimental Measurements bet. Aluminum and Perspex	71
Table 4. 3 – Verification and validation on Case 1 simulated results by experiment 1...	72
Table 4. 4 – Verification and Validation on Case 2 simulated results by experiment 2..	72

ABBREVIATIONS AND NOMENCLATURES

SVE	Solar Vortex Engine
VEG	Vortex Engine Generator
TP	Top Plate
SC	Solar Collector
TBS	Transparent Bounding Structure
D_i	Top Plate inner diameter (m)
D_o	Top Plate outer diameter (m)
A_{tp}	Area of Top Plate
h	Top Plate Height (m)
I_A	Absorbed incident
I_R	Reflected incident
I_T	Transmitted incident

CHAPTER 1

INTRODUCTION

1.1 – Prelude

Based on the World Energy Outlook (WEO) 2014, the “Global energy demand is set to grow by 37% by 2040 in our central scenario” [1]. The demand of natural gas has grown by more than half. There is a rising consumption concentrated in the rest of Asia, Africa, the Middle East and Latin America while a landmark is predicted to be made in the early 2030s when China by-pass United State of America, becoming the largest oil-consuming country. Subsidies given to fossil fuel (\$550billion) in year 2013 were more than 4 times of renewable energy (\$120billion). However, the increase production on non-renewable resources will indirectly cause passive effect on the ecosystem. Thus, there is a will to bring down the demand on fossil fuel. The intergovernmental panels have agreed that only 1000 gigatonnes of CO_2 is allowed to be emitted globally. This is to achieve the goal to allow only 2°C increase in global temperature [1]. This is where the renewable and clean energy are applicable.

Renewable Energy

Renewable energy is defined as energy that replenish naturally. This result in significant energy security and economic benefits. Renewable energy does provide a clean generation with no greenhouse gas emissions. Diversifying energy supply did indeed reduced the dependence on imported fuels. Renewable energy range from Wind, Hydropower, Solar, Geothermal, Biomass and Wave energy. Based on REN21’s report in year 2014, renewable energy contributed 19% to the global final energy consumption and 22% on electricity generation in between 2012 to 2013. As a share of the total energy generated by modern renewables, biomass energy provided 4.2%, hydropower generated 3.8%, other renewable sources (e.g. Wind and Solar) comprised 1.2% and biofuels accounted for 0.8%. [2]. Statistic shows that solar renewable sources have not been fully utilized. Further development and deployment on solar technologies can increase the power supply generation.

Overview on Solar Technologies

Solar energy is energy harvested from light and heat of the Sun. Different technologies like solar heating, photovoltaics, and solar thermal system have been implemented for harnessing. The cost of solar technologies have been decreasing due to technological improvement. Solar thermal electricity (STE) and Solar Photovoltaic Electricity (PV) are competitive in sunny countries against oil generated electricity [3]. STE has been providing cheap and promising energy generation. STE mainly apply Concentrating Solar Power (CSP) and non-concentrating solar power technologies. Parabolic trough, Dish Stirling, and Solar Power Tower are example of CSP while Solar Updraft Tower is placed under non-concentrating category.

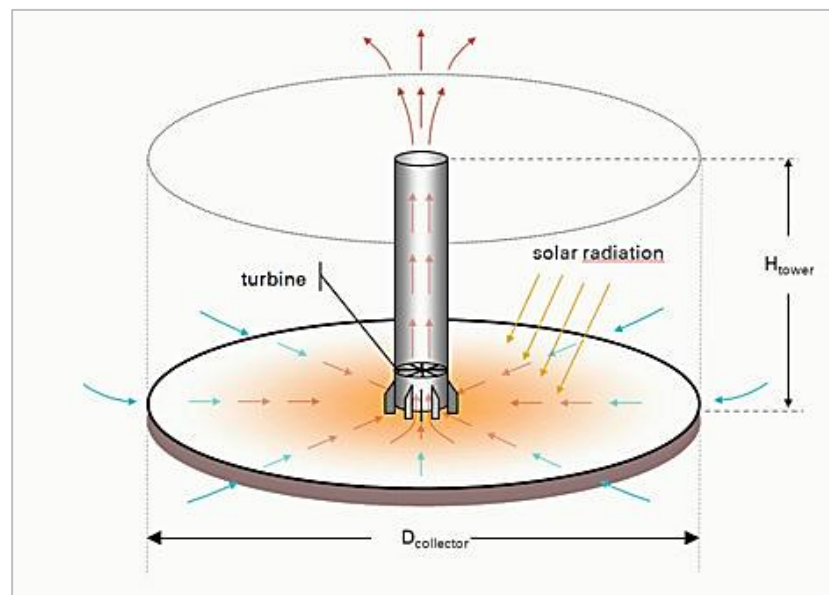


Figure 1. 1 – Schematic of Solar Updraft Tower (SUT) [4]

Solar Updraft Tower (SUT)

As shown in Figure 1.1, Solar Updraft Tower (SUT) is consisted of three elements, namely solar collector (SC), chimney/tower, and wind turbines. The SUT apply the principle of air convection for its operation. Sunlight or solar radiation heats up the air beneath the SC installed at the base of the tower. The resulting natural convection causes hot air to rise in the tower by the chimney effect. Pressure variation in tower causes suction which then

draws in more hot air. The airflow then drives the wind turbine installed within the tower, converting mechanical energy to electrical energy. Large-scale Solar Updraft Tower (SUT) is believed to be capable in generating electricity match to those of conventional power plants [4]. Although taller or higher solar chimney and larger collector area will be able to increase the power output efficiency, higher investment cost will be involved for construction. This is where the Atmospheric Vortex Engine (AVE) is applicable in overcoming the drawback.

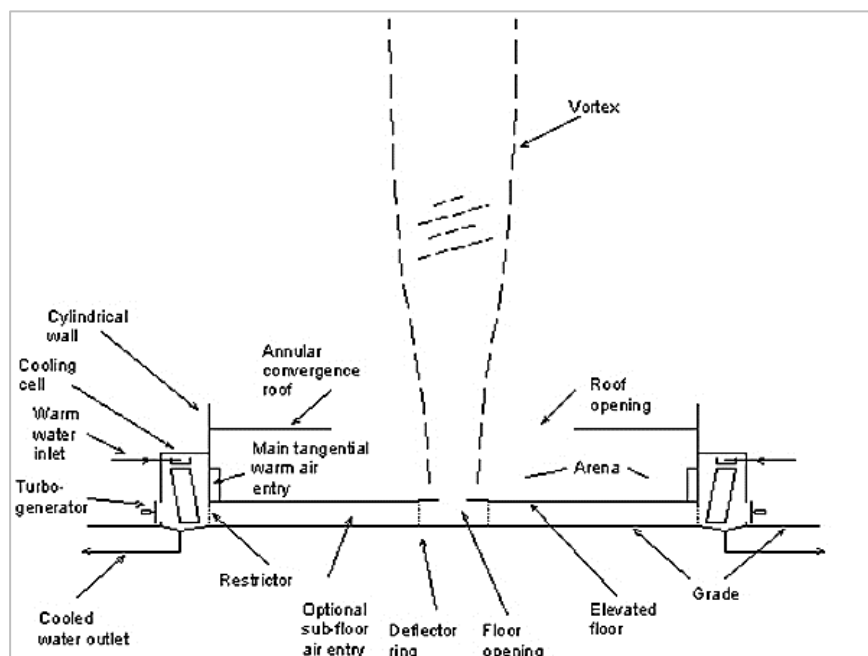


Figure 1. 2 – Side View of Atmospheric Vortex Engine [5]

Solar Vortex Engine (SVE)

As shown in Figure 1.2, Atmospheric Vortex Engine (AVE) was invented with the aim to replace SUT with a lower and less expensive structure. The cost of an Atmospheric Vortex Engine (AVE) plant is only 5% of the total cost of solar chimney with the same capacity. Solar Vortex Engine (SVE) was later proposed as an alternative to AVE. The Solar Vortex Engine (SVE) is a type of AVE which combines the principle of tornadoes and the principle of the solar chimney [5]. Instead of applying heat exchanger or industrial wasted heat energy, the SVE utilized solar radiation to spark the engine operation. The air is

heated in the same manner as the solar updraft tower using solar radiant [6]. Besides, the SVE applies artificially created vortexes and capture the mechanical energy generated during air convection updraft [7]. The vortexes are created by admitting warm or humid air tangentially at the base of a circular wall using guide vanes. The height of a virtual “vortex chimney” could extend much higher into the atmosphere compare to a physical chimney structure. [5].

Top Plate

The same principle of solar thermal system has been applied on the top plate of the Solar Vortex Engine. Top plate is installed on the tower outlet to increase the temperature of air to promote updraft and natural convection. The top plate will be presented in current research based on numerical and experimental approaches.

1.2 – Problem Statement

Solar Vortex Engine (SVE) was proposed and constructed at solar research site located within Universiti Teknologi PETRONAS. Current prototype is not ready for power generation and thus continuous improvement will have to be done to increase natural convection and improve power generation. Solar Collector (SC) was installed as the major heat source for the SVE. However, the low air temperature variation compare to ambient has drag down the engine performance. Top plate was proposed to be installed above the Vortex Engine Generator (VEG) to increase airflow temperature for further improvement on natural convection. However, horizontal top plate does prevent updraft and create fluid cornering. Therefore, this paper is aimed to counter the problems and propose a solution.

1.3 – Objectives

This study was conducted to achieve the following objectives.

1. To evaluate the contribution of the top plate on the performance of Solar Vortex Engine (SVE) by experimental investigation.
2. To simulate and evaluate the flow field within the Solar Vortex Engine (SVE) by CFD technique.
3. To determine the optimum top plate opening diameter and slanting angle in improving solar updraft by CFD technique.

1.4 – Scope of Study

This is a research on Solar Vortex Engine (SVE). This research will focus only on the top plate of the Solar Vortex Engine (SVE). A numerical approach will be applied to study on various parameters of the top plate and their effects on the updraft, air cornering and power generation efficiency of the Solar Vortex Engine. Different top plate parameters, namely type of material (transparency), opening diameter (internal diameter) and slope of canopy are used as the controlling variable while airflow and air temperature are the changing variables. The optimum slope and opening diameter that will improve updraft without compromising the heat transfer efficiency is to be determined in this paper.

The numerical investigation is completed using the Newton-Raphson approach in 1D. Computational Fluid Dynamics (CFD) technique has been used for simulation on Solar Vortex Engine (SVE) within ANSYS Fluent 15 simulation software to predict and calculate the nominal performance.

Experiments were later conducted on a solar vortex engine model that has previously been built on the solar research ground within Universiti Teknologi PETRONAS to validate the numerical and simulation approaches.

CHAPTER 2

LITERATURE REVIEW

2.1 – Solar Vortex Engine

Solar energy is a clean form of renewable energy. Society has been supportive and agreed for the development solar technologies. Researches have been done all over the world to design solar plants and increase their efficiency to fully utilize the solar energy for power generation. Atmospheric Vortex Engine (AVE) is one of the concept proposed by Norman Louat and Louis. M. Michaud. Based on Technical Description by Louis. M. Michaud, “An atmospheric vortex engine (AVE) is a device for producing mechanical energy by means of a controlled tornado-like vortex.” [8]. The thermal source to heat the air come from conventional power plants. While a Solar Vortex Engine (SVE) is the modified version of AVE where the insolation is applied to replace conventional power plants as the main source of thermal energy to heat the air for operation. The top plate or Solar Collector (SC) is the main component to separate air underneath from ambient condition and act as the collector for solar heat energy. This chapter presents a review of the fundamentals as well as the state-of-the-art researches did previously on Solar Vortex Engine (SVE) and the effect of collector or top plate on power generation efficiency.

Vortex Engine is applying a controlled tornado-like vortex instead of a physical tower and using the centrifugal force created by the rotation of a mass of air can prevent horizontal convergence just as good as a solid wall [9].

Figure 2.1 shows a concept of the Solar Vortex Engine (SVE) which utilize solar radiation as heating source to reduce airflow buoyancy, promoting updraft.

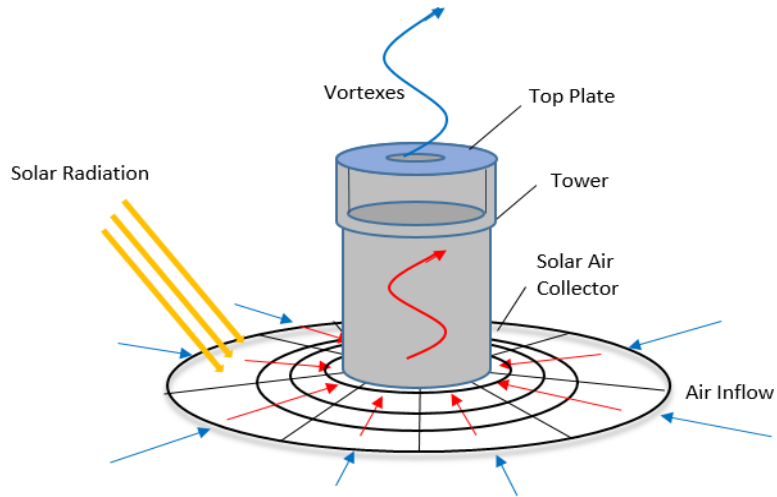


Figure 2. 1 - Concept of Solar Vortex Engine (SVE)

2.2 – Top Plate

The top plate is a flat plate collector which is used for capturing solar radiation, converting solar energy to heat energy. The solar air collector is installed at engine inlet while top plate is installed at engine outlet, implementing the concept of the greenhouse effect that trap short wavelength radiation and reflect long wavelength radiation as shown in Figure 2.2. The thermal performance of a top plate highly depend on the rate of energy incident direct on the collector, the slope, transparency and the rate of energy loss on both front and rear surface and the rate of useful energy collected to heat the air [10].

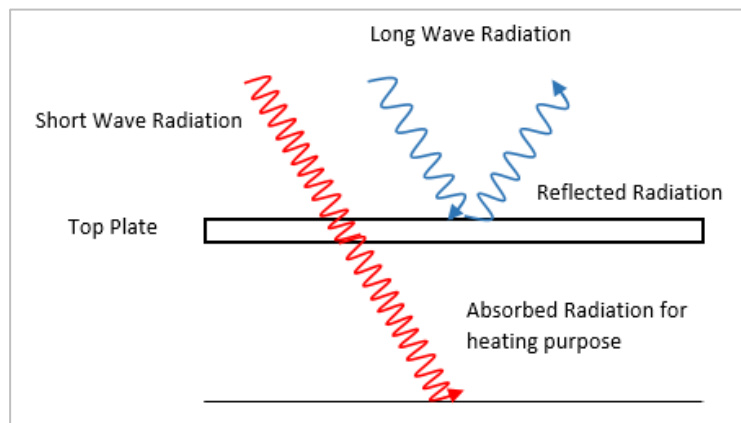


Figure 2. 2 - Concept of Greenhouse Effect Applied on Top Plate

Collectors can be categorized into non-concentrating and concentrating. The top plate applied on the Solar Vortex Engine (SVE) is a flat collector, which is a non-concentrating collector. Thus, the area that intercepts the solar radiation is the area absorbing solar radiation. While concentrating collectors have a bigger collector area than absorber [11].

Many researches have been done to improve the thermal efficiency of collector. Most modeling methodologies were conducted to predict the performance of the solar thermal system. The Solar Vortex Engine apply a circular top plate as second collector and the basic design of the circular solar collector was presented and introduced for the solar chimney power plant of Manzanares prototype in Spain [12].

Al-Kayiem has presented a mathematical modeling on circular configuration solar air collector. With appropriate and justified assumptions, the governing equation on conservation of continuity, momentum and energy balance equation were manipulated to predict the thermodynamic properties of airflow in radial direction at various controlled conditions. Numerical simulation was conducted using Computational Fluid Dynamics (CFD) Analysis. Experimental model was later fabricated to validate numerical result [13].

A research done has applied an experimental approach to investigate on the performance of a solar collector for a Solar Chimney Power Plant (SCPP). Influencing factors have been applied on the statistical methodology ranging from solar radiation intensity and air volume flow rate. The efficiency of collector and graphical relationship with influencing factors were the result findings [14].

A new approach for analyzing solar collector were presented where a conceptual temperature term – equivalent ambient temperature (t_a^*) has been introduced to determine thermal performance when solar collector is exposed to different front and rear ambient temperatures. Hottel-Whillier-Bliss (HWB) Analysis has been done using parameters: Plate Efficiency Factor - F' , Heat Removal Factor - F_R , Overall Heat Loss Coefficient - U_L , and Effective Transmittance-Absorptance Product - $(\tau\alpha)_e$. Heat Transfer is assumed to be steady state. A building-integrated solar collector model for heating effect has been built to demonstrate the concept [10].

On the other hand, one-directional heat transfer analysis and Thermal Equilibrium Equations are applied on the solar collector. The effect of collector radius on power generation of Solar Chimney Power Plant (SCPP) was investigated to determine the maximum radius allow for effective power output. Based on the research, “Under the unloaded conditions, the theoretical power output of an SCPP is directly proportional to the square of the collector radius.” The research conclude that there is a limitation on the allowable collector radius, beyond which the proportional relationship between collector radius and power output is unobtainable [15, 16]

In order to understand the natural convection phenomena, a numerical study have been conducted by passing laminar airflow through an inclined enclosure and investigate the convection under various condition like pressure and temperature. Temperature variation at enclosure inlet and outlet triggered pressure difference and promote air circulation. Continuity equation has been applied for the study to determine the relationship between slope and updraft [17].

The outlet diameter of the solar tower will as well affect the engine performance. A research have been done to study the relationship between collector area, tower height and chimney’s diameter on power output. Manzanares model in Spain has been used as comparison in the study and a mathematical equation relating collector area to air temperature has been derived. Result shows that the chimney outlet diameter has lower impact on power output compare to other parameter. Increasing the tower outlet diameter lead to a rise in air mass flow rate but the increased cross-sectional area tends to reduce the temperature variation between inlet and outlet, lowering the air velocity and rate of natural convection [18].

Kalidasan has conducted a research to investigate on the transparency and refractivity of cover on performance for solar water heater. An incremental approach on number of cover with same material properties has been used and result shows that the instantaneous efficiency of flat plate collector increases with an increase in number of covers only until a certain degree. Further plate increment, in fact, start to reduce system performance. On the other hand, efficiency decreases with an increase in refractive index [19].

2.3 – Airflow

The Top Plate is installed on the Solar Vortex Engine (SVE) to collect solar radiation to heat up the air underneath for operation. The efficiency of the solar collector will directly affect the airflow. Bernardes considered collector as a cavity between two parallel plates. The rise of temperature on collector and shear stress on top layer air in contact with solar collector were considered numerically [20].

Airflow is assumed to be in steady state condition due to low air dynamics. The velocity and temperature distribution equation were considered within the analytical approach where velocity and convection heat transfer increase with air temperature [21]. A numerical model and considered airflow as incompressible due to low variation in air density. Based on the research, “The computational mesh should be finer near the wall to capture the thermal and viscosity boundary layer”. On the contrary, compressible airflow are modeled by Boussinesq where density of air changes with temperature variation [22, 23].

As a conclusion, most studies conducted mainly focus on Solar Collector (SC) and the comparison on the parameters of Solar Chimney to the power performance. Various methods have been applied to improve the collector efficiency and to predict the thermal fluid properties in order to maximize the power generation by thermal plant. However, there is no single study that focus on the modeling of the top plate to increase temperature variation within solar tower which can lead to performance improvement.

In this paper, a geometrical model of Solar Vortex Engine was developed and numerical simulation was applied to determine the top plate efficiency in collecting solar irradiance and to predict air temperature. Experimental investigation was applied to verify and validate on the numerical simulation.

CHAPTER 3 METHODOLOGY

3.1 – Project Approaches

The strategy of approach for this research is outlined in this chapter. The CFD simulation, experiments, data collection process and results analysis are included as well. Theoretical study is conducted on the Solar Collector (SC) of the Solar Vortex Engine (SVE).

Studies conducted are aim to investigate the influence triggered by Top Plate on the updraft and performance of the Solar Vortex Engine (SVE). Numerical approach is used to predict the research findings through modeling and simulation. Experimental approach is used to verify and validate the predictions. Studies conducted on top plate are based on the following element and sequence.

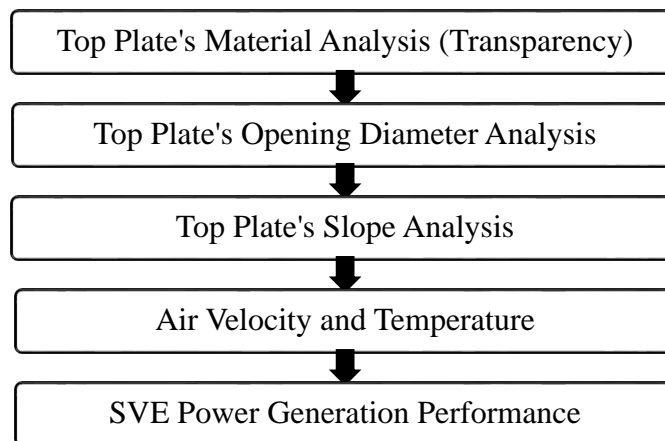


Figure 3. 1 – Study Approach on SVE Top Plate

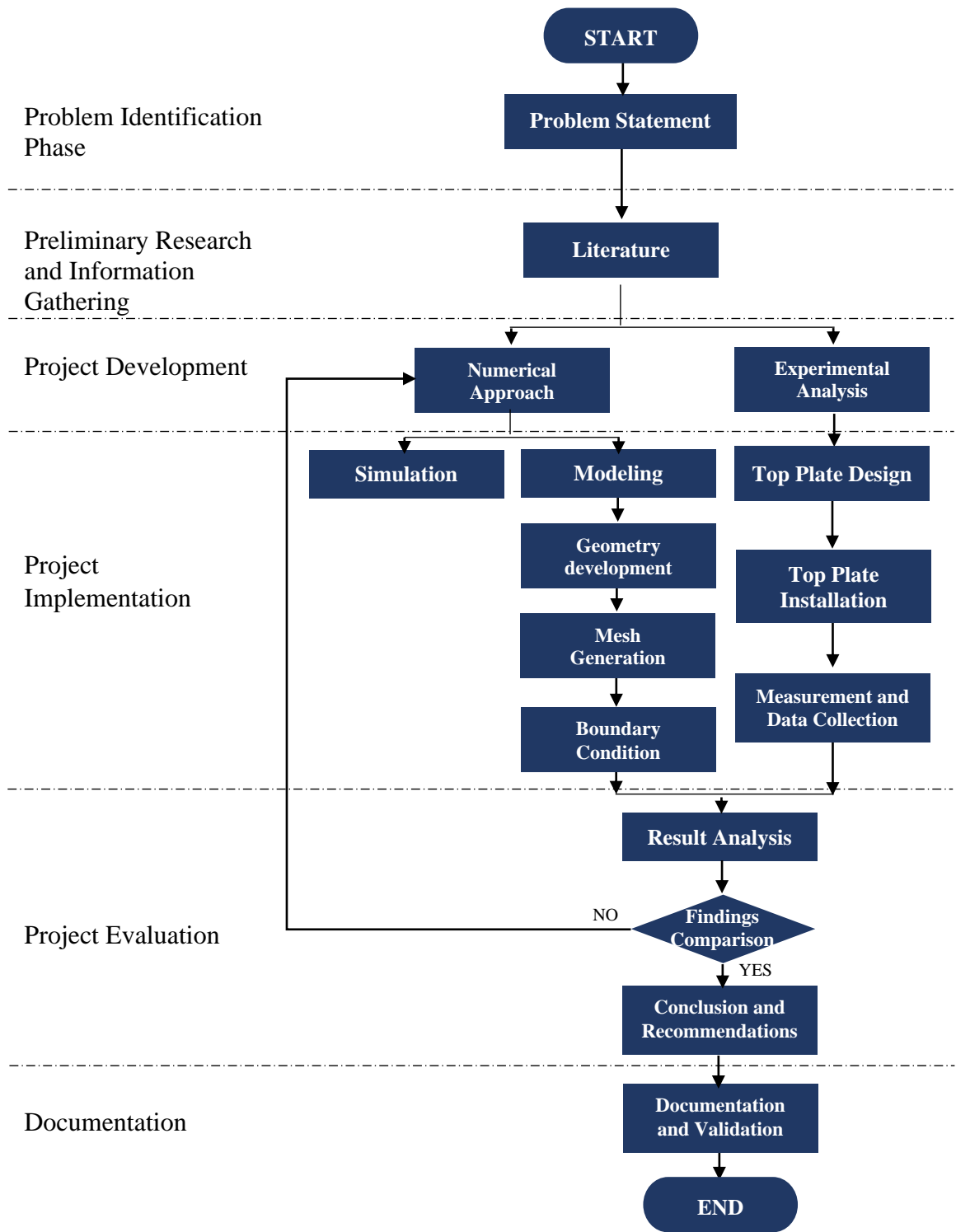


Figure 3. 2 - Flow Chart for Research Methodology

3.2 – Modeling On Solar Vortex Engine

The geometrical modelling was developed using PTC Creo 2.0 Parametric, an Engineering Drawing Commercialized Software. The Vortex Engine Generator (VEG) was constructed at a diameter of 0.9m and with a configuration of 8 rectangular air entry slots, 8 curved guide vanes and a circular base. An outer cylinder with diameter 1.0m of was constructed to embrace the VEG. A top plate was then constructed and slot in between the VEG and an octagonal shaped Transparent Bounding Structure (TBS).

The Transparent Bounding Structure (TBS) of height 0.60m was created based on prototype's parameters to study on air vortexes extending beyond its physical height of vortex engine. This is adequate for the preliminary simulations to investigate on the updraft of airflow. A Boolean function was applied later within ANSYS Design-Modeler to minus out the interior fluid volume from the geometrical frame for simulation purpose.

The geometrical model constructed is showed in Figure 3.3 in an exploded view. The dimensions for VEG is showed in Figure 3.4 below.

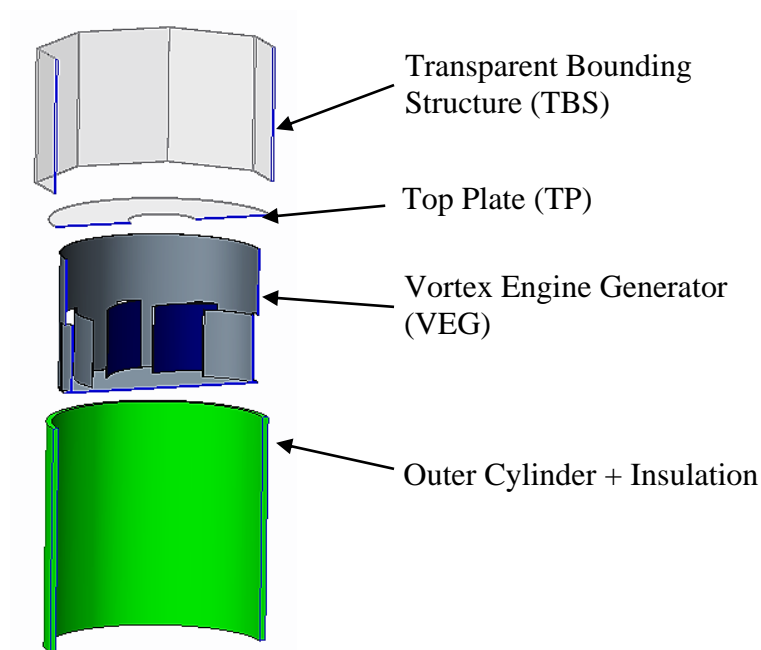


Figure 3. 3 - Sectioned view on Geometrical Modeling for VEG

Table 3. 1 – Parameters for Vortex Engine Generator

Parameters	unit	Value
Height of Transparent Bounding Structure (TBS)	m	0.6
Height of Vortex Engine Generator (VEG)	m	0.6
Height of Outer Cylinder + Insulation	m	1.0

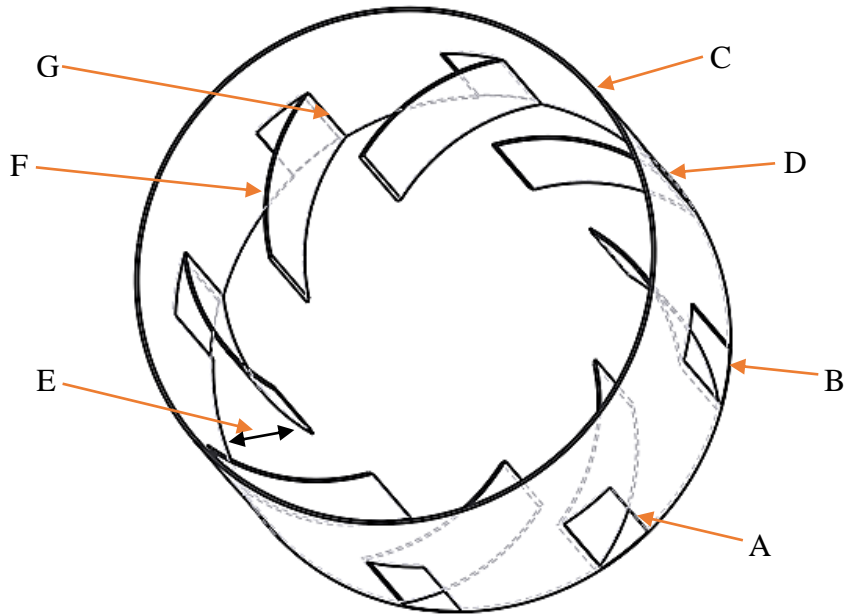


Figure 3. 4 - Configuration for Vortex Engine Generator (VEG)

Table 3. 2 – Dimensions for Vortex Engine Generator (VEG)

Order.	Parameters	Unit	Dimensions
A	Air entry slot height	m	0.3
B	Air entry slot width	m	0.1
C	VEG diameter	m	0.9
D	VEG height	m	0.6
E	Guide vanes angle	Degree, °	25°
F	Guide vanes length	m	0.35
G	Guide vanes height	m	0.3

Figure 3.5 shows the interior fluid body of Vortex Engine Generator (VEG) which was constructed for purpose of numerical simulation.

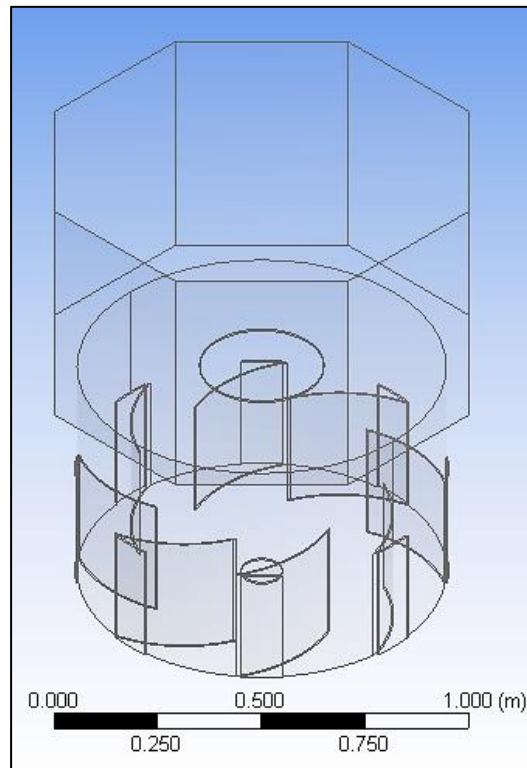
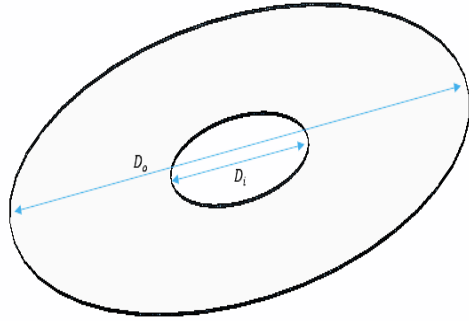


Figure 3. 5 – Fluid Body Structure of Vortex Engine Generator (VEG)

3.3 – Modelling of Top Plate

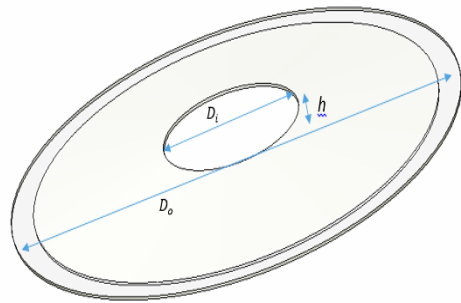
This research mainly focus on the top plate of SVE. A geometrical model for top plate was designed based on available prototype installed in solar research site within Universiti Teknologi PETRONAS to ease testing and experimental purpose. The top plate has an annulus structure with an outer diameter and inner diameter. The top plate can be categorized into two, namely a flat shaped top plate and a concentric circles canopy shaped top plate. Figure 3.6 and figure 3.7 show the configuration for both types of top plate. The area of top plate exposed to solar radiation can be calculated as below:



Where:

$$A_{tp} \text{ Top Plate Area} = \frac{1}{4}\pi D_c^2 - \frac{1}{4}\pi D_o^2 \quad (1)$$

Figure 3. 6 – Annulus Shaped Top Plate



Where:

$$A_{tp} \text{ Top Plate Area} = \pi \left(\frac{D_o}{2} + \frac{D_i}{2} \right) \sqrt{\left(\frac{D_o}{2} - \frac{D_i}{2} \right)^2 + h^2} \quad (2)$$

Figure 3. 7 – Canopy Shaped Top Plate

The top plate has been geometrical constructed with two type of material, namely Aluminum and Perspex for numerical investigation. The variation in material transparency will highly affect the Discrete Ordinates (DO) function in ANSYS to simulate the flow field within Vortex Engine Generator (VEG).

In order to obtain the optimum opening diameter that will improve solar updraft without compromising the heat transfer by solar radiation, another three top plates with different inner diameter (0.3m, 0.5m, and 0.9m) were constructed geometrically. The top plate was removed on the 0.9m case which allowed the Vortex Engine Generator to be fully opened. The dimensional modifications on the flat Solar Top Plate is showed in Figure 3.8 below. Simulations were done on all three diameters to determine the relationship between flow velocity and opening area. The optimum opening diameter simulated was then be made onto a canopy shape (slanted top plate) to promote air updraft as showed in Figure 3.9.

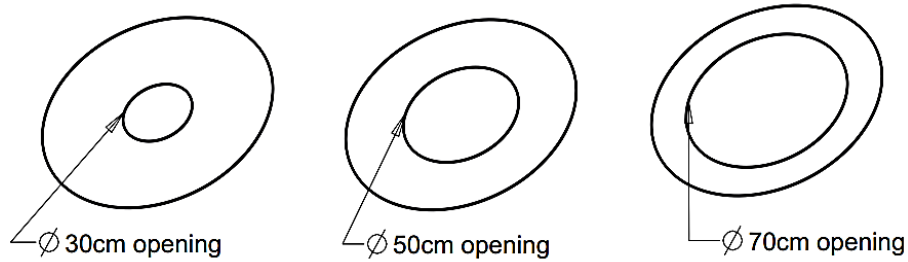


Figure 3. 8 - Proposed opening diameters for top plate

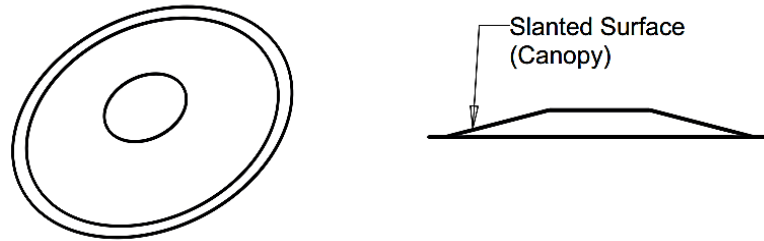


Figure 3. 9 - Proposed Modifications on Solar Top Plate

Table 3.3 below shows the material properties for the Perspex Top Plate.

Table 3. 3 – Material Properties for Top Plate

Properties	Value
Perspex Emmisivity, ϵ_p	0.9
Perspex Transmissivity, τ_p	0.92
Perspex Absorptivity, α_p	0.06
Stefan-Boltzmann constant, σ	$5.67 \times 10^{-8} W/m^2.K^4$

3.4 – Numerical Investigation

A 3D Geometrical Modeling on the SVE based on the prototype’s parameters was developed using PTC Creo 2.0 Parametric. The geometries were then transfer to ANSYS Workbench 15 for further meshing and simulation. Computational Fluid Dynamics (CFD) simulation techniques were applied to simulate physical phenomena and to predict on the dynamic behavior and thermo-properties of air within 3-D cylindrical coordinates. Finite Volume Method (FVM) was used to discretize the Navier-Stokes Equations, continuity equation and energy equation [24].

3.4.1 Mesh Generation

Mesh independency tests were conducted preliminary by changing the relevance center to identify the appropriate cell size or element number which provide the most stable and

accurate result with convergence criteria met. The default maximum face size provided by the system (ANSYS Fluent) was used as reference and further meshing were done by decreasing the maximum face size by a value of 0.01 for up to a total of 11 trials. Further decrement on max face size will lead to number of elements to exceed 512,000 cells which is not allowed under ANSYS educational package. The aspect ratio, number of nodes and elements were recorded for analysis and selection. Percentage of differences between current value and last trials (predecessor) were calculated to determine stability of outlet velocity. Refer to *Appendix B* for the full mesh independency analysis. Figure 3.10 below shows the mesh generated on the interior fluid body model of Vortex Engine Generator (VEG).

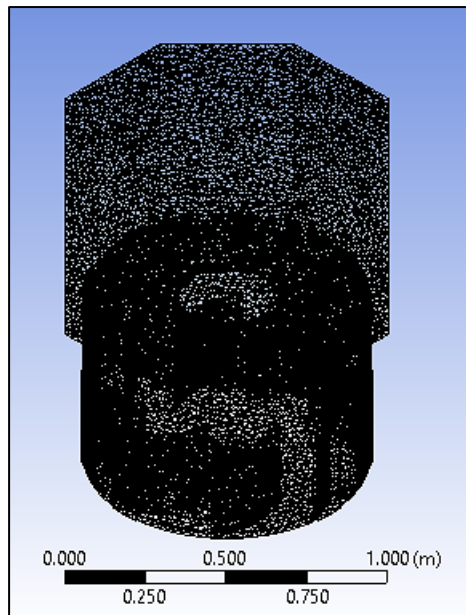


Figure 3. 10 – Mesh Generated on VEG model

3.4.2 Numerical Simulations

Simulations in Fluent employed Boussinesq Model for natural convection [25]. This model assume density remains a constant value in all solved equations, except for the buoyancy term in the momentum equation. Simulations were conducted based on unsteady $k - \varepsilon$ turbulence model. The Semi Implicit Method for Pressure Linked Equation – Consistent (SIMPLEC) algorithm was applied for second order discretization for pressure, momentum and energy to obtain more converged solution.

Discrete Ordinates (DO) has been applied under the radiation model to represent the solar insolation or radiation load passing through the transparent Perspex to heat up the air underneath. The amount of radiation is highly depend on the solar insolation available and the value was obtained from solar calculator pre-build in ANSYS Fluent 15. Global irradiance was employed in solar calculator which include transmitted, absorbed and reflected irradiance. Thus, the amount of intensity transmitted (Global Irradiance):

$$I_0 = I_T + I_A + I_R \quad (3)$$

3.4.3 Governing Equations

Various working principle and governing equations have been applied in numerical simulation done with ANSYS Fluent 15. Bernoulli's Equation, Conservation of Momentum and Energy Balance Equation were applied to studies the flow field within Vortex Engine Generator (VEG).

1. Ideal Gas Law

Top plate is installed to increase the outlet temperature to promote better updraft. Idea Gas Law can be applied to determine the relationship between air temperature on air density and pressure.

$$P = \rho RT \quad (4)$$

2. Air Continuity Equation

The flow of air within tower for Solar Vortex Engine is treated to be under confined flow condition with inlet and outlet. Continuity Equation [26] has been used to identify the suitable opening area on the top plate without sacrificing airflow velocity. The flow is assumed to be incompressible where increment in temperature is counterbalanced by pressure under ideal gas law. Continuity equation based on cylindrical coordinates is applicable to the top plate simulation. [27, 28].

$$\nabla \cdot (\rho V) = 0 \quad (5)$$

$$\frac{1}{r} \frac{\partial (r p v_r)}{\partial r} + \frac{1}{r} \frac{\partial (p v_\theta)}{\partial \theta} + \frac{\partial (p v_z)}{\partial z} = 0 \quad (6)$$

where ρ is the airflow density, V is the airflow updraft velocity and t is the time.

3. Navier-Stokes Equations on Cylindrical Polar Coordinates [26]

$$\begin{aligned}
 r \quad \rho \left(v_r \frac{\partial v_r}{\partial r} + \frac{v_\theta}{r} \frac{\partial v_r}{\partial \theta} - \frac{v_\theta^2}{r} + v_z \frac{\partial v_r}{\partial z} \right) & \quad (7) \\
 & = -\frac{\partial p}{\partial r} + pg_r + \mu \left(\frac{1}{r} \frac{\partial}{\partial r} \left(r \frac{\partial v_r}{\partial r} \right) - \frac{v_r}{r^2} + \frac{1}{r^2} \frac{\partial^2 v_r}{\partial \theta^2} - \frac{2}{r^2} \frac{\partial v_\theta}{\partial \theta} + \frac{\partial^2 v_r}{\partial z^2} \right)
 \end{aligned}$$

$$\begin{aligned}
 \theta \quad \rho \left(v_r \frac{\partial v_\theta}{\partial r} + \frac{v_\theta}{r} \frac{\partial v_\theta}{\partial \theta} + \frac{v_r v_\theta}{r} + v_z \frac{\partial v_\theta}{\partial z} \right) & \quad (8) \\
 & = -\frac{1}{r} \frac{\partial p}{\partial \theta} + pg_\theta + \mu \left(\frac{1}{r} \frac{\partial}{\partial r} \left(r \frac{\partial v_\theta}{\partial r} \right) - \frac{v_\theta}{r^2} + \frac{1}{r^2} \frac{\partial^2 v_\theta}{\partial \theta^2} + \frac{2}{r^2} \frac{\partial v_r}{\partial \theta} + \frac{\partial^2 v_\theta}{\partial z^2} \right)
 \end{aligned}$$

$$\begin{aligned}
 z \quad \rho \left(v_r \frac{\partial v_z}{\partial r} + \frac{v_\theta}{r} \frac{\partial v_z}{\partial \theta} + v_z \frac{\partial v_z}{\partial z} \right) & = -\frac{\partial p}{\partial z} + pg_z + \mu \left(\frac{1}{r} \frac{\partial}{\partial r} \left(r \frac{\partial v_z}{\partial r} \right) + \frac{1}{r^2} \frac{\partial^2 v_z}{\partial \theta^2} + \frac{\partial^2 v_z}{\partial z^2} \right) & \quad (9)
 \end{aligned}$$

4. Conservation of Mass [26]

Conservation of Mass principle was applied to investigate the inlet flow rate and outlet flow rate based on air updraft velocity. Incompressible flow is assumed for the operation fluid.

$$\begin{aligned}
 m_{inlet} & = m_{outlet} & (10) \\
 \rho A_{inlet} V_{inlet} & = \rho A_{outlet} V_{outlet} \\
 A_{inlet} V_{inlet} & = A_{outlet} V_{outlet}
 \end{aligned}$$

Preliminary simulation was conducted to seek for improvement on replacement of material transparency specification. The top plate material was changed from opaque aluminum to semi-transparent Perspex characteristic. Further simulations were conducted independently on different top plate opening diameter ranging from 0.3m, 0.5m 0.7m to 0.9m. The optimum opening diameter will then be implemented to canopy shaped top plate. The canopy shaped top plate was aimed for the investigation on the relationship between air-cornering underneath top plate with top plate slanting angle. Several slanting angles (8.53°, 10°, 20°, 30° and 40°) were selected for simulations to identify the optimum angle in reducing air cornering without compromising the air updraft and temperature. The simulation findings were later analyzed and validated through experiments. Convergence criterion was achieved when the ratio of maximum mass imbalance for each control volume is less than 0.01, the velocity and $k - \varepsilon$ viscous reduce to 0.001, while Discrete Ordinates and energy reduce to 10^{-6} in residual monitor.

3.4.4 Numerical Simulation Setup

The setup for simulation within ANSYS Fluent 15 is as below:

1. Solver Type – Pressure Based, Absolute Velocity Formulation and Steady time scheme.
2. Model Setup with Energy Equation
 - Viscous = $k - \varepsilon$ model for turbulent flow.
 - ✓ RNG – Swirl dominated flow and $S = 0.07$
 - ✓ Near – Wall Treatment = Standard Wall Functions
 - ✓ Options – Full Buoyancy Effects
 - Radiation = Discrete Ordinates (DO)
 - ✓ Solar Load – DO Irradiation with Solar Calculator
 - ✓ Longitude 100.98' E and Latitude 4.42' N
 - ✓ Timezone = +8 GMT with North (Z=-1) and East (X=1)
 - ✓ Day 18, Month 2, Hour 13, Minute 0
 - ✓ Solar Irradiation Method = Fair Weather Conditions
 - ✓ Sunshine Factor =1

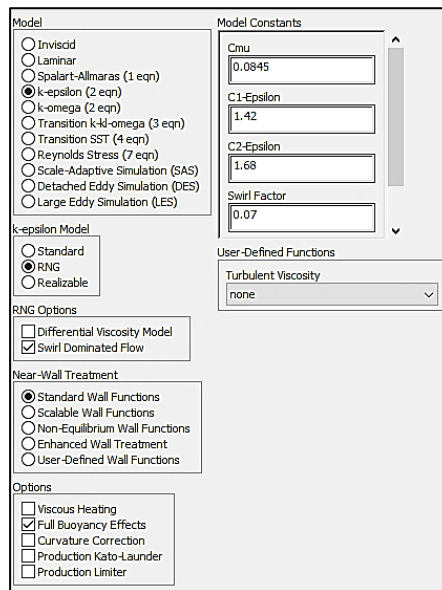


Figure 3. 11 - ANSYS Fluent 15 Viscous Model Setup

3. Materials – Fluid (Air), Solid (Aluminum) and Solid (Perspex)
 - Fluid (Air)
 - ✓ Density = Boussinesq (1.225kg/m^3)

- ✓ Air Thermal Expansion Coefficient = 0.00303/K
 - Solid (Aluminum)
 - ✓ Properties = Opaque
 - ✓ Thermal Conductivity = 202.4W/m.K
 - ✓ Density = 2719kg/m³
 - ✓ Specific Heat = 871J/kg.K
 - Solid (Perspex)
 - ✓ Properties = Semi-Transparent
 - ✓ Thermal Conductivity = 0.189W/m.K
 - ✓ Density = 1200kg/m³
 - ✓ Specific Heat = 1200J/kg.K
4. Boundary Conditions – As described in section 3.4.5
5. Solution Method –
- Pressure–Velocity Coupling – SIMPLEC with Skewness Correction: 0
 - Spatial Discretization –
 - ✓ Gradient – Green-Gauss Cell Based
 - ✓ Pressure – PRESTO!
 - ✓ Momentum – Second Order Upwind
 - ✓ Energy – Second Order Upwind
 - ✓ Turbulent Kinetic Energy – Second Order Upwind
 - ✓ Turbulent Dissipation Rate – Second Order Upwind
 - ✓ Discrete Ordinates – Second Order Upwind
6. Solution Controls – Relaxation Factors
- Pressure - 0.3
 - Momentum – 0.01
 - Density, Body Forces, and Energy – 0.5
7. Solution Initialization – Compute from main inlets (Air entry slots)

3.4.5 Boundary Conditions

Case 1 Boundary Conditions

Case 1 was simulated with Aluminum Top Plate and consideration of Solar Radiation. Boundary conditions were selected based on Experiment 1 parameters.

Table 3. 4 – Boundary Condition for Case 1

Surfaces/ Components	No. of Items	Boundary Type	Boundary Conditions
Transparent Bounding Structure (TBS)	8	Wall	Material = Perspex Constant temperature = 315K Stationary with no slip condition
Top Plate	1	Wall	Material = Aluminum Stationary with no slip condition and constant temperature = 316K
Top Plate opening	1	Outflow	Opening Diameter = 0.3m
Inner cylinder (VEG)	1	Wall	Material = Aluminum Constant temperature = 316K Stationary with no slip condition
Curved Vanes	8	Wall	Material = Aluminum Constant temperature = 316K Stationary with no slip condition
Air entry slots	8	Velocity-Inlet	Constant normal Velocity = 0.3m/s Constant temperature = 312K
Base inlet	1	Velocity-Inlet	Constant normal Velocity = 0m/s ** Constant temperature = 316K
Ambient Condition	-	-	Constant Temperature = 314K

** The base inlet air flow velocity was set to be 0m/s as the base opening will be covered or closed in future experimental works.

Case 2 Boundary Conditions

Case 2 was simulated with Perspex Top Plate (0.3m Opening Diameter) and consideration of Solar Radiation. Boundary conditions were selected based on Experiment 2 parameters.

Table 3. 5 – Boundary Condition for Case 2

Surfaces/ Components	No. of Items	Boundary Type	Boundary Conditions
Transparent Bounding Structure (TBS)	8	Wall	Material = Perspex Constant temperature = 315K Stationary with no slip condition
Top Plate	1	Wall	Material = Perspex Stationary with no slip condition and constant temperature = 322K
Top Plate opening	1	Outflow	Opening Diameter = 0.3m
Inner cylinder (VEG)	1	Wall	Material = Aluminum Constant temperature = 325K Stationary with no slip condition
Curved Vanes	8	Wall	Material = Aluminum Constant temperature = 325K Stationary with no slip condition
Air entry slots	8	Velocity-Inlet	Constant normal Velocity = 0.7m/s Constant temperature = 322K
Base inlet	1	Velocity-Inlet	Constant normal Velocity = 0m/s ** Constant temperature = 325K
Ambient Condition	-	-	Constant Temperature = 314K

** The base inlet air flow velocity was set to be 0m/s as the base opening will be covered or closed in future experimental works.

Case 3 Boundary Conditions

Case 3 was simulated with changing variable of Perspex Top Plate (0.5m, 0.7m, 0.9m Opening Diameter) and consideration of Solar Radiation. Boundary conditions were selected based on Experiment 2 parameters.

Table 3. 6 – Boundary Condition for Case 3

Surfaces/ Components	No. of Items	Boundary Type	Boundary Conditions
Transparent Bounding Structure (TBS)	8	Wall	Material = Perspex Constant temperature = 315K Stationary with no slip condition
Top Plate	1	Wall	Material = Perspex Stationary with no slip condition and constant temperature = 322K
Top Plate opening	1	Outflow	Opening Diameter = 0.5m, 0.7m, 0.9m
Inner cylinder (VEG)	1	Wall	Material = Aluminum Constant temperature = 325K Stationary with no slip condition
Curved Vanes	8	Wall	Material = Aluminum Constant temperature = 325K Stationary with no slip condition
Air entry slots	8	Velocity-Inlet	Constant normal Velocity = 0.7m/s Constant temperature = 322K
Base inlet	1	Velocity-Inlet	Constant normal Velocity = 0m/s ** Constant temperature = 325K
Ambient Condition	-	-	Constant Temperature = 314K

*** The base inlet air flow velocity was set to be 0m/s as the base opening will be covered or closed in future experimental works.*

Case 4 Boundary Conditions

Case 4 was simulated with changing variable of Canopy Shaped Perspex Top Plate (8.53', 10', 20', 30' and 40' slanting angle) and consideration of Solar Radiation. Boundary conditions were selected based on Experiment 2 parameters.

Table 3.7 – Boundary Condition for Case 4

Surfaces/ Components	No. of Items	Boundary Type	Boundary Conditions
Transparent Bounding Structure (TBS)	8	Wall	Material = Perspex Constant temperature = 315K Stationary with no slip condition
Top Plate	1	Wall	Material = Perspex Stationary with no slip condition and constant temperature = 322K
Top Plate opening	1	Outflow	Opening Diameter = 0.3m Slanting angle = 8.53', 10', 20', 30', 40'
Inner cylinder (VEG)	1	Wall	Material = Aluminum Constant temperature = 325K Stationary with no slip condition
Curved Vanes	8	Wall	Material = Aluminum Constant temperature = 325K Stationary with no slip condition
Air entry slots	8	Velocity-Inlet	Constant normal Velocity = 0.7m/s Constant temperature = 322K
Base inlet	1	Velocity-Inlet	Constant normal Velocity = 0m/s ** Constant temperature = 325K
Ambient Condition	-	-	Constant Temperature = 314K

*** The base inlet air flow velocity was set to be 0m/s as the base opening will be covered or closed in future experimental works.*

3.5 – Experimental Approach

All the experimental procedures, measurements instruments, prototype construction and modifications have been included in this section. Configurations on SVE prototype and measurements have been illustrated with figures.

Experiments are conducted with the aims to verify and validate a hypothesis while a hypothesis is an expectation on how a particular process and phenomena works. In every experiments, there are changing variable(s), dependent variable(s) and fixed variable(s). Experiments rely on repeatable steps or procedures and logical analysis of the results. Results or outcomes of the experiment will either support or disprove the hypothesis.

This experiment is conducted to answer the “What-if” question. Modification and improvements (Changing Variables = “What-if”) were done on the pre-installed prototype. Sensors were installed for experimental measurements and measuring results are the Dependent Variables. Experimental measurements were done on a pretest-posttest basis. First measurement was done before intervention factor place which an opaque aluminum top place was installed above the VEG. Same measurements were done later after the intervention factor took place in which three transparent top plate with different orifice diameter were installed above the VEG. Comparison on pretest and posttest results were made to determine the causal effect from the modifications.

The experimental testing on Solar Vortex Engine is categorized as Field Experiment. The outcome of the experiment is observed in a natural setting rather than a contrived laboratory experiment. It has a higher external validity. However, field experiment would suffer higher possibility of contaminations.

Experimental implementation must take into account and make possible control on the confounding factors. Confounding factor is any factors that would mar the accuracy or repeatability of the experiment or the ability to interpret the results. Example of confounding factors would be the experimental errors or uncertainties in measurements.

3.5.1 Experimental Setup for Solar Vortex Engine (SVE)

The Solar Vortex Engine (SVE) is consisted on a Vortex Engine Generator (VGE), Solar Collector (SC) and Transparent Bounding Structure (TBS). The prototype for SVE was fabricated previously based on before-hand research and is located at Solar Research Site in Universiti Teknologi PETRONAS. This pre-built prototype has been applied as the experimental model for this research.

The working environment of the Solar Vortex Engine prototype installed at the solar research site in Universiti Teknologi PETRONAS is as below:

- Location Altitude: 24.23m
- Latitude and Longitude: $4.42^{\circ}N$, $100.98^{\circ}E$
- Average wind velocity: 1.4m/s
- Average solar intensity: $200-1000W/m^2$
- Ambient temperature: 300-304K
- Ambient pressure: 100.2kPa

Two experiments were conducted to verify on the numerical simulations and to determine the contribution of transparent top plate on the performance of Solar Vortex Engine. Experiment 1 was conducted to with an opaque Aluminum Top Plate to investigate the air flow velocity and temperature Experiment 2 was conducted with a Perspex Top Plate where all other parameters remain constant. The results obtained from experiment 1 were applied as the reference or baseline value to prove on any modification made on the prototype. By changing the transparency of the top plate, the solar intensity became the changing variable between the two experiments. Multiple parameters were measured ranging from solar updraft velocity, airflow tangential velocity and radial velocity, airflow and surface temperature and to name a few.

Figures below shows the construction of Solar Vortex Engine (SVE).



Transparent
Bounding
Structure
(TBS)

Thermal
Insulation

Vortex Engine
Generator
(VGE)

Solar
Collector
(SC)

Figure 3. 12 - Solar Vortex Engine Testing Unit installed at UTP Solar Research Site



Top Plate
opening
(Central hole)

Aluminum
Top Plate

Figure 3. 13 – Top View of Solar Vortex Engine (SVE) with Aluminum Top Plate



Figure 3. 14 – Top View of Solar Vortex Engine (SVE) with Perspex Top Plate

3.5.2 Components and Dimensions for Solar Vortex Engine

Table 3. 8 – Components and Dimensions for Solar Vortex Engine

System Components	Materials Properties		Dimensions	
	Description	Value	Items	Value
Transparent Bounding Structure (TBS) / Protector	Perspex thickness, t_p	5 mm	Height, h_{TBS}	0.6 m
	Perspex emissivity, ϵ_p	0.9		
	Perspex transmissivity, τ_p	0.92		
	Perspex absorptivity, α_p	0.06		
	Density, ρ	1200kg/m ³		
	Specific Heat, C	1200J/kg.K		
	Thermal Exp. Coef.	0.003031/K		
Thermal Insulation	Fiberglass thickness, t_f	0.0254	Radius, r_f	0.5 m
	Fiberglass thermal conductivity, t_p	0.04 W/m.K		

Outer Cylinder	Aluminum thickness	2 mm	Radius, r_{OC}	0.5 m
	Aluminum thermal conductivity	25 W/m.K	Height, h_{OC}	1.0 m
Inner Cylinder	Aluminum thickness	2 mm	Radius, r_{IC}	0.45 m
			Height, h_{IC}	0.6 m
			Air entry slot number, N	8
			Air entry slot width, w_s	0.1 m
			Air entry slot height, h_s	0.3 m
	Aluminum thermal conductivity	25 W/m.K	Guide vanes number, N	8
			Guide vanes height, h_v	0.3 m
			Guide vanes deflection angle, θ_v	25
			Base radius, r_{ob}	0.45 m
			Base inner radius, r_{ib}	0.05 m
SC	Steel chassis	1.5 inch	Angle of canopy slope	8.53°
	Perspex emissivity	0.9		
	Perspex transmissivity	0.92	Outer radius	4.4 m
	Perspex absorptivity	0.06		
	Perspex surfaces roughness,	0	Inner radius	0.5 m
	Density, ρ	1200kg/m ³		
	Specific Heat, C	1200J/kg.K	Outer height	0.24 m
	Thermal Exp. Coef.	0.003031/K	Inner height	0.79 m
Ground	Sand, Crash Stone and pebble stone layers' absorptivity,	~ 0.7	Outer radius	4.4 m

3.5.3 Experimental Positioning For Measurements

Experimental measurements were divided into Fixed Measurements and Transient Measurements. All measurements were done with measuring instruments mentioned in last section which includes: GRAPHTEC DATA LOGGER GL820 for temperature measuring, Digital Reader KIMO-AMI 300 with Multi Probes for Velocity, Temperature,

Humidity and Pressure measuring, and Solarimeter KIMO-SL 200 Instrument for solar radiation measuring. Details of measuring instruments were attached in Appendix A.

Fixed measurements method applied GRAPHTEC DATA LOGGER GL820 with type J thermocouples and were installed at certain fixed position on Solar Vortex Engine (SVE) and data recording is done automatically by the instrument at specified interval. No manual recording and monitoring is required.

Positioning of experimental measurements are illustrated as below in Figure 3.15. Thermocouples type J have been installed at position 1 to 9 in radial direction of the Solar Collector (SC) for measurements of ground, air flow and collector surface temperature. Thermocouples 1, 2 and 3 were placed under the pebble stones while thermocouples 4, 5 and 6 were placed at middle height underneath solar collector. Thermocouples 7, 8 and 9 were installed at top surface of SC. Thermocouple 10 was placed on VEG base aluminum to measure surface temperature while Thermocouple 11 was placed in the middle at top plate opening to measure air outflow temperature. Two more thermocouples were installed at position 13 and 14 to measure surface temperature of VEG interior wall and top plate surface temperature.

Transient measurements method involved the manual measuring with Digital Reader KIMO-AMI 300 at specified location within SVE. The measuring interval or frequency depend solely on user and an hour interval has been applied. The transient measurements were done at position 11, 12, 14, 16, and 17. Position 11 was meant to measure air outflow temperature, velocity, humidity, and volume flow rate while position 12 recorded the ambient temperature, velocity and humidity for comparison purpose. Solarimeter has been used to measure solar intensity directed above and underneath the top plate at position 14. Air inflow temperature and velocity were recorded with hotwire probe at position 16 and airflow tangential and radial velocity were measured at position 17.

The temperature recorded by Thermocouples type J was saved in Excel files format and was directly transferred to an USB memory drive connected to the Graphtec Data Logger GL820. Transient experimental measurements on solar intensity, temperature, velocity and humidity were captured manually on an hourly basis starting from 9a.m. to 5p.m. in a day. The data were later analyzed and compiled as well in Chapter 4.

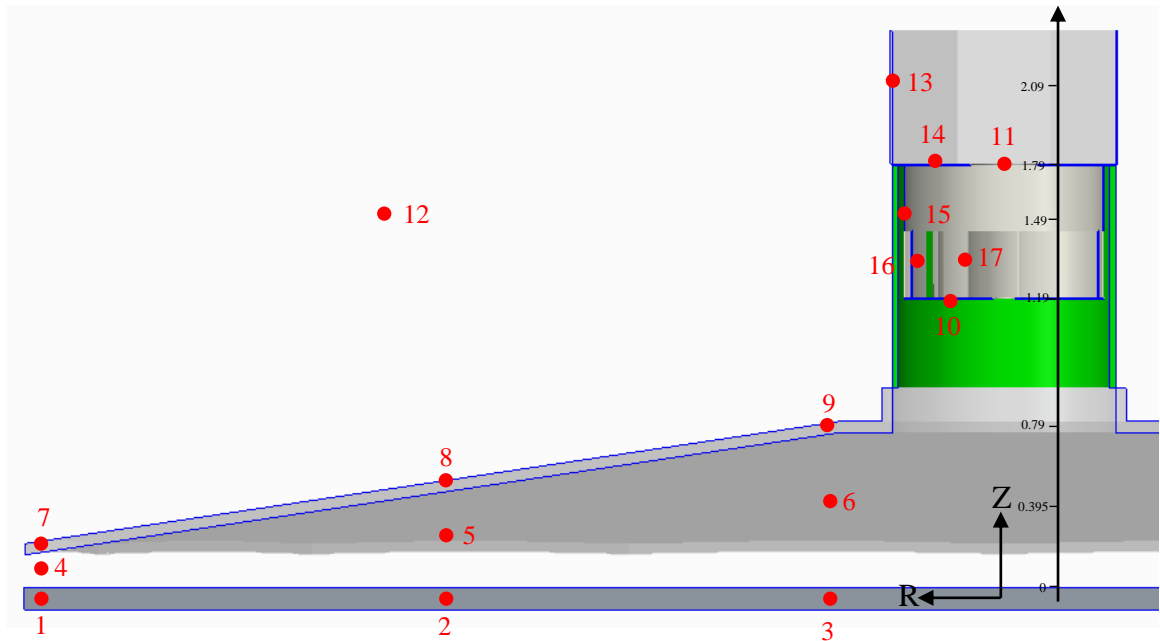


Figure 3. 15 - Sectional Schematic for Experimental Measurements Positions

Table 3. 9 – Experimental Measuring Positions with Instruments

Items	Positions	Parameters	Positioning Dimensions		Probe
			R – axis (m)	Z –axis (m)	
Ground	1	Temperature	4.4	0	Thermocouples
	2		2.4	0	
	3		0.5	0	
Air flow under SC	4	Temperature	4.4	0.12	Thermocouples
	5		2.4	0.27	
	6		0.5	0.395	
SC	7	Temperature	4.4	Canopy Surface	Thermocouples
	8		2.4		
	9		0.5		
VEG	10	Temperature	0.3	1.19	Thermocouples
	15	Temperature	0.5	1.49	Thermocouples
	16	Temperature	0.45	1.29	Hotwire
		Velocity			
	17	Tangential Velocity	0.2	1.29	Hotwire
Radial Velocity					

Outlet	11	Temperature	0	1.79	Thermocouple
		Velocity			Hotwire
		Vol. flow rate			Airflow Meter
		Humidity			
Ambient	12	Temperature	-	-	Hotwire
		Velocity			Airflow Meter
		Humidity			
TBS	13	Temperature	0.5	2.09	Thermocouple
Top Plate	14	Temperature	0.3	1.79	Thermocouple
		Solar Intensity			Solarimeter

3.6 – Gantt Chart

3.6.1 FYP 1

Table 3. 10 – Gantt Chart for FYP 1

No	Task	%	WEEK													
			1	2	3	4	5	6	7	8	9	10	11	12	13	14
Stage 1																
1	Title Selection	100	■													
	Title understanding	100	■													
Stage 2																
2	Research on Vortex Engine and Solar Top Plate	100	■													
	Search for related Research Papers	100	■	■												
	Download ANSYS Fluent 15 Software and PTC Creo 3.0	100	■													
	Research on mesh generation	100		■	■											
Stage 3																
3	Identification of Problem Statement	100			■											
	Identification of Objectives	100			■											
	Preparation of Key milestones	100			■											
	Literature Review	100	■	■	■	■	■	■	■	■	■	■	■	■	■	■
	Comparison on previous researches	100			■	■	■	■	■							
	Preparation of First Draft Proposal	100	■	■	■	■	■	■	■							
	Extended Proposal and Proposal Defense	100							■							
Stage 4																
4	Geometrical Modeling Development	100									■					
	Simulation (Trial and Error)	100									■	■				
	Simulation and Prototype Fabrication	100									■	■				

3.7 – Project Key Milestone

Geometrical Modeling, simulations and fabrication of prototype (top plates) are conducted within FYP 1. Mesh independence test was applied to identify the most suitable cells number in determining an accurate result.

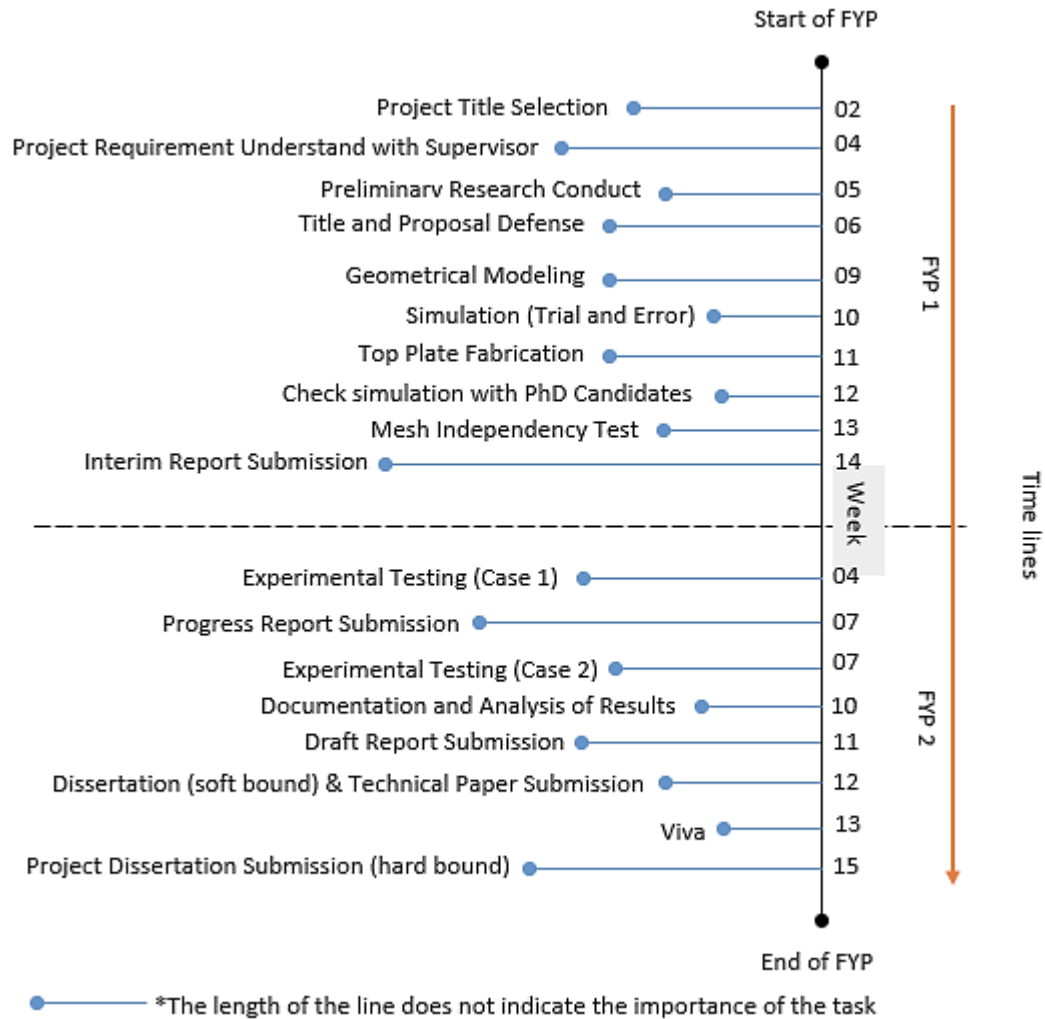


Figure 3. 16 – Key Milestone for FYP

3.8 – Summary

All the required information on the approaches of this research has been compiled within this chapter. The methodology started with the conceptual design of the Solar Vortex Engine and followed by the geometrical modelling for numerical simulation. Boundary condition and setup adopted has been placed under numerical procedure. The dimensional information and fabrication of prototype have been included as well in this chapter.

CHAPTER 4

RESULT AND DISCUSSION

4.1 Foreword

Solar Vortex Engine (SVE) utilized solar thermal system to heat up airflow underneath collector to promote natural free convection, generating low pressure within vortex engine, leading to constant air supply from higher pressure ambient air. Top plate was installed to further improve updraft by generating larger temperature variation within Vortex Engine Generator (VEG), lowering air buoyancy and leading to lower internal pressure. Transparent Top plate allows the penetration of solar radiation and apply solar energy as the source of energy supply to heat up air. This research was done to improve top plate efficiency in order to raise power plant performance. With the correct material selected for the construction on top plate, the efficiency on collector in capturing solar radiation increased. Higher temperature can be obtained from the airflow underneath the top plate, leading to a larger temperature variation compare to ambient air. Airflow velocity (natural convection) increased due to the temperature variation. Efficiency in converting airflow kinematic energy into mechanical energy was increased as well, promoting the power plant generation performance.

Results and findings obtained are discussed and analyzed in this chapter. Comparisons were made between numerical results and experimental measurements for validation purpose.

4.2 Numerical Simulation Results

Computational Fluid Dynamics Method (CFD) was adopted to simulate the physical phenomena within Vortex Engine Generator (VEG). Simulations findings are showed in contours, vectors and X-Y plots. Several cases have been simulated for comparison purpose and seek for parameters' improvement due to the modifications did on the top plate. The optimum opening diameter and slanting angle on canopy shaped top plate are included at the end of this section. Mesh independency tests were conducted at the very first place before any iterations to determine the best mesh size for most accurate result.

4.2.1 Mesh Independency Test (MIT)

A few runs on simulating the same parameters are conducted through Mesh Independency Test to identify the appropriate elements number and cells size which provide the stable result. Lowest mesh size was selected among the stabled trials in order to achieve lowest duration for simulation. Laminar flow and zero energy have been applied in the test to accelerate convergent. The default mesh size provided by ANSYS Fluent 15 was treated as the first simulation and act as a reference. A decrement of 0.01m on maximum face size was adopted for further trials.

Smoothing operation tends to reposition nodes based on the average of the neighbors' nodes. Reposition strategy improves the mesh skewness but relaxes the clustering of node points. Smoothing can be categorized into Laplace smoothing where all types of meshes are applicable and Skewness based smoothing for triangular and tetrahedral meshes. With Fine smoothing, the minimum cell size and maximum cell size are limit to $2.057 \times 10^{-4}m$ and $4.115 \times 10^{-2}m$. The default meshing provided by ANSYS has Coarse Relevance Center and Medium Smoothing. A Medium Relevance Center and Medium Smoothing was adopted as the second trial while Fine Relevance Center and High Smoothing was applied for third trial.

The aspect ratio, elements number, maximum velocity, maximum pressure and percentage difference were considered and monitored for mesh size selection. Finally, **trial 4** with Max Face Size of 0.027m, an aspect ratio of 12.40 and cells number of 211,833 was selected due to approximately zero percentage difference compare to predecessor. Stability was obtained in trial 4. Although trial 10 recorded the lowest aspect ratio, it was not selected due to the larger percentage difference. Figure 4.1 and 4.2 shows the stability of maximum velocity and pressure against trials and their aspect ratio. Refer to Appendix B.1 for full statistical table on mesh independency test conducted at inlet velocity of 0.5m/s.

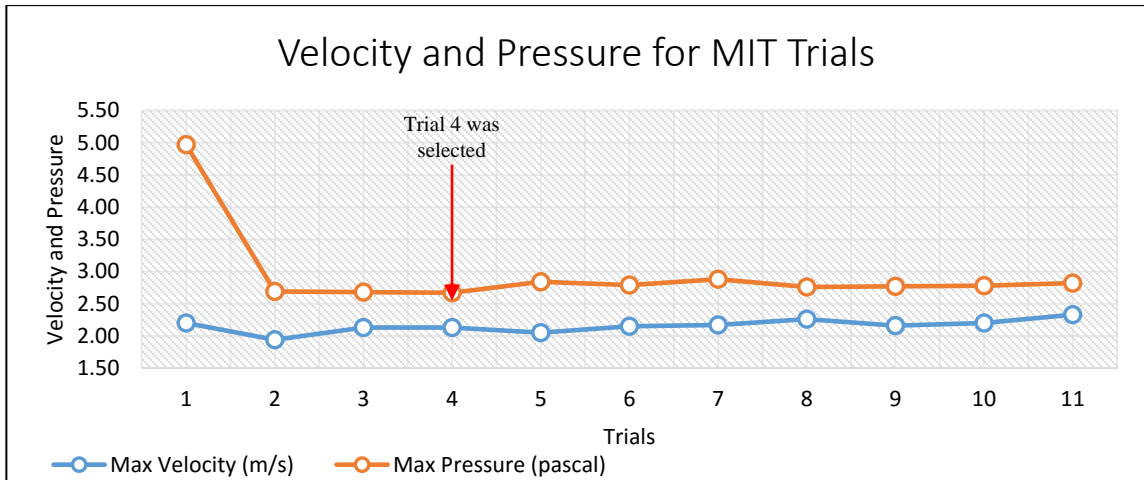


Figure 4. 1 - Graph of Maximum Simulated Velocity and pressure vs Trials on MIT

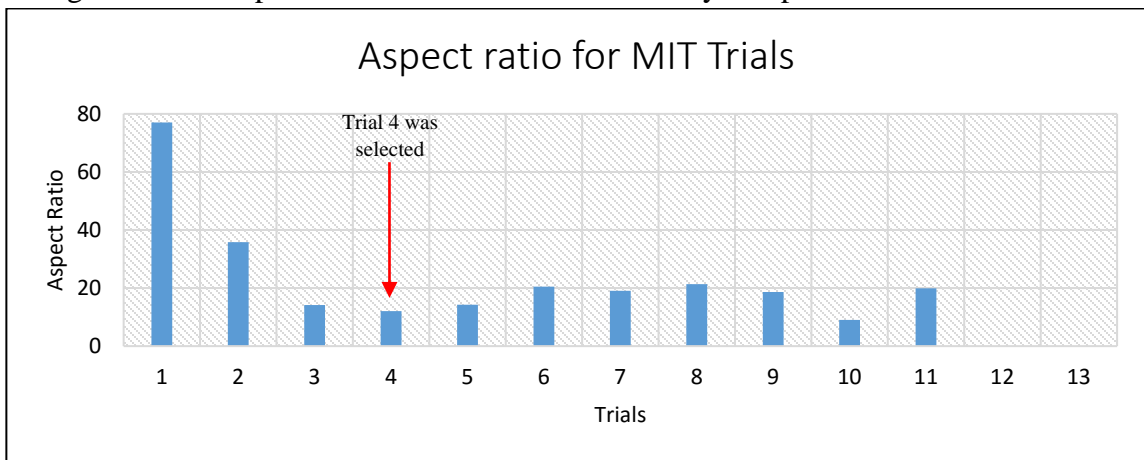


Figure 4. 2 - Graph of Aspect Ratio vs Trials on Mesh Independency Test

The inlet flow rate at 8 air inlet slots and top plate single outlet flow rate were calculated and compared simultaneously within Mesh Independency Test. An average of outflow velocity at top plate opening has been applied on the calculation on outlet flow rate. Figure 4.3 below shows the approaches in obtaining the average outlet velocity.

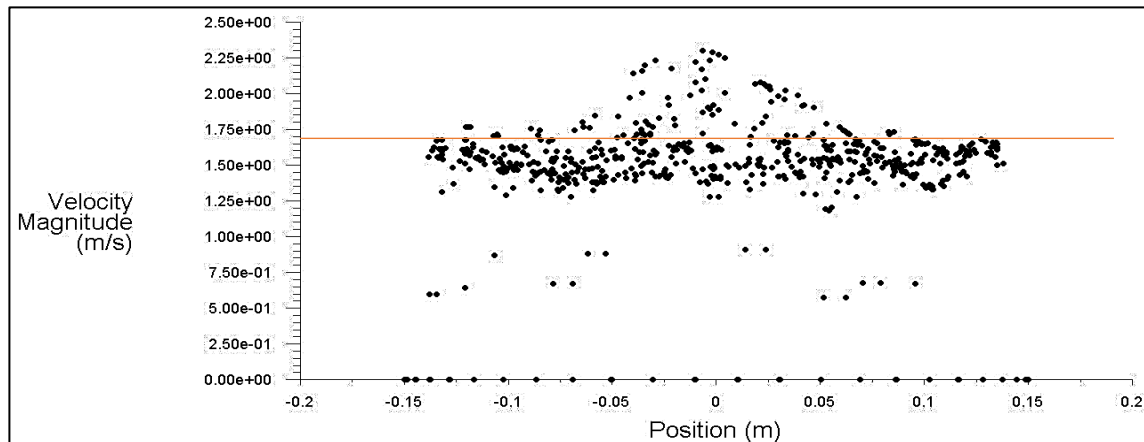


Figure 4. 3 - XY Plot for Top Plate Outlet Velocity on Trial 11

Table 4. 1 - Inlet and Outlet Flow rate for 11 trials

Trials	Inlet Flow Rate (m^3/s)	Outlet Flow Rate (m^3/s)	Percentage Difference
1	0.12	0.125	0.043
2	0.12	0.124	0.031
3	0.12	0.120	0.002
4	0.12	0.120	0.002
5	0.12	0.123	0.025
6	0.12	0.122	0.013
7	0.12	0.115	0.040
8	0.12	0.128	0.066
9	0.12	0.122	0.019
10	0.12	0.124	0.031
11	0.12	0.124	0.031

Based on Figure 4.4, the outlet flow rates for several trials were matching with the inlet flow rate of $0.12m^3/s$. The Conservation of mass principle was achieved in the trials. A low percentage difference was recorded. Calculation on inlet flow rate and outlet flow rate are shows as below. Trial 11 has been applied as sample calculation.

$$Q_{inlet} = 8 * A_{inlet} V_{inlet} = 8(0.1m \times 0.3m)(0.5 m/s) = 0.12m^3/s \quad (16)$$

$$Q_{outlet} = 1.75m/s[\pi(0.15)^2] = 0.1237m^3/s \quad (17)$$

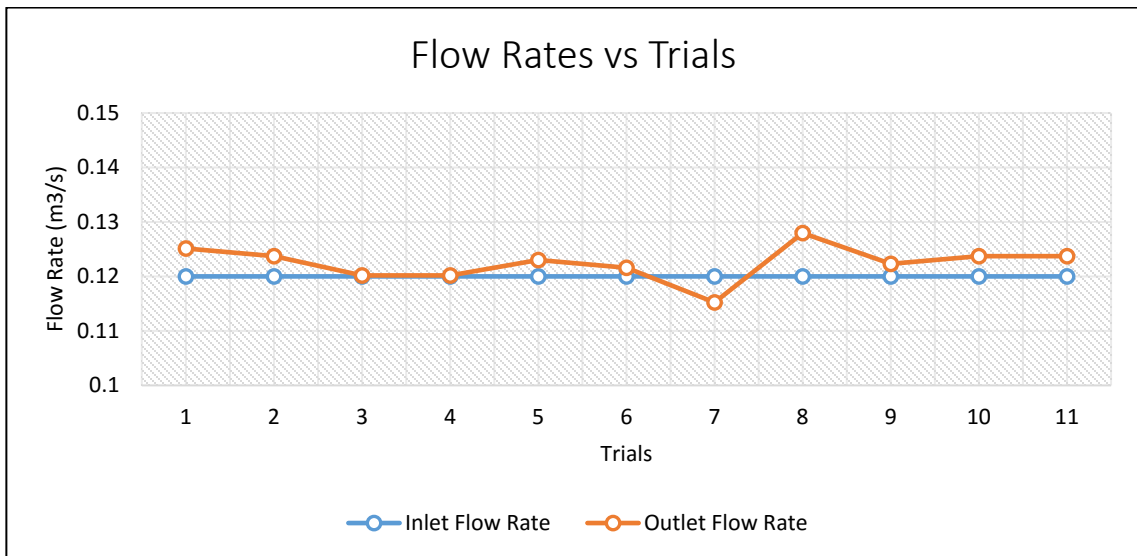


Figure 4. 4 - Graph on Flow Rates vs Trials

4.2.2 Numerical Investigation on Top Plate Material

Preliminary simulation (Case 1) was conducted on Aluminum Top Plate (TP) with consideration on solar radiation. Discrete ordinates (DO) function has been selected within ANSYS Fluent 15 to investigate and predict the effect on solar updraft the flow temperature due to the solar radiation. Simulated result from case 1 was applied as a reference or baseline information for comparison on further simulation. Experiment 1 was then conducted with Aluminum Top Plate (TP) to verify on the simulated result and boundary conditions.

Case 2 simulation was conducted with Perspex Top Plate to predict the improvement compare to case 1. Perspex material properties was entered into numerical setup and semi-transparency feature has been selected to allow the penetration of solar radiation into the Vortex Engine Generator (VEG) during simulation. Discrete Ordinates (DO) has been selected as well in case 2 simulation. Experiment 2 was then conducted to validate on the boundary conditions and simulated results.

Numerically simulated result ranging from static temperature, static pressure, velocity magnitude, and tangential velocity were compared and displayed as below.

Solar Radiation Analysis

Solar intensity was the changing variable between the two cases. Solar radiation was simulated in both cases by Discrete Ordinates (DO) setup. Discrete Ordinates considered all the radiation intensity ranging from direct normal solar radiation, diffuse solar irradiation on both vertical and horizontal surfaces and ground reflected solar irradiation.

Opaque Aluminum top plate tended to absorb most of the direct solar radiation, raising only its own temperature. Solar radiation was blocked and reflected. It was beyond reaching the interior atmosphere of VEG. Thus, as shown in Figure 4.5, a low intensity of $2.24e+03W/m^2$ was simulated within the VEG.

On the other hand, Perspex Top Plate allowed the solar radiation to penetrate to heat up the interior wall and airflow of VEG. Thus, from Figure 4.6, case 2 with Perspex configuration received peak incident radiation of $4.71e+03W/m^2$ below the top plate and reduced further down. Most of the interior airflow received an average radiation intensity

of $3.18e+03W/m^2$ which was higher compare to case 1 with aluminum configuration. Higher radiation intensity is beneficial in raising airflow temperature and improve engine performance.

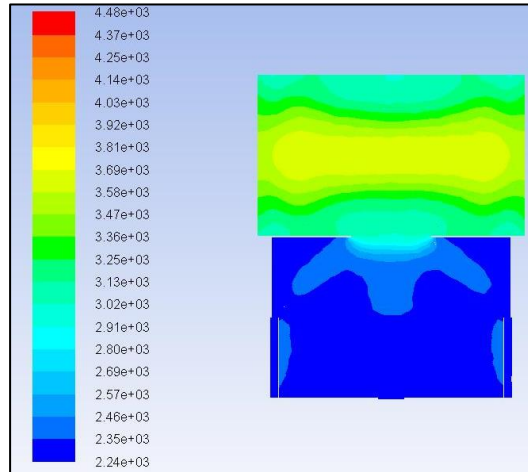


Figure 4. 5 – Case 1 Sectional Incident Radiation Contour (Aluminum)

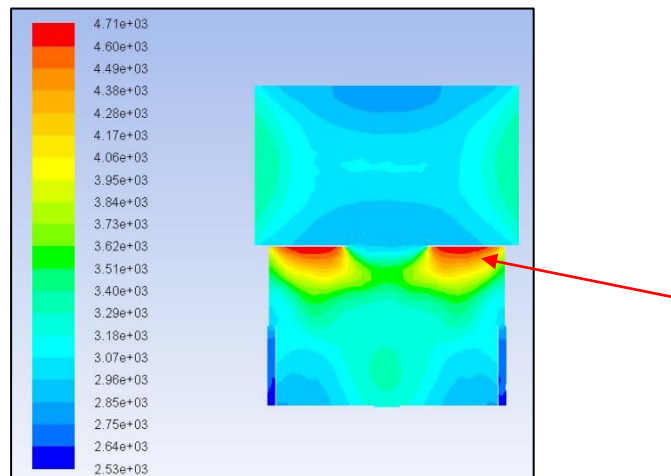


Figure 4. 6 – Case 2 Sectional Incident Radiation Contour (Perspex)

Temperature Distribution

Solar intensity has been very much affected the temperature distribution of the interior flow field within the Vortex Engine Generator (VEG). Interior wall and airflow temperature were directly proportional to the solar intensity. The higher the solar intensity, the higher the top plate efficiency and thus, more useful heat gain was created.

As aluminum top plate blocked most of the solar intensity, a lower wall and airflow temperature were simulated. As shown in Figure 4.7, the wall achieved maximum temperature of 316K (43°C) while airflow achieve maximum temperature of 314K (41°C). The temperatures simulated have been very much match with the experimental measurements. A comparison between simulated results and experimental measurements was done and is included at the end of this chapter.

Case 2 on the other hand, simulated a higher wall and airflow temperature due to the higher solar intensity. The wall achieved a maximum value of 325K (52°C) while airflow reached peak value of 323K (50°C). The modification on top plate transparency has increased the airflow thermal quality by approximately 9°C.

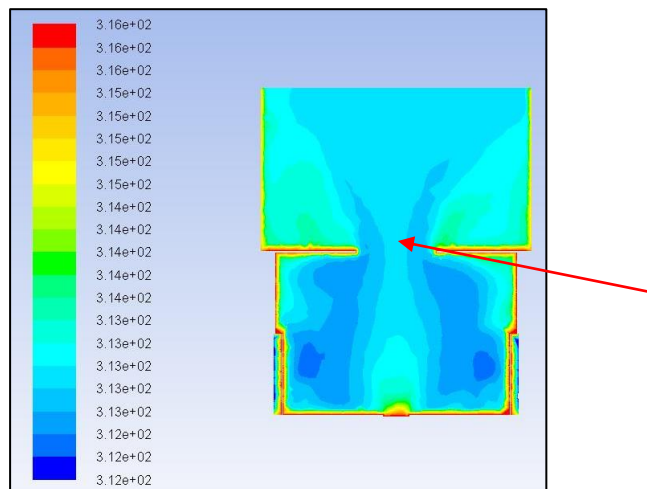


Figure 4. 7 – Case 1 Sectional Static Temperature Contour on (Aluminum)

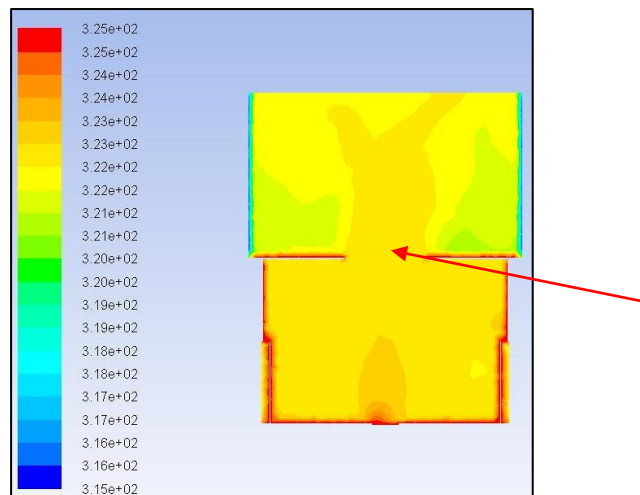


Figure 4. 8 – Case 2 Sectional Static Temperature Contour on (Perspex)

Velocity Magnitude Distribution

There are two methods in driving vertical airflow, namely (1) direct action of temperature in reducing air buoyancy which also known as natural convection and (2) application of vertical pressure gradient in creating a suction effect [29]. Increase in solar intensity led to a higher airflow temperature which then promote natural convection or solar updraft. A higher velocity was simulated on the side way (Green contour) in both cases due to the present of vortexes. A lower velocity of approximately 0m/s appeared at the center of flow field within the VEG. As shown in Figure 4.9, aluminum top plate prevent the penetration of solar radiation and thus a lower temperature and velocity was simulated in case 1. The maximum velocity achieved was 1.88m/s and an average outlet velocity of 1.32m/s was simulated at the top plate orifice. Case 2 in contrast simulated a higher velocity magnitude as penetrated solar intensity increased. Maximum velocity of 4.57m/s and average outlet velocity of 2.28m/s were achieved as shown in Figure 4.10. As conclusion, the solar radiation penetration did promoted better updraft and the velocity has been improved by 0.96m/s.

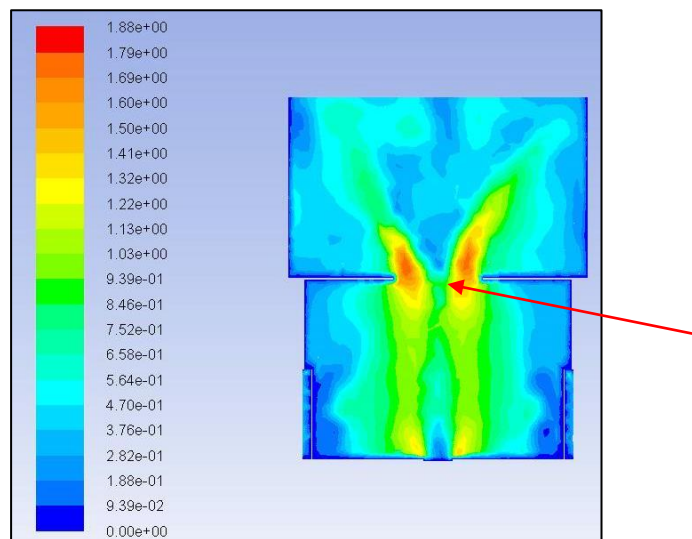


Figure 4. 9 – Case 1 Sectional Velocity Magnitude Contour (Aluminum)

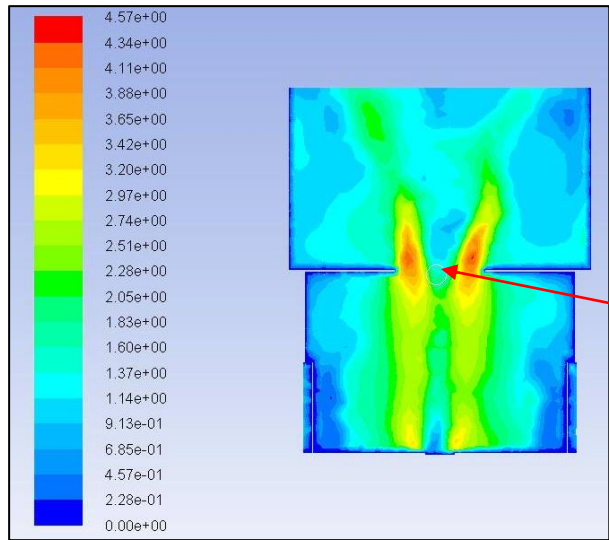


Figure 4. 10 – Case 2 Sectional Velocity magnitude Contour (Perspex)

Static Pressure Distribution

The application of solar intensity to raise airflow temperature led to a higher outlet volume flow rate and velocity. When the outlet flow rate increased, a low pressure domain was created within the Vortex Engine Generator (VEG), creating a stack effect to draw in air.

As shown in Figure 4.11 and 4.12, Case 1 with aluminum top plate was simulated with a higher interior pressure compare to case 2 with Perspex Top Plate. In creating a stack effect within the Vortex Engine Generator (VEG), a lower interior pressure distribution will be beneficial to draw in more air from Solar Collector (SC), increasing the inlet velocity.

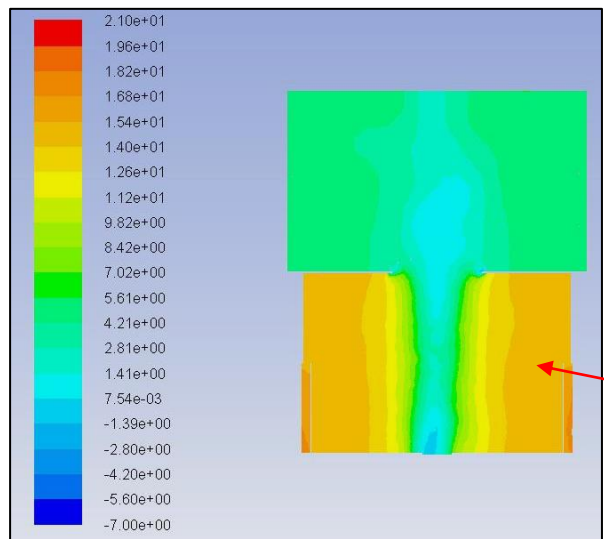


Figure 4. 11 – Case 1 Sectional Pressure Contour (Aluminum)

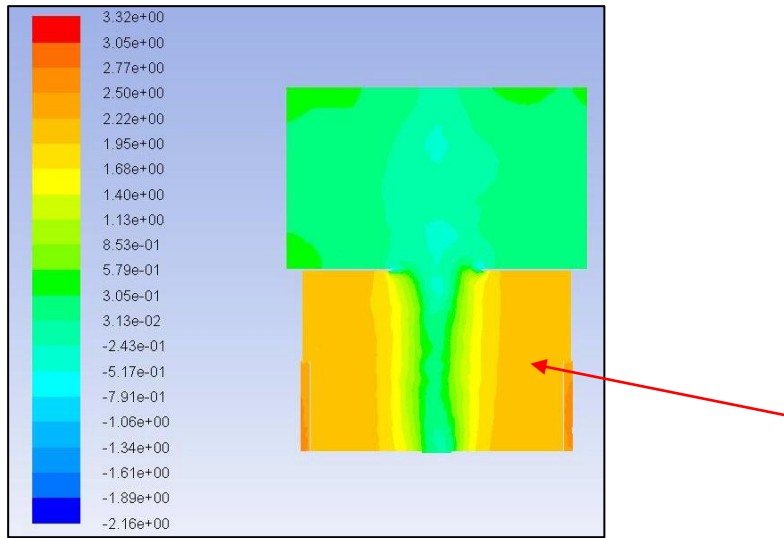


Figure 4.12 – Case 2 Sectional Pressure Contour (Perspex)

Tangential Velocity Analysis

A raise in outlet volume flow rate tended to create a stack effect within the VEG. In obey to the continuity equation or conservation of mass principle, the inlet flow rate has been improved. As guide vanes was installed to direct the airflow to artificially create vortexes, an increased in inlet mass flow rate indeed enhanced the tangential velocity within VEG.

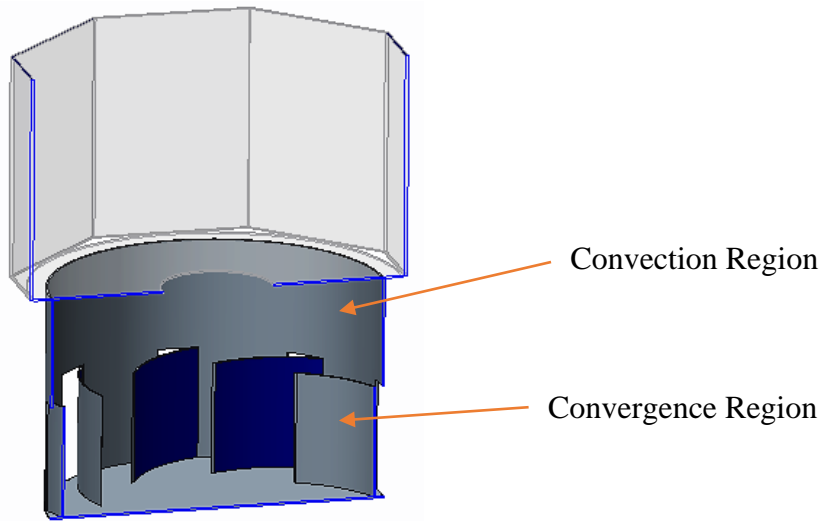


Figure 4.13 – Illustration on Vortex Engine Generator

The simulated vector of tangential velocity at both convergence and convection regions with Case 1 Aluminum Top plate are showed in Figure 4.14 and 4.15. A lower tangential velocity was simulated in case 1 where an aluminum top plate was applied, only 1.66m/s of maximum tangential velocity was achieved.

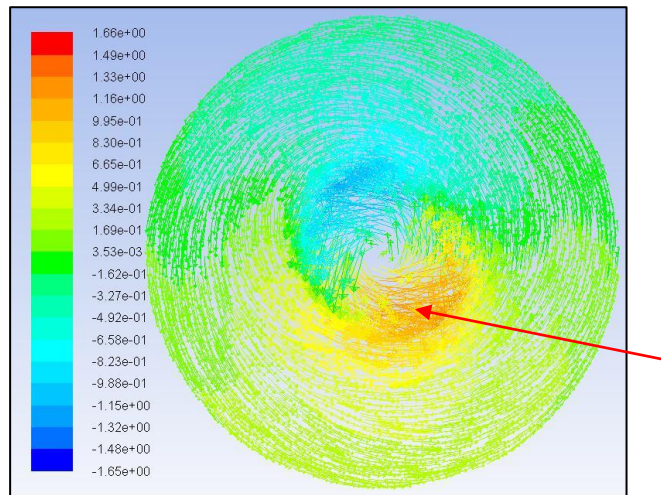


Figure 4. 14 – Case 1 Tangential Velocity at Convection Region (Aluminum)

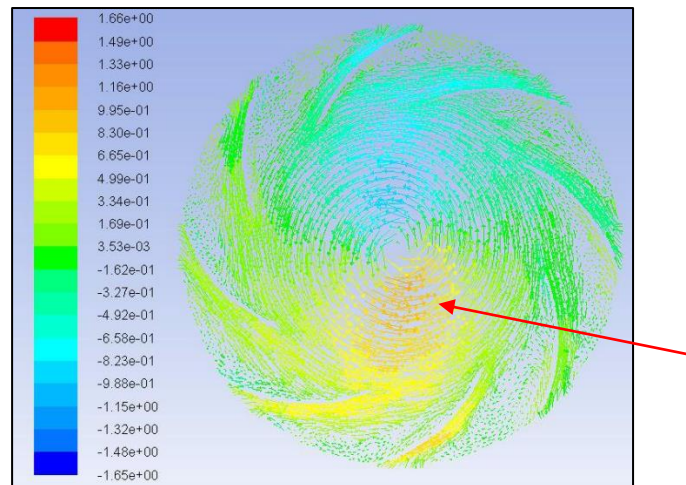


Figure 4. 15 – Case 1 Tangential Velocity at Convergence Region (Aluminum)

On the contrary, as shown in Figure 4.16 and 4.17, Case 2 attain a maximum tangential velocity of 3.90m/s on both convection and convergence regions. As conclusion, the tangential velocity was improved with the replacement of Perspex Top plate which allow the penetration of solar radiation to heat up the airflow within the Solar Vortex Engine Generator. The tangential velocity has been improved by 31.74%.

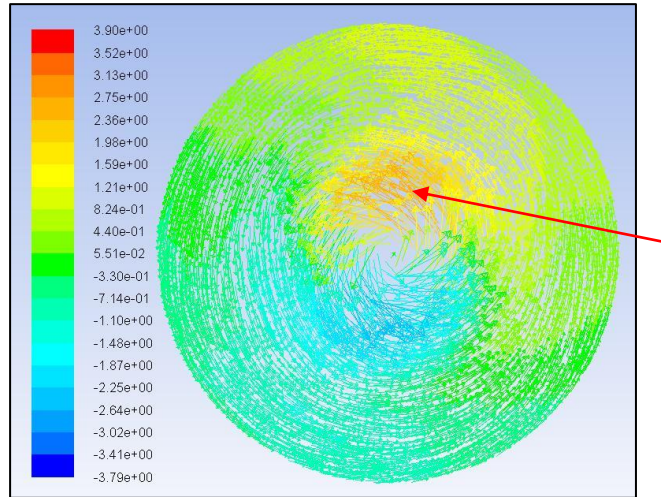


Figure 4. 16 – Case 2 Tangential Velocity at Convection Region (Perspex)

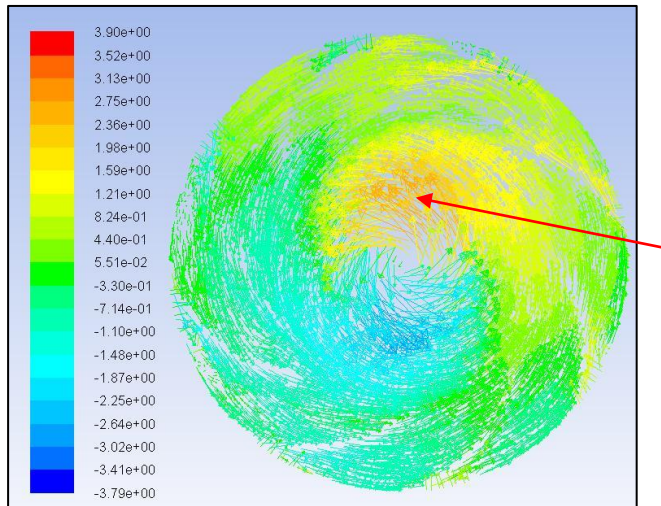


Figure 4. 17 – Case 2 Tangential Velocity at Convergence Region (Perspex)

Vorticity Magnitude

Vorticity is directly proportional to the tangential velocity. Increase in tangential velocity led to a higher vorticity. As shown in Figure 4.18, case 1 with aluminum configuration was simulated with maximum vorticity of 304/s and 0.672/s in most of the interior atmosphere (dark blue region). On the other hand, maximum vorticity increased by 181% in case 2, achieving a value of 855/s. As shown in Figure 4.19, on average, a higher vorticity of 2.07/s was simulated in case 2 compare to case 1.

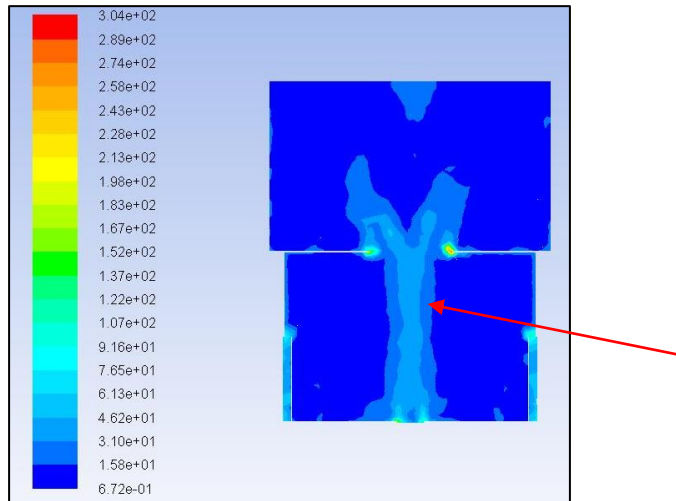


Figure 4. 18 – Case 1 Sectional Vorticity Contour (Aluminum)

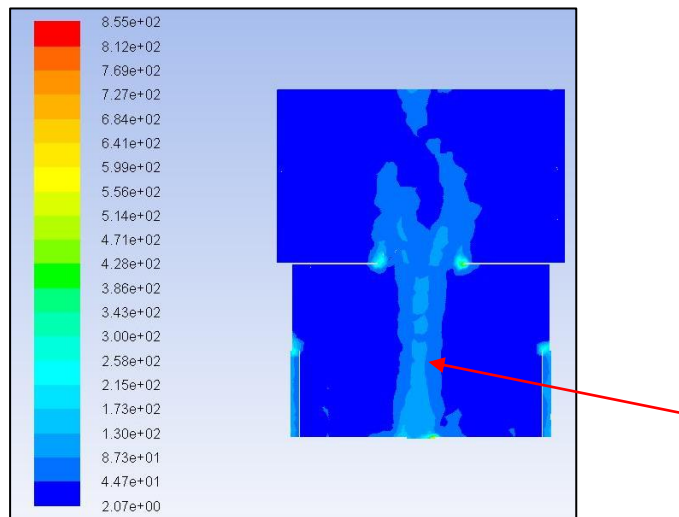


Figure 4. 19 – Case 2 Sectional Vorticity Contour (Perspex)

In summary, the top plate material replacement from opaque Aluminum to transparent Perspex has been numerically proved on its worthiness. The contribution of the top plate has been evaluated and all-round improvement has been observed from the simulations. The temperature distribution, velocity magnitude and pressure have been improved due to a lift on penetrated solar intensity.

4.2.3 Numerical Investigation on Top Plate Opening Diameter

Numerical simulation has been conducted to determine the optimum opening diameter or the inner diameter, D_i of the top plate that will increase engine performance without compromising the solar updraft and artificially created vortices. Small opening diameter

will tend to drag down vertical updraft velocity and create air-cornering underneath while large diameter will reduce top plate area that expose to solar radiation, decreasing efficiency. 3 opening diameter, namely 0.3m, 0.5m, 0.7m, and 0.9m (no top plate) were simulated before experimental fabrication for verification. The airflow updraft velocity magnitude is the prioritized parameter. The opening diameter which provide the highest velocity magnitude will be selected for experimental fabrication.

Static Temperature Distribution

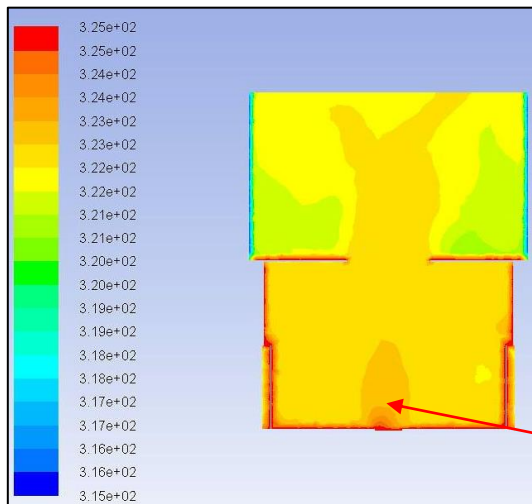


Figure 4. 20 – Sectional Temperature Contour at Perspex opening diameter 0.3m

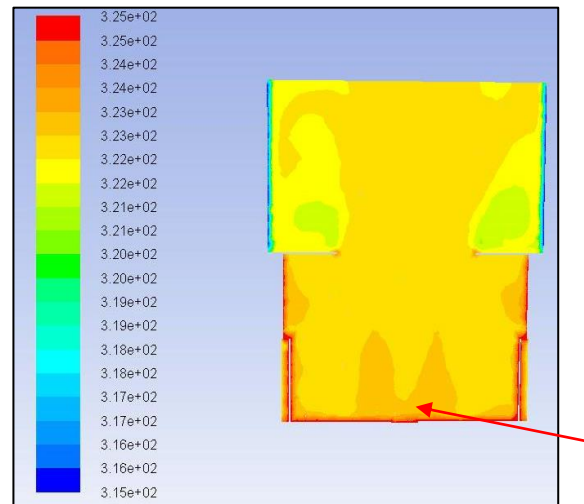


Figure 4. 21 – Sectional Temperature Contour at Perspex opening diameter 0.5m

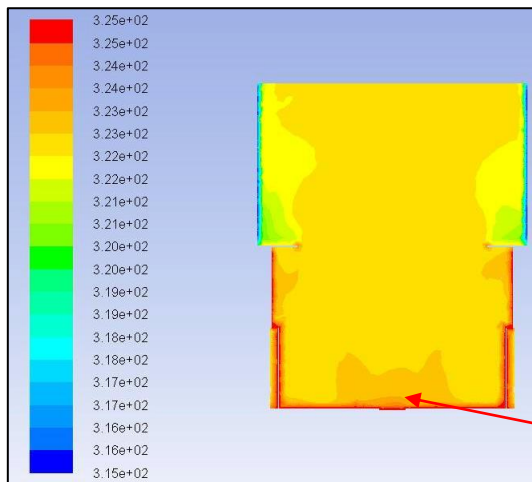


Figure 4. 22 – Sectional Temperature Contour at Perspex opening diameter 0.7m

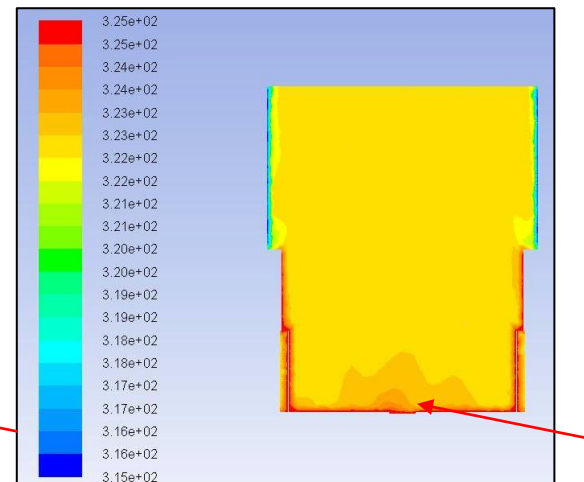


Figure 4. 23 – Sectional Temperature Contour at Perspex opening diameter 0.9m

From the simulations, as shown in Figure 4.20, 4.21, 4.22 and 4.23, the orange region with temperature of 324K (51°C) increased in area when the top plate opening diameter increased. Although the volume flow rate has been improved with opening diameter, a lower interior airflow temperature was simulated. As shown in simulation, the concentrated high temperature region at the base center (dark orange region) started to disperse and slowly decreased when the top plate opening diameter was increased.

Velocity Magnitude

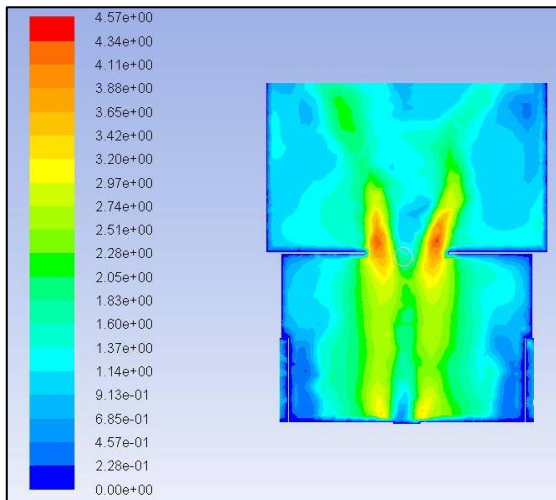


Figure 4.24 – Sectional Velocity Contour at Perspex opening diameter 0.3m

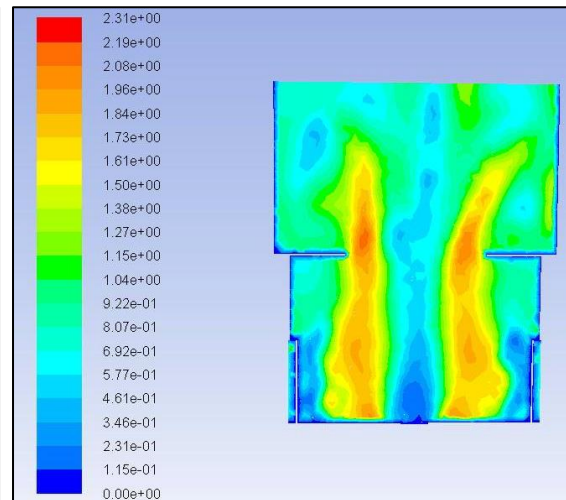


Figure 4.25 – Sectional Velocity Contour at Perspex opening diameter 0.5m

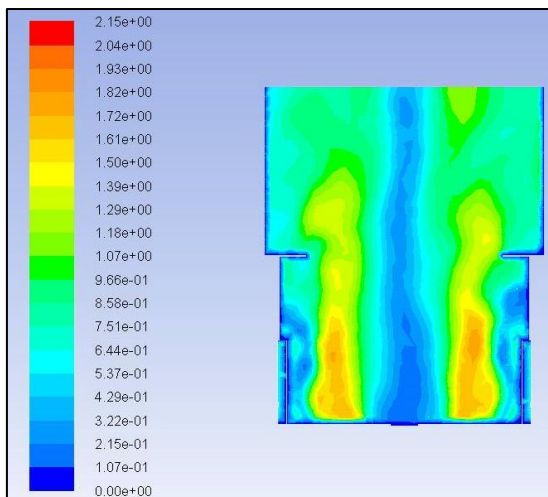


Figure 4.26 – Sectional Velocity Contour at Perspex opening diameter 0.7m

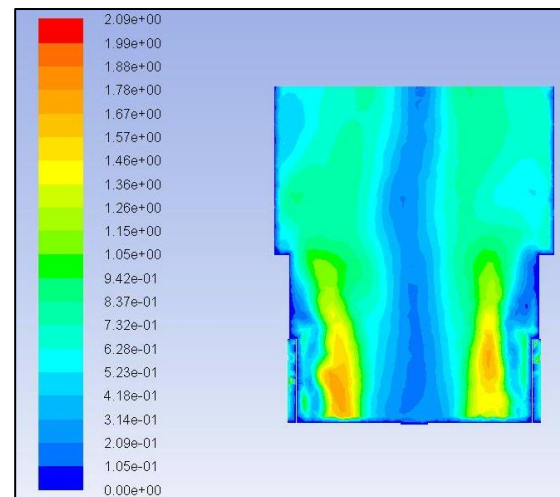


Figure 4.27 – Sectional Velocity Contour at Perspex opening diameter 0.9m

Volume flow rate is directly proportional to both flow area and flow velocity. Increase in opening diameter tends to increase flow area, leading to a larger volume flow rate. Besides,

increase in opening diameter allowed a better vortex to be artificially simulated. A complete tornado flow field was simulated in opening diameter of 0.9m where the top plate was removed. However, increase in opening diameter led to a lower airflow velocity magnitude. As shown in figure 4.24, 4.25, 4.26 and 4.27, the maximum velocity started to decrease with opening diameter. As the solar updraft is the top priority in the modification, the opening diameter of 0.3m was selected as the optimum top plate.

4.2.4 Numerical Investigation on Slanting Angle for Canopy Shaped Top Plate

Static Temperature Distribution

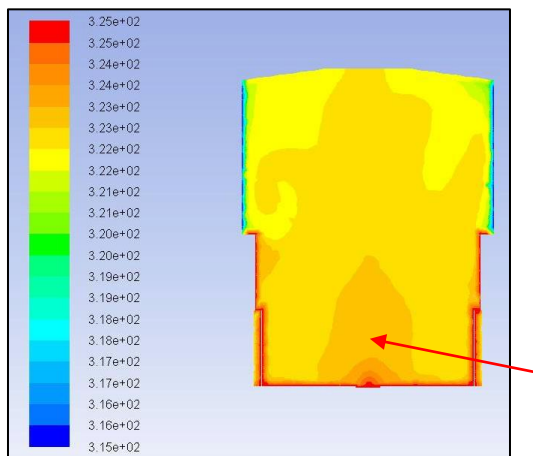


Figure 4. 28 – Sectional Temperature Contour at Perspex 8.53° slanting angle

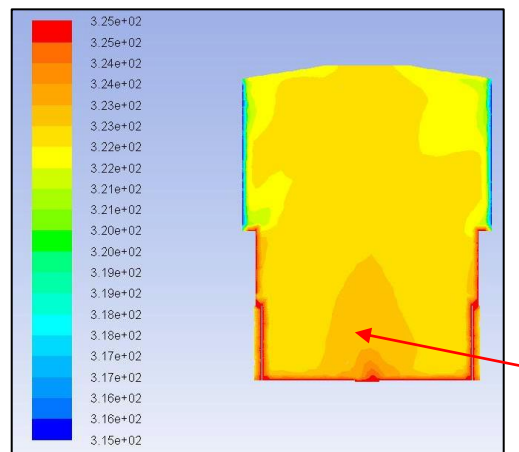


Figure 4. 29 - Sectional Temperature Contour at Perspex 10° slanting angle

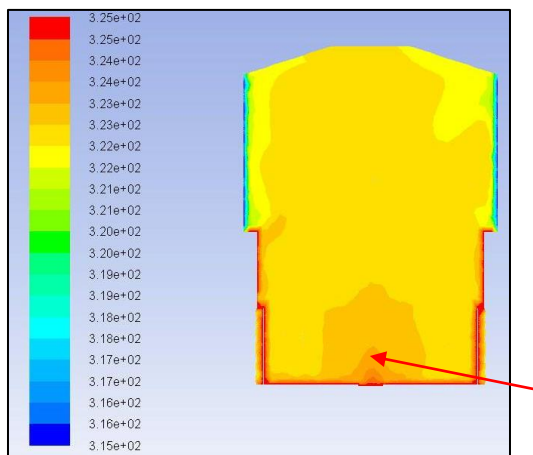


Figure 4. 30 - Sectional Temperature Contour at Perspex 20° slanting angle

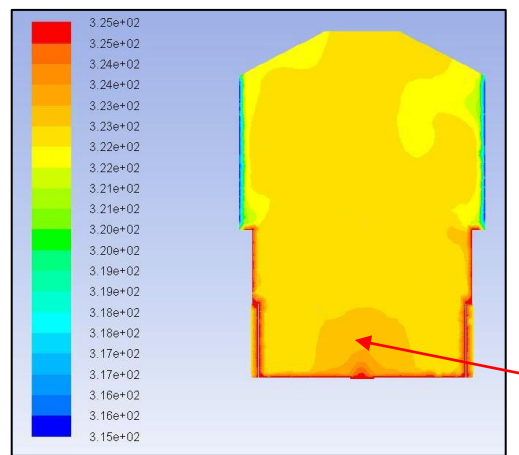


Figure 4. 31 - Sectional Temperature Contour at Perspex 30° slanting angle

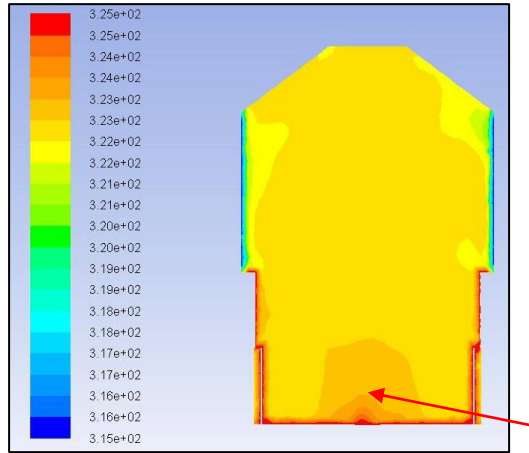


Figure 4.32 - Sectional Temperature Contour at Perspex 40° slanting angle

Velocity Magnitude

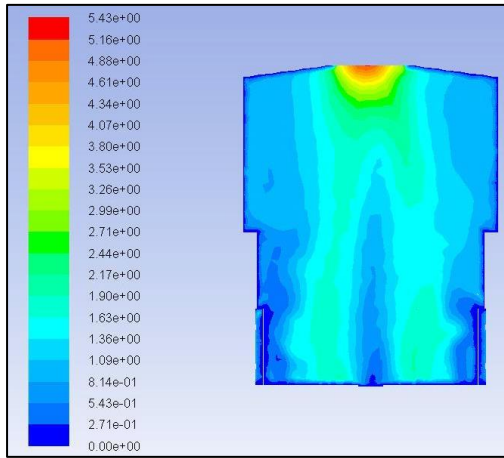


Figure 4.33 – Sectional Velocity Contour at 8.53° slanting angle

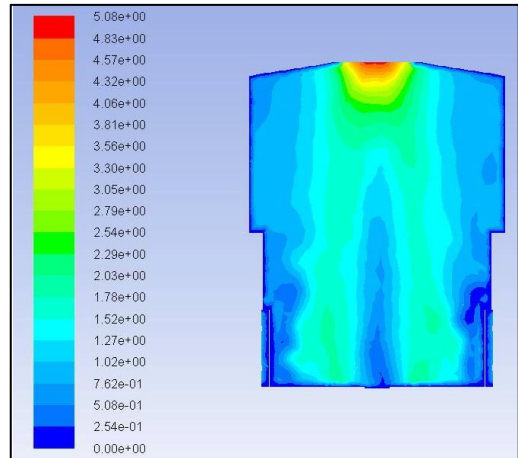


Figure 4.34 - Sectional Velocity Contour at 10° slanting angle

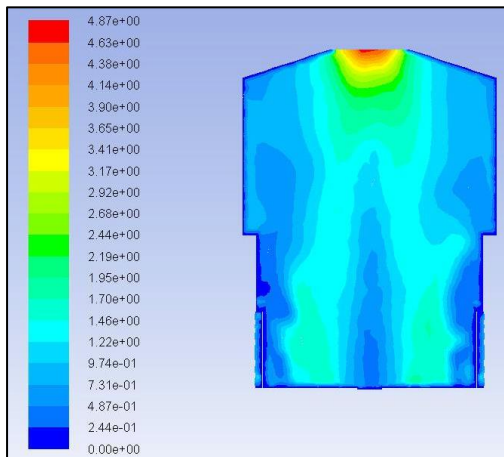


Figure 4.35 - Sectional Velocity Contour at 20° slanting angle

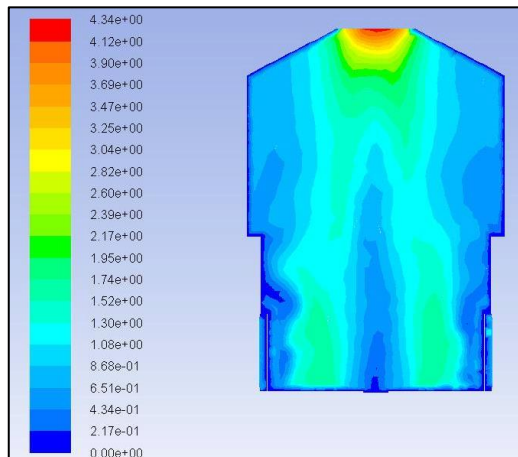


Figure 4.36 - Sectional Velocity Contour at 30° slanting angle

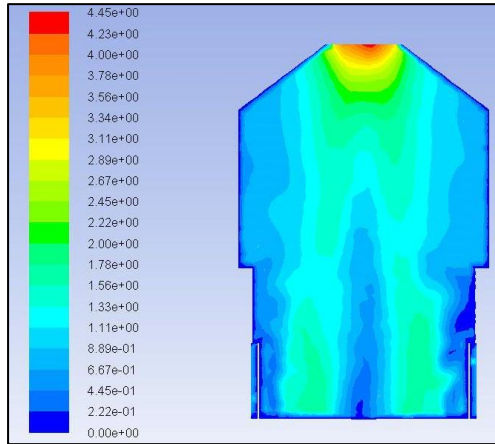


Figure 4. 37 - Sectional Velocity Contour at 40° slanting angle

The canopy shaped top plate was simulated at various angle starting from the reference angle of 8.53° which was obtained from the Solar Collector (SC) of in-situ SVE prototype. Further increment on slanting angle to 10°, 20°, 30° and 40° were simulated and the results are showed in above. As shown in Figure 4.28 to 4.32, the increment on slanting angle did not caused any major effect on the airflow temperature. However, the efficiency of the top plate in providing solar radiation reduced with slanting angle. A decreasing trend was observed at the base center region where the area of dark orange region with 325K (52°C) reduced with top plate slanting angle.

The top plate slanting angle has vast effect on the airflow velocity magnitude. Moving from 8.53° to 40°, the maximum velocity achieved at the outlet was in a decreasing trend. The maximum velocity simulated for various angle are plotted in Figure 4.38. The slanting angle of 8.53° was selected as the optimum slope for Perspex Top Plate (TP).

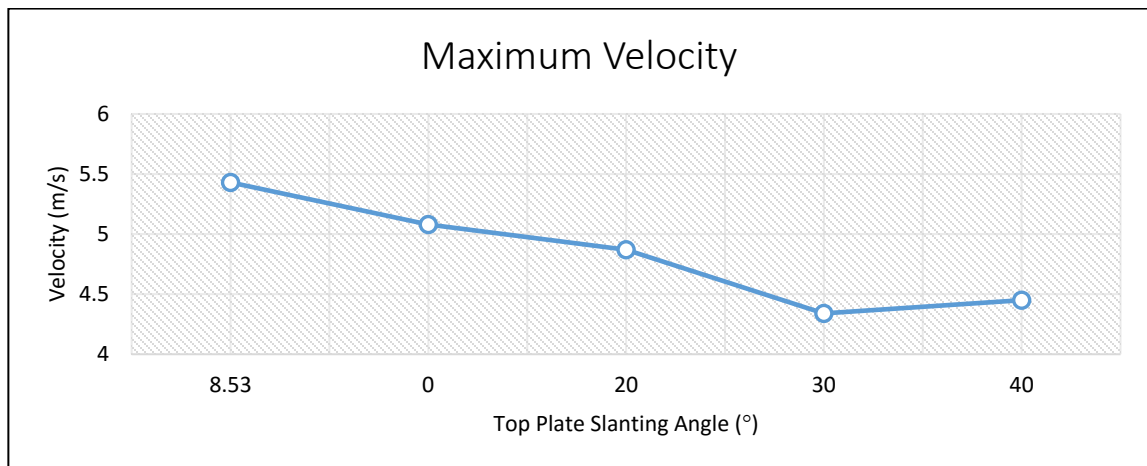


Figure 4. 38 – Maximum Velocity Simulated on Various Top Plate Slanting Angle

4.3 Experimental Results

4.3.1 Solar Collector

The Solar Collector (SC) apply solar radiation to create a greenhouse effect in order to heat up the air underneath and spark-on the operation of Solar Vortex Engine (SVE). Thus, experimental measurements mainly focused on the temperature distribution and solar intensity direct to the Solar Collector (SC). A total of 9 Thermocouples have been installed to investigate on temperature distribution within Solar Collector (SC). Sensors' positioning is as shown under section 3.5.3. Each experiments were conducted for a duration of 4 days to obtain the average data. The measurements obtained were then analyzed and attached as below.

Solar Intensity

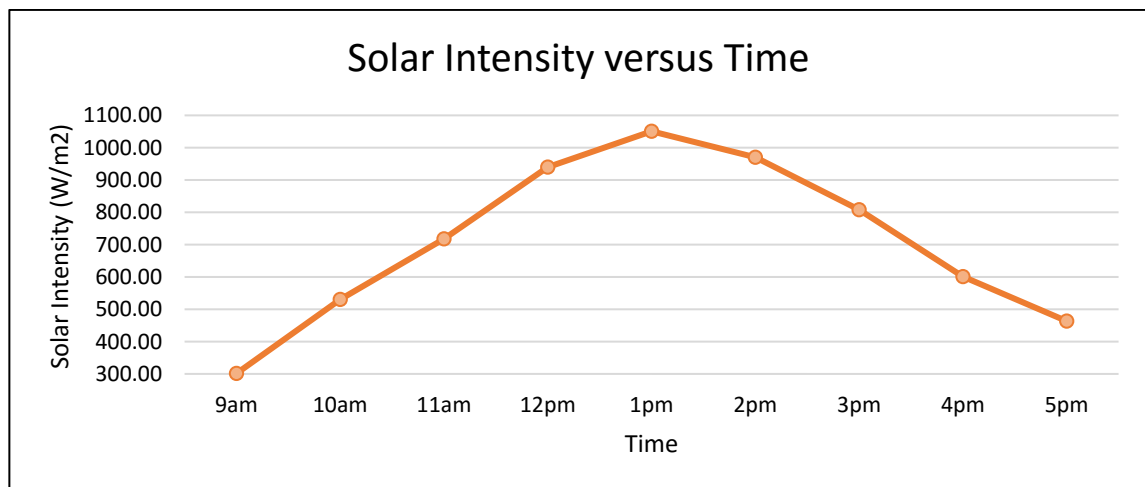


Figure 4. 39 – Solar Intensity against Time

Figure 4.39 shows the solar intensity directed to the solar collector in a day. The plot was constructed based on the average value obtained from 8 days of experiment. The solar intensity increased in the morning and decreased after 1pm. The peak solar intensity recorded was $1050.75W/m^2$.

Temperature

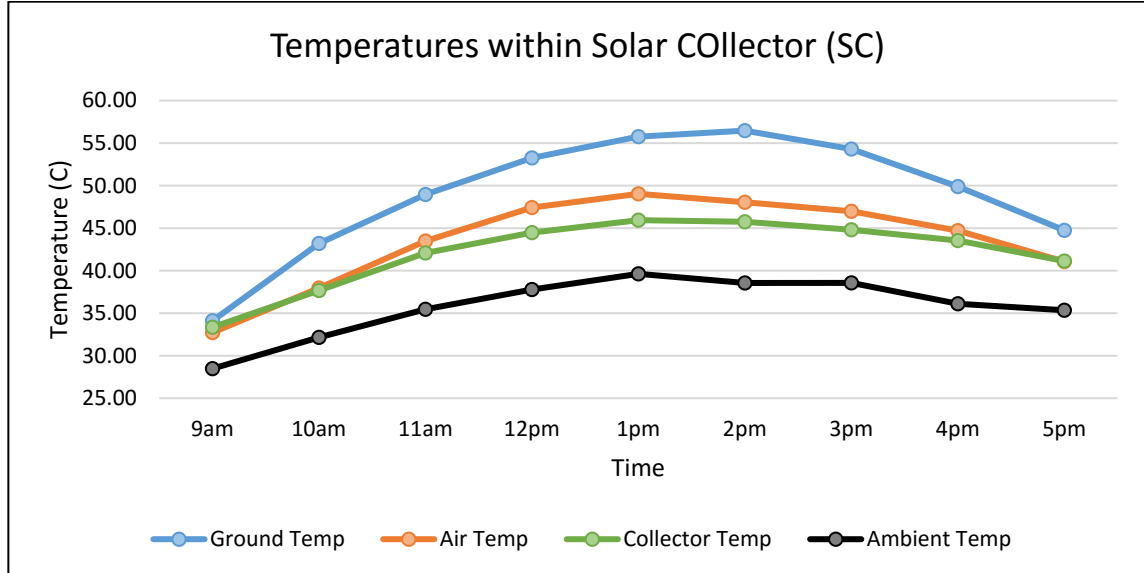


Figure 4. 40 – Temperatures within Solar Collector (SC)

As shown in Figure 4.40, the ambient temperature was increasing proportionally with the solar intensity at the beginning of experiment and decreases afterward. A maximum value of approximately 40°C was achieved at 1pm when the solar intensity peaked. The same trend was observed on the ground temperature, airflow temperature and collector temperature. The ground achieved the highest temperature compare to air and collector as the newly installed Pebble Stones were painted in black to create a blackbody effect. The painted Pebble stones tend to have a higher absorptivity than collector and airflow. The thermal energy stored within the Pebble Stones allowed the ground structure to achieved peak value at 2pm even solar intensity started to reduce after 1pm.

The collector has a higher temperature than the air at 9am due to the low solar intensity. The air was not heat compare to the collector and ground. However, the air temperature surpass the collector temperature at 10am when the solar intensity increased.

As conclusion, temperatures within the solar collector (ground, airflow and collector) was directly proportional to the solar intensity. The higher the solar radiation, a higher airflow temperature was obtained and supplied to the Solar Vortex Engine (SVE).

4.3.2 Vortex Engine Generator

The Perspex Top Plate (TP) was proposed and installed with the aims to improve solar updraft and efficiency of the Solar Vortex Engine (SVE). The contribution of top plate in enhancing the performance of Solar Vortex Engine (SVE) was evaluated by experimental investigation and the results were plotted in this section.

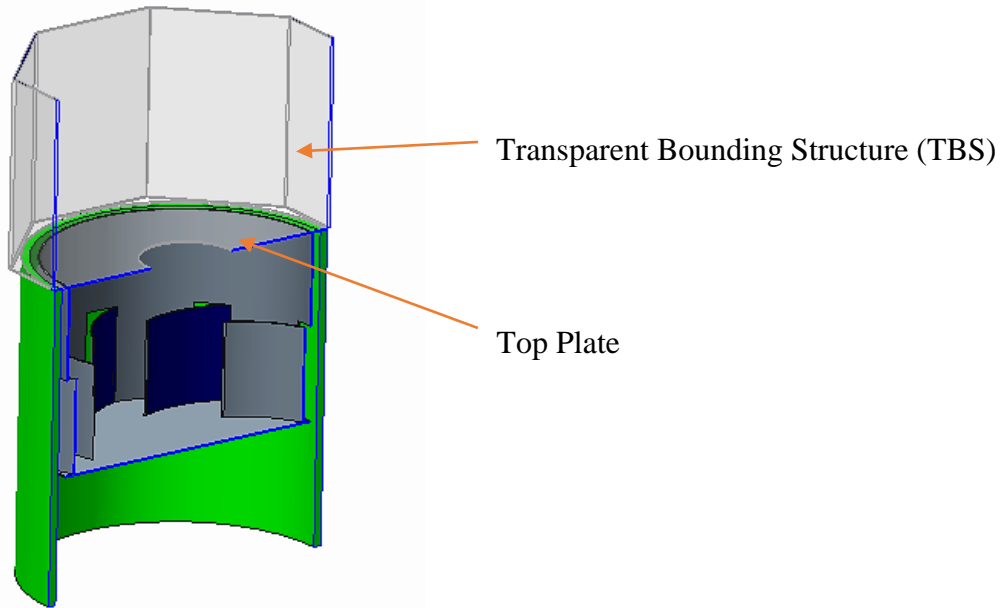


Figure 4. 41 – Illustration on VEG Top Plate and TBS

Solar Intensity

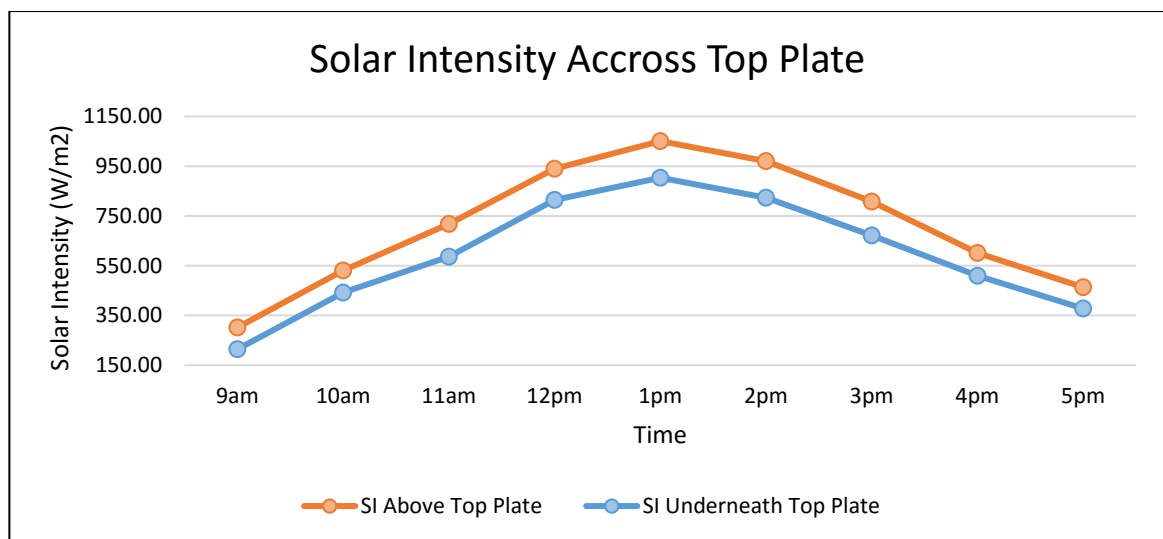


Figure 4. 42 – Solar Intensity against Time

As shown in Figure 4.42, solar intensity recorded approximately $300W/m^3$ at the start of experiment at 9am in the morning and keep increasing till the peak hour at 1pm. A maximum solar incidence of $1050W/m^3$ was recorded above the Solar Collector while $903W/m^3$ was recorded after the filtration by transparent Perspex Solar Collector (SC). 86% of solar intensity was allowed to penetrate, reaching the VEG interior atmosphere. Solar intensity tends to reduce after 1pm and reached approximately $460W/m^3$ at the end of experiment on 5pm.

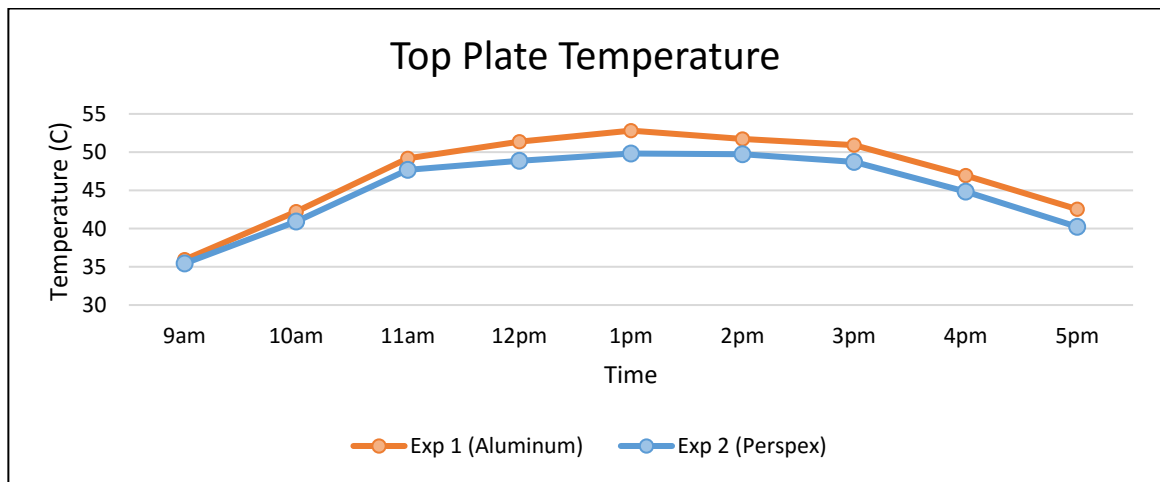


Figure 4. 43 – Measured Top Plate Temperature against Time

As shown in figure 4.43, as Aluminum material has a higher thermal conductivity compare to Perspex, a higher surface temperature was recorded on the aluminum top plate. The aluminum top plate temperature increased with the solar intensity till a peak value of approximately $53^{\circ}C$ was achieved. On the contrary, lower surface temperature was recorded on Perspex top plate due to the low thermal conductivity. However, the Perspex top plate did allowed a higher solar intensity to penetrate and warm the interior atmosphere of Vortex Engine Generator (VEG). This is where the solar heat gain is applicable.

Solar heat gain is defined as the temperature increment in physical object, space or structure results from solar radiation, while Solar Heat Gain Coefficient (SHGC) is defined as “the ratio of the solar heat gain entering the space through the fenestration product to the incident solar radiation.” Solar heat gain included directly transmitted solar heat and absorbed solar radiation which is then reradiated, conducted or converted into the space. Although the Aluminum material owns a higher thermal conductivity, the

Perspex possess a higher Solar Heat Gain Coefficient (SHGC) which allows high percentage of Solar Incident to penetrate, reaching the interior airflow and inner wall to create the greenhouse effect within the Vortex Engine Generator (VEG). Higher reflectivity and shading coefficient of aluminum tends to reflect and block most of the solar radiation.

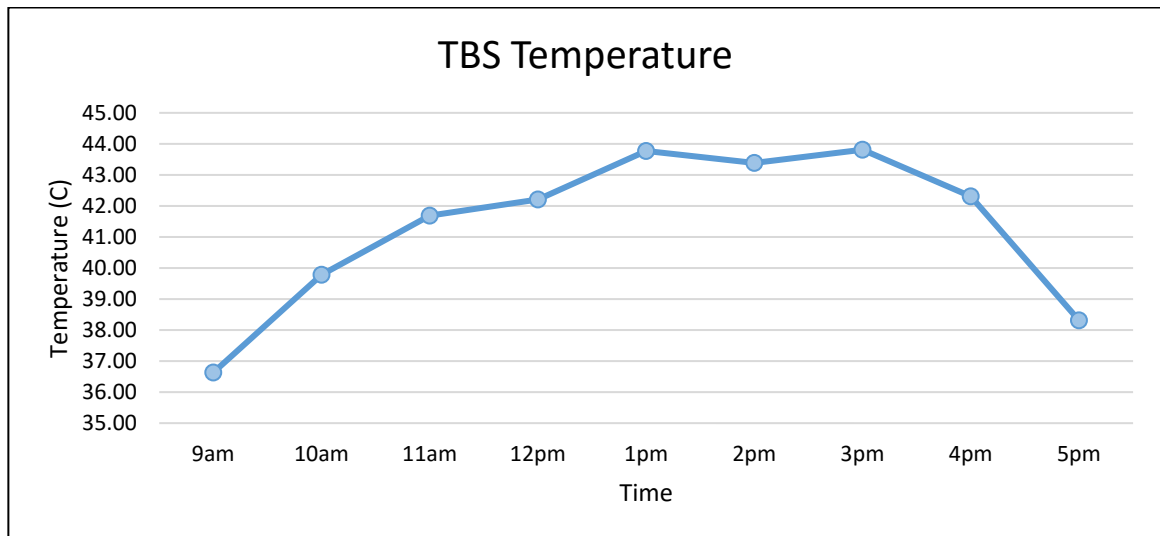


Figure 4. 44 – Temperature of Transparent Bounding Structure (TBS) against Time

Figure 4.44 were plotted based on measured temperature behavior on Perspex TBS surface in both experiments. Type J Thermocouples have been applied and stick closely to the surface for measurements. Automatic data recording was applied with Graphtec Data-logger GL280 for temperature measurements on 5 minutes interval. The data was recorded with the aim to verify on simulation boundary conditions. A peak value of 44°C was recorded on Transparent Bounding Structure (TBS). The experimental results were in match with boundary condition where the temperature entered into the simulation setup was 315K (42°C).

Temperature

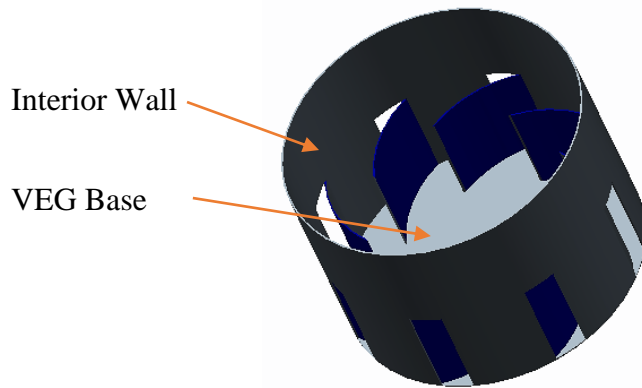


Figure 4. 45 – Illustration on VEG Interior Wall and Base

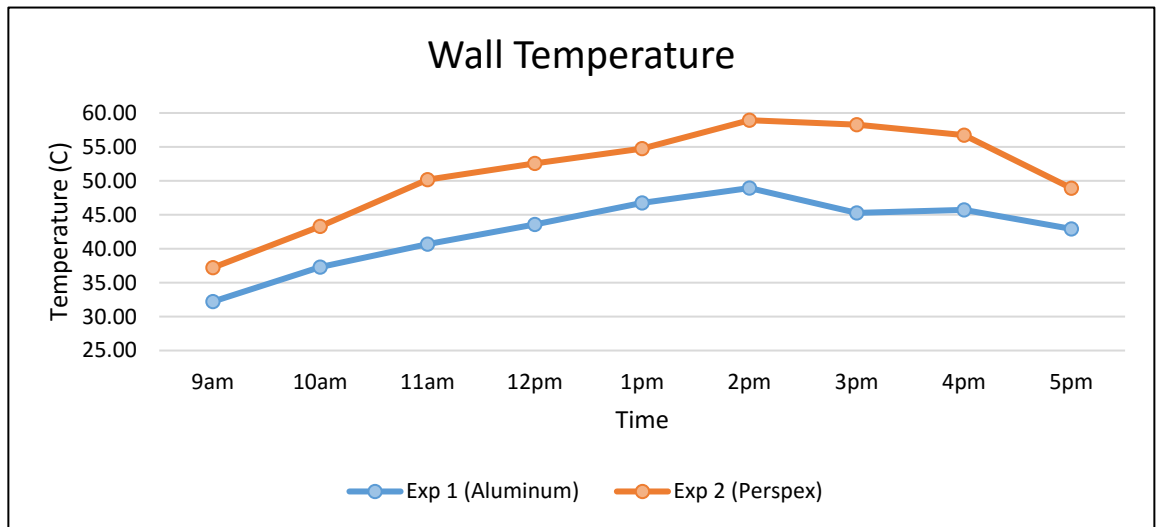


Figure 4. 46 – Interior Wall Temperature of VEG against Time

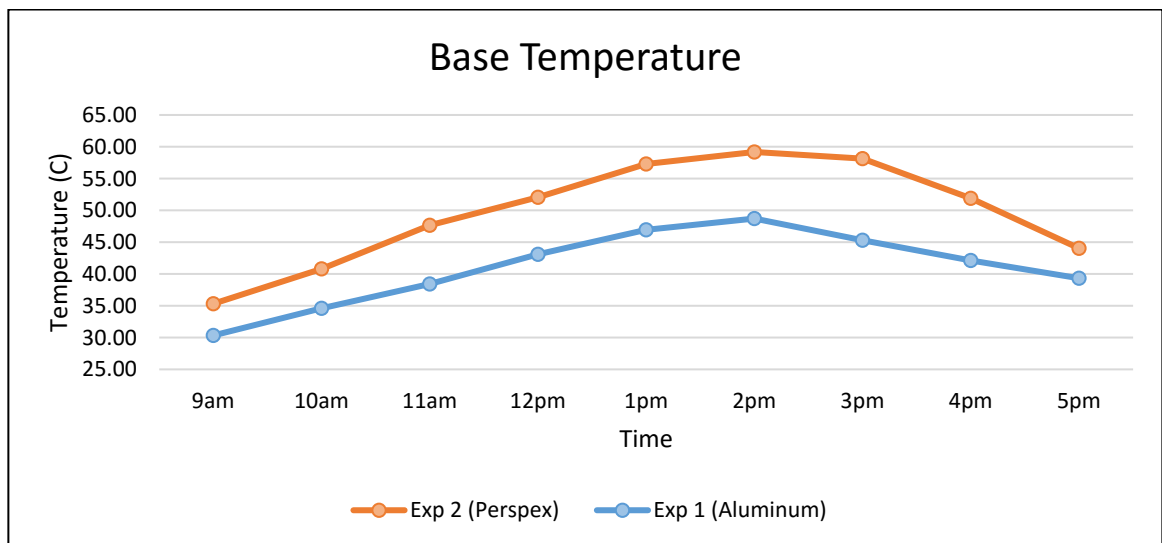


Figure 4. 47 – Measured Base Temperature for VEG against Time

Base on figure 4.42, Perspex Top Plate (TP) only filter approximately $100W/m^2$ of Solar Radiation, which allow $903W/m^2$ of Solar Radiation to pass through top plate, reaching the inner wall and base of Vortex Engine Generator (VEG). Thus, higher wall and base temperatures were recorded in figure 4.46 and figure 4.47. Due to the change in solar intensity during the day, the wall and base temperature vary accordingly. With Perspex Top Plate (TP), a higher interior component temperature was registered. A peak wall temperature of $58.94^{\circ}C$ was obtained at 2pm while a peak base temperature of $59.17^{\circ}C$ was obtained at 2pm with the Perspex Top Plate (TP) installed. Maximum wall temperature of only $48.94^{\circ}C$ and base temperature of $48.70^{\circ}C$ were obtained at 2pm with Aluminum Top Plate (TP). The worthiness of top plate transparency modification was once again proved.

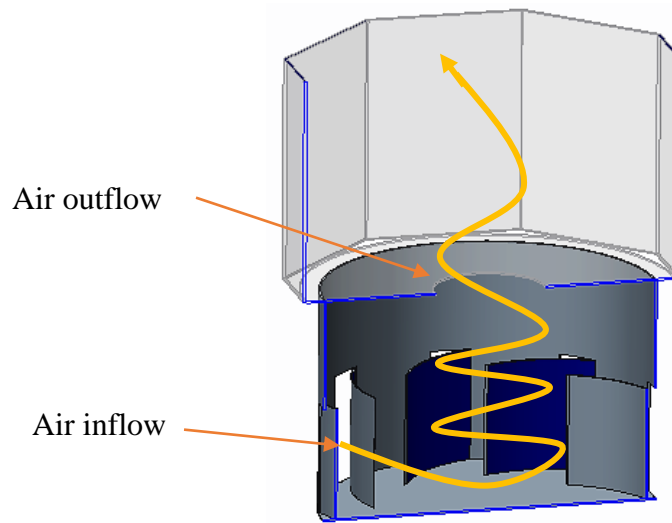


Figure 4. 48 – Illustration on VEG inflow and outflow

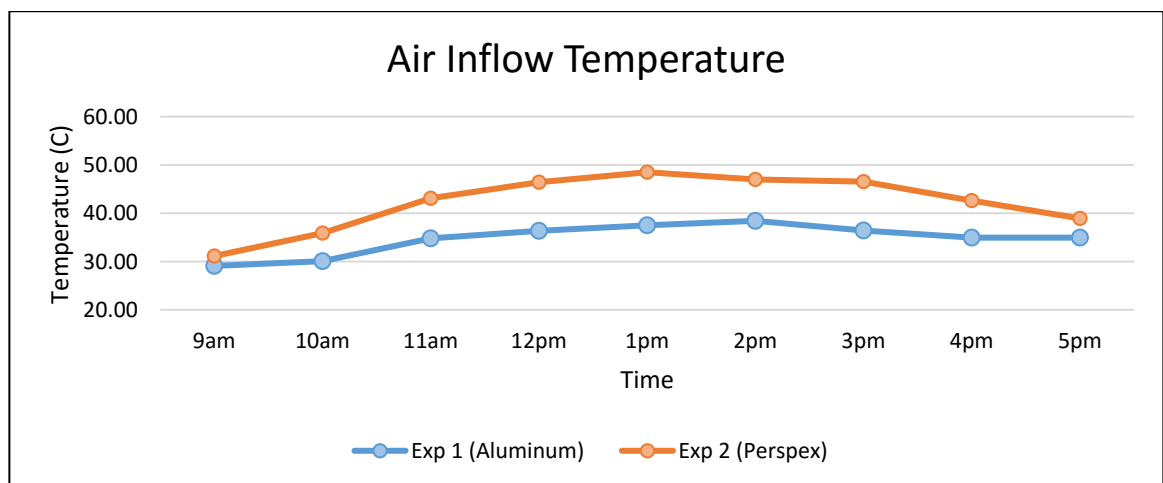


Figure 4. 49 – Measured Transient Behavior of Air Inflow Temperature

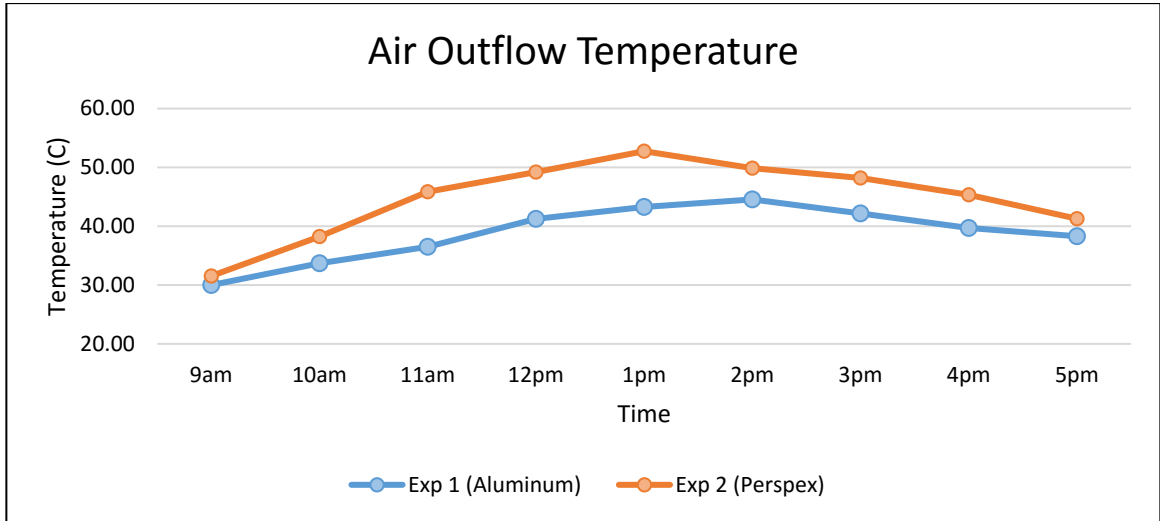


Figure 4. 50 – Measured Transient Behavior of Air Outflow Temperature

As shown in figure 4.49 and figure 4.50, the penetrated solar radiation was converted to useful heat energy which as well improved the air inflow and outflow temperature. Experiment 2 was conducted for a duration of 4 days with a Perspex Top Plate and airflow temperature recorded was higher compared to experiment 1 with Aluminum Top Plate. Experiment 1 with Aluminum achieved peak temperature of 38.43°C (inlet) and 44.55°C (outlet) at 2pm while Experiment 2 with Perspex tended to accelerate the heating effect and reached higher peak value of 48°C (inlet) and 52°C (outlet) at 1pm. The difference in air outflow temperature is 7.45°C.

Relative Humidity (RH%)

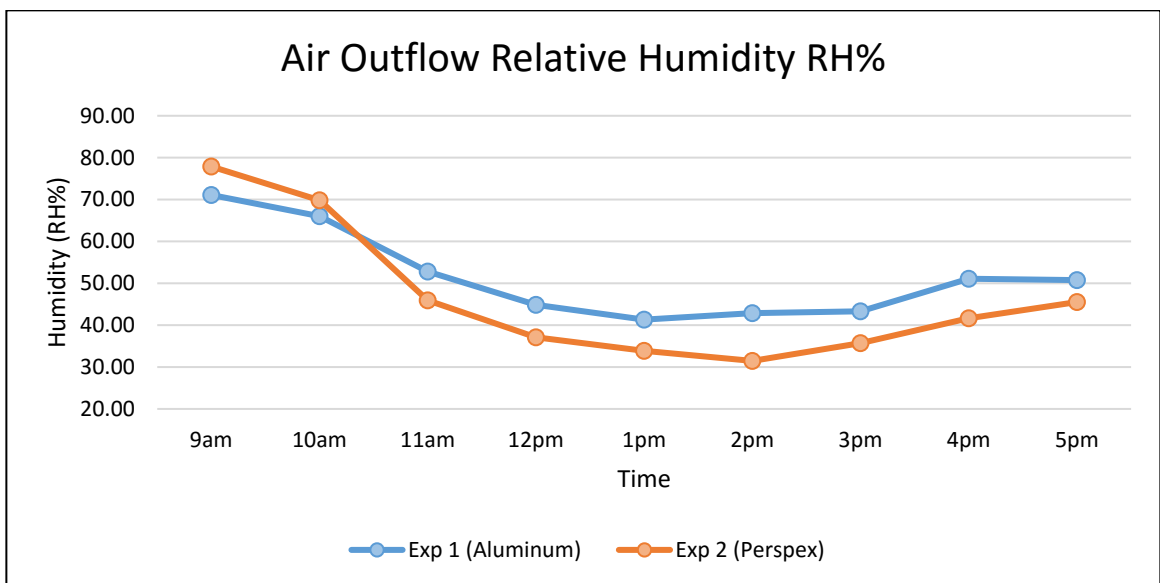


Figure 4. 51 – Air Outflow Humidity (RH %) against Time

Relative humidity is defined as the ratio (in percentage) of the actual amount of moisture content in the air to the maximum amount that can be present at that temperature. The dew point temperature is achieved if a given sample of air contain relative humidity of 100%. Relative humidity is affected by actual temperature and dew point temperature at a relationship of:

$$RH = 100 - 5(t - t_d) \quad [30]$$

When the “ t ” increases, relative humidity tends to decrease. This is because warm air can hold up more water vapor compare to cool air, thus relative humidity falls when temperature rises during peak hours with condition that no moisture is added to the air.

As shown in Figure 4.51, the replacement of Perspex Top Plate (TP) allows the penetration of solar radiation into the Vortex Engine Generator (VEG) which indeed raised the temperature of airflow and interior aluminum walls, a lower relative humidity of 31.48% was recorded in second experiment 2 compare to 42.88% in first experiment conducted with Aluminum Top Plate (TP). These prove the performance enhancement provided from the replacement of Perspex Top Plate (TP).

Velocity

The increment in airflow temperature have lowered the air buoyancy, which then enhanced the solar updraft. Higher value of velocities were recorded with the replacement of Perspex Top Plate (TP) in experiment 2. Due to the increased air inflow and outflow temperature, vast improvement in both inlet and outlet velocity was observed in figure 4.52 and figure 4.53. Both inlet and outlet airflow velocity have been recorded using the hotwire probe. Peak value of approximately 0.28m/s was recorded in experiment 1 (Aluminum) while the inlet air velocity reached peak value of 0.81m/s due to the increased amount of solar intensity in raising airflow temperature.

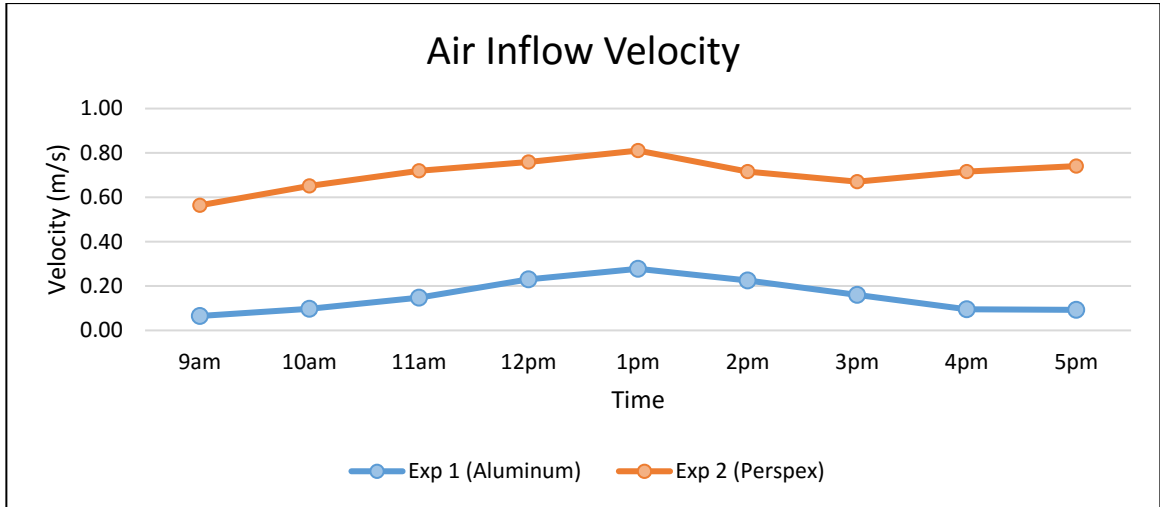


Figure 4. 52 – Measured Transient Behavior of Air Inflow Velocity

The same trend occurred on the outlet air velocity. The airflow velocity increased with solar intensity and tended to maintain the velocity after 1pm where the solar intensity started to reduce. The outlet velocity reached peak value of 2.11m/s at 2pm in Experiment 2 (Perspex) which was an hour delay compare to inlet velocity. The maximum recorded velocity in experiment 1 (Aluminum) was only 1.45m/s. Thus, the replacement of a transparent Perspex Top Plate (TP) did proved its worthiness in improving engine performance and enhance flow field within the Solar Vortex Engine (SVE). Figure 4.53 shows the outlet velocity for both experiments.

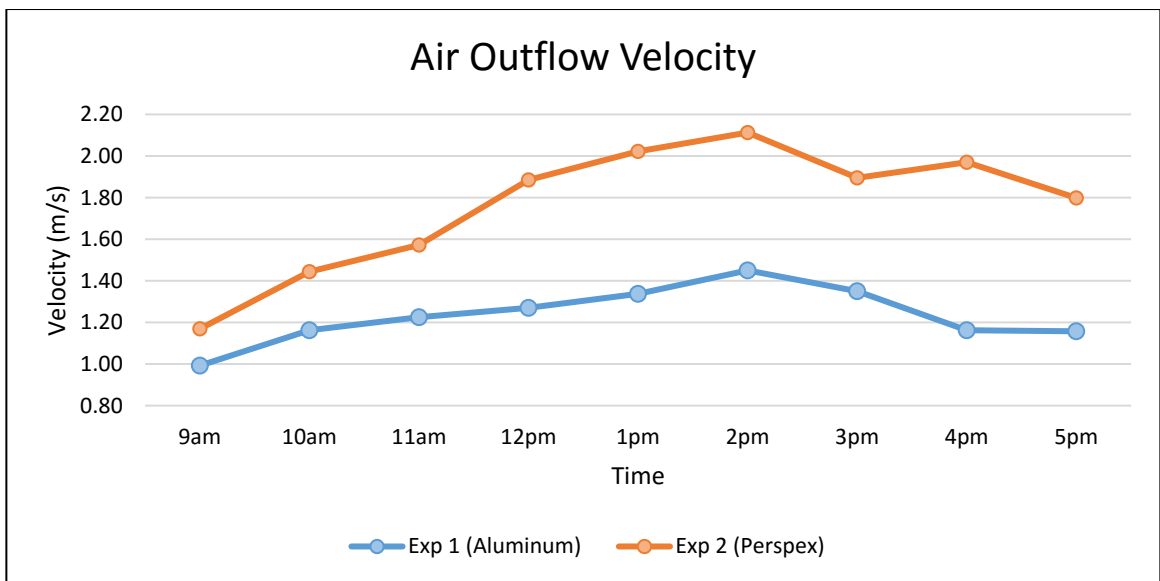


Figure 4. 53 - Measured Transient Behavior of Air Outflow Velocity

Figure 4.54 shows the percentage of enhancement on the outlet velocity between experiment 1 (Aluminum) and experiment 2 (Perspex). The highest percentage of enhancement (69%) occurred at 4pm where the outlet velocity decreased in experiment 1 (Aluminum) while outlet velocity in experiment 2 (Perspex) tended to maintain at approximately 2m/s.

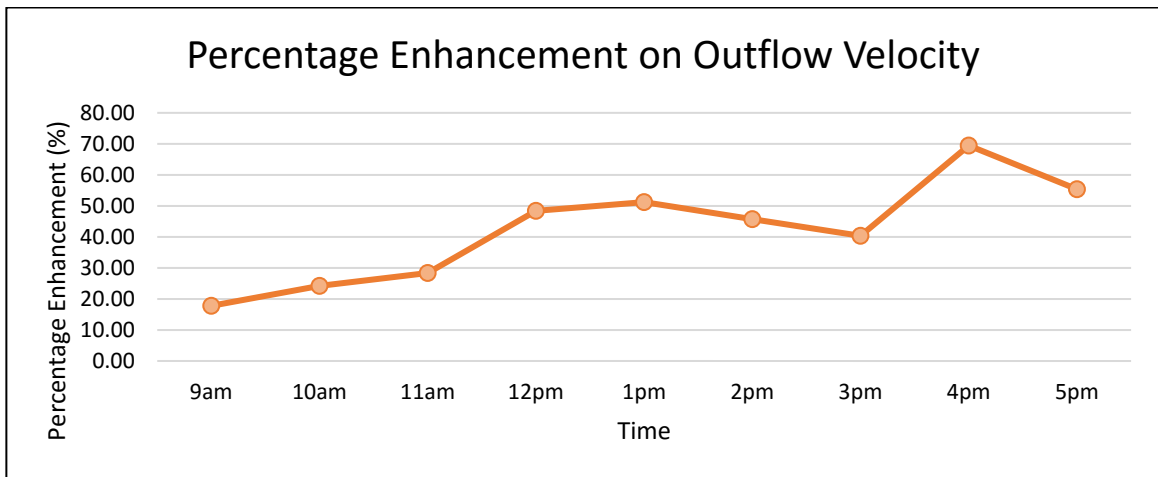


Figure 4. 54 – Percentage Enhancement in Outflow Velocity against Time

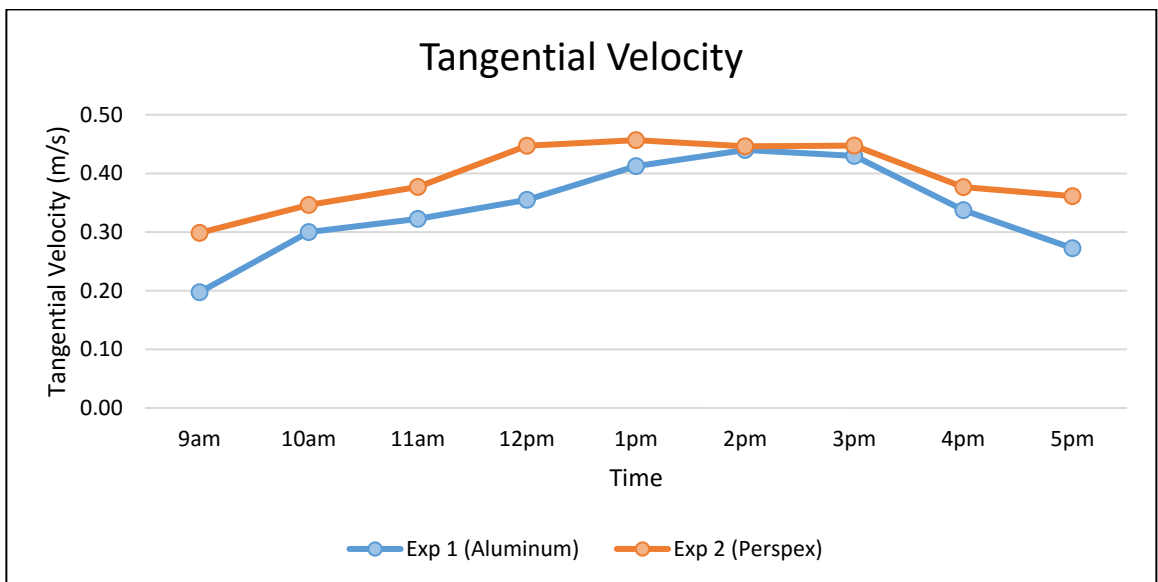


Figure 4. 55 – Measured Transient Behavior of Tangential Velocity against Time

The solar radiation did not just enhanced the solar updraft, but as well improve the tangential velocity of airflow within the Vortex Engine Generator (VEG). A peak value of 0.44m/s was achieved at 2pm in experiment 1 (Aluminum) while 0.46m/s was achieved at 1pm in experiment 2 (Perspex).

Volume Flow Rate

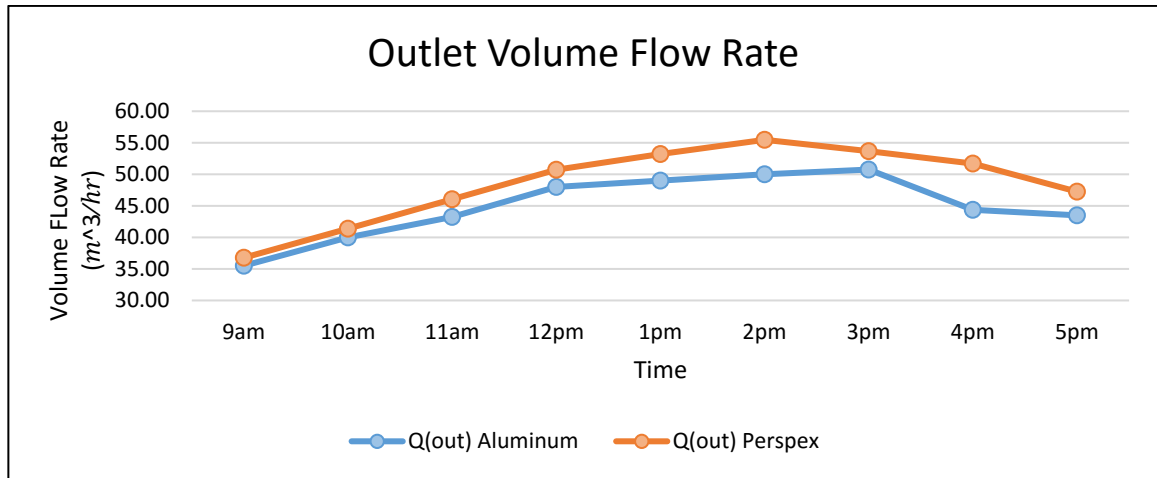


Figure 4. 56 – Measured Outlet Volume Flow rate against Time

The outlet velocity is proportional to the outlet volume flow rate. Outlet volume flow rate in unit of m^3/hr increased when temperature and velocity of outlet airflow increased. With transparent Perspex, peak value of $55.48m^3/hr$ was recorded in experiment 2 at 2pm. Increasing the outlet volume flow rate will indeed raise the power generation performance of Solar Vortex Engine (SVE).

4.4 Summary

Both numerical simulations and experimental results for Vortex Engine Generator (VEG) have been presented and discussed in this chapter. Validation and verification on simulation boundary conditions and results have been done by experimental investigation and the percentage error for each parameter were listed as below. Comparisons between experiment 1 (Aluminum) and experiment 2 (Perspex) have been made as well to show on the worthiness in replacing the top plate.

Table 4. 2 – Comparison on Experimental Measurements bet. Aluminum and Perspex

	Maximum Experimental Measurements				
	Air Inlet Temperature	Air Outlet Temperature	Air Inlet Velocity	Air Outlet Velocity	Tangential Velocity
Experiment 1 (Aluminum)	38.43°C	44.55°C	0.28m/s	1.45m/s	0.44m/s
Experiment 2 (Perspex)	48.51°C	52.75°C	0.81m/s	2.11m/s	0.46m/s

Percentage Enhancement (%)	26.23%	18.41%	189%	45.52%	4.55%
----------------------------	--------	--------	------	--------	-------

Table 4. 3 – Verification and validation on Case 1 simulated results by experiment 1

	Air Inlet Temperature	Air Outlet Temperature	Air Inlet Velocity	Air Outlet Velocity	Tangential Velocity
Experiment 1 (Aluminum)	38.43°C	44.55°C	0.28m/s	1.45m/s	0.44m/s
Simulation Case 1	312 (39°C)	±314K (41°C)	0.3m/s	±1.32m/s	0.334m/s
Percentage Difference	1.48%	7.97%	7.14%	8.97%	24%

Table 4. 4 – Verification and Validation on Case 2 simulated results by experiment 2

	Air Inlet Temperature	Air Outlet Temperature	Air Inlet Velocity	Air Outlet Velocity	Tangential Velocity
Experiment 2 (Perspex)	48.51°C	52.75°C	0.81m/s	2.11m/s	0.46m/s
Simulation Case 2	322K (49°C)	±323K (50°C)	0.7m/s	±2.28m/s	±0.44m/s
Percentage Error	1.01%	5.21%	13.58%	8.05%	4.35%

In summary, the replacement of Perspex top plate did improved both the airflow temperature and velocity magnitude. The air outflow velocity from the top plate has been improved by 45% while temperature has been raised by 18%. At last, the maximum achieved experimental measurements were applied to verify on the simulated result. All the parameters have acceptable percentage error except the air inlet velocity into the Vortex Engine Generator (VEG) and the tangential velocity simulated in case 1 (Aluminum). The percentage error of inflow and case 1 tangential velocity exceeded 10% of acceptable range.

CHAPTER 5

CONCLUSION AND RECOMMENDATIONS

The objective to evaluate the contribution of top plate on the performance of Solar Vortex Engine (SVE) has been achieved by experimental investigation. Based on results, the replacement of aluminum top plate with semi-transparent Perspex top plate did prove its worthiness in increasing interior flow temperature and creating better updraft. Lower interior pressure has been achieved due to the increased outflow velocity, drawing in higher air inlet velocity.

The flow field within the Solar Vortex Engine (SVE) has been successfully simulated by CFD technique. Vortices were simulated within the Vortex Engine Generator. Most of the parameters are in match with the experimental measurements. The optimum opening diameter for flat top plate has been identified by CFD technique. Increasing the outlet diameter lead to a rise in air mass flow rate but the increased cross-sectional area tends to reduce the temperature variation between inlet and outlet, lowering the air velocity and rate of natural convection. Besides, the suitable angle for the canopy shaped top plate has been simulated and evaluated by CFD technique. Increasing the slanting angle of canopy shape top plate did resolve the air-cornering issue, but the outlet velocity has been reduced.

In conclusion, current prototype of Solar Vortex Engine (SVE) was constructed with less-expensive material and yet still is generating a peak updraft velocity of 2.11m/s. with further modification and improvement on the prototype, the Solar Vortex Engine (SVE) will be ready for power generation. Figure 5.1 below shows the proposed model for the Vortex Engine Generator (VEG) where the guide vanes and entry slots are suggested to extend into the convection region. The flat and canopy shaped top plate were proposed to be implement simultaneously on a prototype.

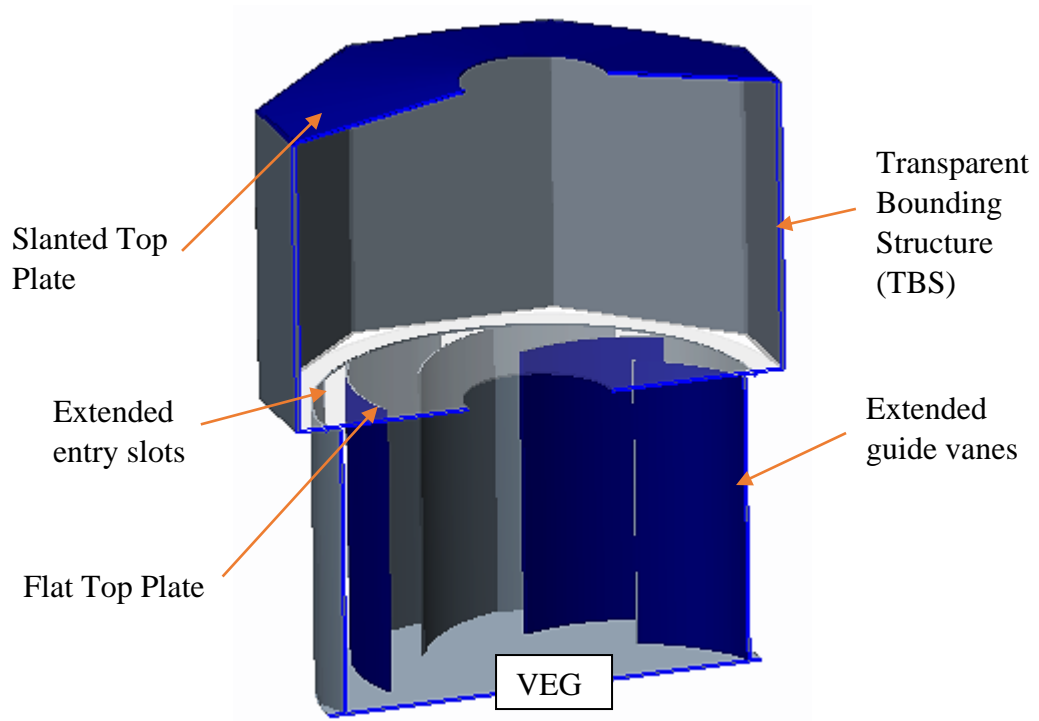


Figure 5. 1 – Proposed Model of Vortex Engine Generator (VEG)

REFERENCE

- [1] “*Executive Summary - World Energy Outlook 2014*,” International Energy Agency - IEA, 2014.
- [2] “*Renewables 2014 - Global Status Report*,” REN21, pp. 21, 2014.
- [3] C. Philibert, “*Solar Energy Perspectives*,” International Energy Agency – IEA, 2011.
- [4] J. Schlaich, R. Bergermann, W. Schiel and G. Weinrebe, "*Design of Commercial Solar Updraft Tower Systems—Utilization of Solar Induced Convective Flows for Power Generation*," *Journal of Solar Energy Engineering*. Vol. 127. pp. 117-124, 2005.
- [5] L. M. Michaud, “*The Atmospheric Vortex Engine*”, AVEtec Energy Corporation, 2008.
- [6] A. T. Mustafa, H. H. Al-Kayiem and S. I. U. Gilani, “*A Review of the Vortex Engine*,” *The Sustainable City VIII*, Vol 2, pp. 911-920, 2013.
- [7] S. Rathnavel and K. Vijaya sankaran, “*Design and Analysis of an Atmospheric Vortex Engine*”, *International Journal of Research in Aeronautical and Mechanical Engineering*, Vol. 3, Issue. 2, pp. 1-9, Feb, 2015.
- [8] L. M. Michaud, “*Atmospheric Vortex Engine - US7086823 B2*,” Google Patents, 2006
- [9] V. H. Hidalgo Diaz and N. Chen “*Application of Vortex Process to Cleaner Energy Generation*,” *Applied Mechanics and Materials*, Vol. 71-78, pp. 2196-2203, 2011
- [10] K. T. K. Ho. and D. L. Loveday, “*New Approach for Analyzing Solar Collectors Subjected to Unequal Front/Rear Ambient Temperatures: The Equivalent Ambient Temperature Concept, Part 1: Modeling*,” *Journal of Solar Energy Engineering*, Vol. 124, no. 3, pp. 262, 2002.
- [11] W. Contributor, “*Solar Thermal Collector*,” *Wikipedia - The Free Encyclopedia*, 2015.
- [12] J. Schlaich, W. Schiel, K. Friedrich, G. Schwarz, P. Wehowsky, W. Meinecke, et al., “*The Solar Chimney – Transferability of Results from the Manzanares Solar Chimney Plant to Larger Scale-Plants*”, *Tech. Rep.*, Schlaich Bergermann and Partner, Civil Engineering, Stuttgart, Germany. pp 5-33, 1995.

- [13] A. T. Mustafa, H. H. Al-Kayiem and S. I. U. Gilani, “*Investigation and Evaluation of The Solar Air Collector Model to Support The Solar Vortex Engine,*” *ARPJ Journal of Engineering and Applied Sciences*, Vol. 10, no. 12, pp. 5309-5319, July, 2015.
- [14] H. Huang *et al.*, “*Experimental Performance of A Solar Collector in Solar Chimney Power Plant System,*” *International Conference on Electrical and Control Engineering*, pp. 3718-3721, 2010.
- [15] A. M Saleh, “*Modeling of Flat-Plate Solar Collector Operation in Transient States,*” *Purdue University*, May, 2012.
- [16] J. Y. Li, P. H. Guo and Y. Wang, “*Effects of Collector Radius and Chimney Height on Power Output of A Solar Chimney Power Plant with Turbines*”, *Renewable Energy* 47 - Elsevier, pp. 21-28, 2012.
- [17] U. Prasophingchana, W. Pirompugd, P. Laipradit, and K. Boonlong, “*Numerical Study of Natural Convection of Air in an Inclined Square Enclosure,*” *International Journal of Material, Mechanics and Manufacturing*, Vol. 1, No. 2, pp. 131 – 135, May, 2013
- [18] M. H. Ali, “*Analysis Study of Solar Tower Power Plant and Its Configuration Effects on Its Performance in Iraq (Baghdad City),*” *Modern Applied Science*, Vol. 7, No. 4, pp. 55 – 69, March, 2013
- [19] B. Kalidansan and T. Srinivas, “*Study on Effect of Number of Transparent Covers and Refractive Index on Performance of Solar Water Heater,*” *Journal of Renewable Energy*, Vol. 2014, Sept, 2014
- [20] M. A. dos S. Bernades, A. Voß, G. Weinrebe. “*Thermal and Technical Analyses of Solar Chimneys,*” *Solar Energy* 75 – Elsevier, pp. 511-524, 2003.
- [21] E. Gholamalizadeh, S. H. Mansouri, “*A Comprehensive Approach to Design and Improve A Solar Chimney Power Plant: A Special Case – Kerman Project,*” *Applied Energy* 102 - Elsevier, pp. 975-982, 2013.
- [22] A. Asnaghi, S. m. Ladjevardi, “*Solar Chimney Power Plant Performance in Iran,*” *Renewable and Sustainable Energy Reviews* 16 – Elsevier, pp. 3383-3390, 2012

- [23] G. Xu, T. Ming, Y. Pan, F. Meng and C. Zhou, “*Numerical Analysis On The Performance of Solar Chimney Power Plant System,*” Energy Conversion and Management 52 – Elsevier, pp. 876-883, 2011
- [24] D. Natarajan, “Numerical Simulation of Tornado-Like Vortices,” University of Western Ontario, London, Ontario, Canada, pp. 109, 2011
- [25] Boussinesq - ANSYS Fluent 15 Help User Guideline, Now, 2013
- [26] B. R. Munson, D. F. Young, T. H. Okiishi, and W. W. Huebsch, “*Fundamentals of Fluid Mechanics,*” John Wiley and Sons (Asia) Pte Ltd, Ed. 6, pp. 188 and 307, 2010
- [27] S. W. Yuan, “*Foundations of Fluid Mechanics,*” Englewood Cliffs, N.J. :Prentice-Hall, 1967
- [28] D. J. Acheson, “*Elementary Fluid Dynamics,*” Oxford University Press, 1990.
- [29] A. T. Mustafa, H. H. Al-Kayiem and S. I. U. Gilani, “A Review of Convective and Artificial Vortices for Power Generation”, Int. J. Sus. Dev. Plann. Vol. 10, No. 5, pp. 650-665, 2015
- [30] M. G. Lawrence, “The Relationship Between Relative Humidity and the Dewpoint Temperature in Moist Air – A Simple Conversion and Applications”, American Meteorological Society, 225-233, 2005

Appendix A – Measuring Instruments

Table A. 1 - Specifications on GRAPHTEC DATA LOGGER GL820

	Descriptions								
Instrument 1	GRAPHTEC DATA LOGGER GL820								
Figure									
Features	<ol style="list-style-type: none"> 1. Provide isolated input method which ensures signals are not corrupted by inputs to other channels, eliminating wiring concerns. 2. Suitable for measurements on voltage, temperature, pulse, humidity, and logic signals. 3. Suitable for combined measurements of different phenomena like temperature / humidity and voltage. 4. Provide 2GB Internal Flash Memory to secure long term data measurements 5. Support direct data saving into external USB memory stick. 6. Support direct-Excel graphical display. 								
Specifications	<ol style="list-style-type: none"> 1. 5.7 inch wide TFT color LCD with resolution of VGA: 640 x 480 dots. 2. Operational voltage range: 20Mv to 50V. 3. Operational humidity range: 0 to 100%RH (B-530) 4. Provide standard configuration of 20 analogue input channels. 5. Provide extension up to 200 channels with extension base kit (B-537). 6. Provide maximum sampling rate up to 10ms. 7. Thermocouple type J: Nickel Constantan <table border="1" style="margin-left: auto; margin-right: auto;"> <thead> <tr> <th style="text-align: center;">Measurement Range</th> <th style="text-align: center;">Measurement Accuracy</th> </tr> </thead> <tbody> <tr> <td style="text-align: center;">$-200^{\circ}\text{C} \leq TS \leq -100^{\circ}\text{C}$</td> <td style="text-align: center;">$\pm 2.7^{\circ}\text{C}$</td> </tr> <tr> <td style="text-align: center;">$-100^{\circ}\text{C} \leq TS \leq 100^{\circ}\text{C}$</td> <td style="text-align: center;">$\pm 1.7^{\circ}\text{C}$</td> </tr> <tr> <td style="text-align: center;">$100^{\circ}\text{C} \leq TS \leq 1100^{\circ}\text{C}$</td> <td style="text-align: center;">$\pm(0.05\% \text{ of reading} + 1.0^{\circ}\text{C})$</td> </tr> </tbody> </table>	Measurement Range	Measurement Accuracy	$-200^{\circ}\text{C} \leq TS \leq -100^{\circ}\text{C}$	$\pm 2.7^{\circ}\text{C}$	$-100^{\circ}\text{C} \leq TS \leq 100^{\circ}\text{C}$	$\pm 1.7^{\circ}\text{C}$	$100^{\circ}\text{C} \leq TS \leq 1100^{\circ}\text{C}$	$\pm(0.05\% \text{ of reading} + 1.0^{\circ}\text{C})$
Measurement Range	Measurement Accuracy								
$-200^{\circ}\text{C} \leq TS \leq -100^{\circ}\text{C}$	$\pm 2.7^{\circ}\text{C}$								
$-100^{\circ}\text{C} \leq TS \leq 100^{\circ}\text{C}$	$\pm 1.7^{\circ}\text{C}$								
$100^{\circ}\text{C} \leq TS \leq 1100^{\circ}\text{C}$	$\pm(0.05\% \text{ of reading} + 1.0^{\circ}\text{C})$								
Applications	Applied as data logger for SVE fixed positions experimental temperature measuring.								

Before experimental measurements are conducted, a calibration is required on the thermocouples type J to ensure trustworthy of the instruments. Calibration on thermocouples type J was done with a digital thermometer and a calibration curve was plotted with equation:

$$y = 0.7939x + 6.1547$$

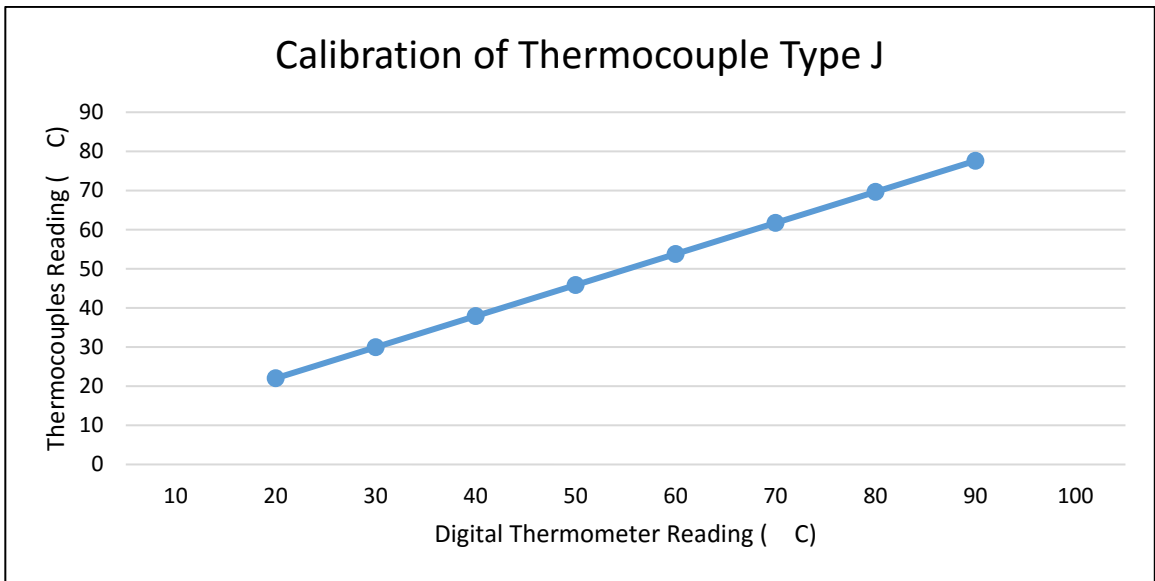


Figure A. 1 – Calibration on Thermocouple Type J against Digital Thermometer

Where X represents the digital thermometer reading and Y represents the thermocouples type J reading.

Thermocouple is a sensor that measure the change in temperature using a welded junction, generating different voltage. Data logger will then interpret the voltage variation and record the respective measuring temperatures.

Table A. 2 - Specifications on Digital Reader KIMO-AMI 300

	Descriptions
Instrument 2	Digital Reader KIMO-AMI 300 with Multi Probes
Figure	
Features	<ol style="list-style-type: none"> 1. Support multiple probes for air flow properties. 2. Suitable for measurements of air temperature, humidity, velocity and pressure. 3. Apply software: Datalogger 10 <ul style="list-style-type: none"> • Allow transfer of measured values from instrument to computer. • Allow 12,000 measurements points or 50 datasets.
Specifications	<ol style="list-style-type: none"> 1. Provide color graphic display with resolution 320 x 240 pixels and dimension of 70 x 52mm. Able to display 4 to 6 measurements simultaneous. 2. Operating Environment: Neutral gas 3. Operating Temperature: 0 to 50°C 4. Storage temperature: -20 to +80°C
Applications	Applied as data logger for SVE fixed positions experimental temperature measuring.

Digital Reader KIMO-AMI 300 utilizes different probes to measurement various variables. Digital reader can be applied for measurements with either automatic or manual method. Datalogger-10 application has been represented as a function of time on the graph and chart. Table A.3 shows the measuring probes.

Table A. 3 - Specifications on Measurements Probes for Digital Reader KIMO-AMI 300

Probes	Figure	Probes' Specifications		
Standard and Telescopic Hotwire Probe		Air Velocity	Measuring Ranges	0.15 to 3 m/s
			Accuracy	±3% of reading ± 0.03m/s
			Resolution	0.01m/s
		Temperature	Measuring Ranges	−20°C to + 80°C
			Accuracy	±0.3% of reading ± 0.25°C
			Resolution	0.1°C
		Air Flow	Measuring Ranges	0 to 99,999m ³ /h
			Accuracy	±3% of reading ± 0.03 * cm ² (area)
			Resolution	1m ³ /h
Vane		Air Velocity	Measuring Ranges	0.3 to 3 m/s
			Accuracy	±3% of reading ±0.1m/s
			Resolution	0.01m/s
		Temperature	Measuring Ranges	−20°C to + 80°C
			Accuracy	±0.4% of reading ±0.3°C
			Resolution	0.1°C
		Air Flow	Measuring Ranges	0 to 99,999m ³ /h
			Accuracy	±3% of reading ± 0.03 * cm ² (area)
			Resolution	1m ³ /h



Enviroterm Sdn. Bhd. 369410-P
 Lot 5035, Jalan 18/62, Taman Sri Sardang,
 43300 Seri Kembangan, Selangor D. E.,
 Malaysia
 Tel: 03-89434558 Fax: 03-89436012

CALIBRATION CERTIFICATE

Customer : Universiti Teknologi Petronas
 31750 Tronoh, Perak, Malaysia

Instrument Identity

Instrument Description	: Multifunction Micromanometer	Calibration Certificate No	: J11696R1
Brand	: KIMO	Issue Date	: 12-Sep-14
Model	: AMI 300	Calibration Date	: 07-Aug-14
Version of Model	: 2008	Next Calibration Due Date*	: 07-Aug-15
Serial No	: 14040820		

Measurement Function and Parameters : The multifunction handheld meter consists of base instrument cater for multiple plug-in modules and probes, the base instrument is ready to measure multiple parameters and access for these measuring parameters which are dependent on the availability of the following modules and probes.

No	Parameters	Availability	Calibration
(1)	Standard Hotwire Anemometry Probe	Included	Calibrated
(2)	SMART-Plus Ø 100mm Vane Anemometry Probe	Included	Calibrated
(3)	SMART-Plus Standard Hygrometry Probe	Included	Calibrated
(4)	Tachometry Probe	Not included	Not required**
(5)	Pressure Module, ± 500 Pascal	Included	Calibrated
(6)	Current and Voltage Module	Included	Calibrated
(7)	Climatic Module	Not included	Not required**
(8)	Carbon Dioxide Probe	Not included	Not required**
(9)	Carbon Monoxide / Temperature Probe	Not included	Not required**
(10)	Thermocouple Module	Not included	Not required**
(11)	Thermocouples Probe(s)	Not included	Not required**
(12)	Carbon Dioxide / Temperature / Hygrometry Probe(s)	Not included	Not required**
(13)	Carbon Dioxide / Temperature Probe(s)	Not included	Not required**

** Calibration performed base on availability on the probe(s) and Module(s) selected as above and as agreed by the owner, details of calibration data on selected probes and modules as per attached pages.

Laboratory's Environmental

Temperature : 24.2 ± 0.5 °C
 Relative Humidity : 49.9 ± 3 %
 Barometric Pressure : 1001.0 ± 50 mBar
 Laboratory Location : Enviroterm Sdn. Bhd., Seri Kembangan, Selangor

Base Instrument Condition:

As Found Condition : Physically and functionally are in good condition and all measured values were in tolerance
 As Left Condition : Calibrated, measured values are in tolerance for parameter tested

Results of Calibration

The data recorded at the time of calibration performed. The Expanded Measurement Uncertainty is at 95% level of confidence based on the ISO Guide to the Expression of Uncertainty in Measurement. Coverage Factor = 2

Calibrated by:

W L Low
 Senior Technician



Approved Signatory:

S K Yoo
 Quality Manager

This certificate is issued in following the guidelines and conditions as recommended in ISO 17025:2005, copyright of this certificate is owned by the issuing laboratory and may not be replaced other than in full except with the prior written approval of the Head of the issuing laboratory. * Next Calibration Due Date as recommended by original equipment manufacturer. The customer should be aware that any number of factors may causes this instrument to drift out of calibration before the specified calibration interval has expired.

Figure A. 2 – Certification of Calibration for Digital Reader



Enviroterm Sdn Bhd 269410-P
 Lot 5025, Jalan 18/62, Taman Sri Serdang,
 43300 Seri Kembangan, Selangor, D. E.,
 Malaysia
 Tel: 03-89434558 Fax: 03-89436012

Measuring Probe Identity

Probe Description : SMART-Plus Ø 100 mm vane probe Calibration Certificate No : J11856R1
 Model : HE 100 Serial No : 14027291
 Measurement Function :

Measurement	Range	Accuracy
(1) Vane Anemometry	0.25 to 3 m/s	± 3% of reading ± 0.1 m/s
	3.1 to 35 m/s	± 1% of reading ± 0.3 m/s
(2) Temperature	-20 to 80 °C	± 0.4% of reading ± 0.3 °C

Measuring Probe Condition

As Found Condition : Physically and functionally are in good condition and all measured values were in tolerance
 As Left Condition : Calibrated, measured values are in tolerance for parameter tested

Calibration Procedure

Policy and Procedure at the calibration laboratory has been performed in accordance with the following appropriate procedures:
 @ In-house's procedure : ETM/CPIA/V10

CALIBRATION DATA

AIR VELOCITY

AS FOUND DATA					AS LEFT DATA				
Testing Points	Reference (m/s)	UUT (m/s)	Deviation (m/s)	Status (I/O)*	Testing Points	Reference (m/s)	UUT (m/s)	Deviation (m/s)	Status (I/O)*
1	0.00	0.00	0.00	I	1	0.00	0.00	0.00	I
2	1.05	1.10	- 0.05	I	2	1.00	1.02	- 0.02	I
3	2.54	2.61	- 0.07	I	3	2.55	2.60	- 0.05	I
4	5.06	5.2	- 0.1	I	4	5.07	5.2	- 0.1	I
5	7.51	7.7	- 0.2	I	5	7.56	7.7	- 0.1	I
6	10.13	10.3	- 0.2	I	6	10.18	10.3	- 0.1	I
7	15.02	15.2	- 0.2	I	7	15.09	15.2	- 0.1	I
8	20.01	20.2	- 0.2	I	8	20.08	20.2	- 0.1	I
9	25.11	25.3	- 0.2	I	9	25.12	25.3	- 0.2	I
10	29.03	29.3	- 0.3	I	10	29.02	29.2	- 0.2	I

TEMPERATURE

AS FOUND DATA					AS LEFT DATA				
Testing Points	Reference (°C)	UUT (°C)	Deviation (°C)	Status	Testing Points	Reference (°C)	UUT (°C)	Deviation (°C)	Status
1	25.1	25.1	0.0	I	1	25.0	25.0	0.0	I

*I UUT data recorded are in-tolerance as new instrument specification published by manufacturer.
 *O UUT data record are out-of-tolerance against as new instrument specification, the Correction Factor may be applicable on UUT as deviation value stated above.

Calibration Standard Used and Traceability

This certificate is issued to certify that this instrument has been calibrated under the stated environmental conditions using standard reference instrument, calibration has been accomplished by comparison with standards maintained by Enviroterm Sdn Bhd. Accuracy and stability of standards maintained by Enviroterm Sdn Bhd are traceable to following:

No	Equipment used	Model	Certificate No.	Serial No.	Calibration Due	Traceability
1	Hot Wire-Wind Tunnel	8380	EC151	275	18-Apr-15	In-house / NML
2	Thermometer	TK-100	EQ138	9507221	19-Mar-15	In-house / NML

Results of Calibration

The data recorded at the time of calibration performed. The Expanded Measurement Uncertainty is at 95% level of confidence based on the ISO Guide to the Expression of Uncertainty in Measurement. Coverage Factor = 2

This certificate is issued in following the guidelines and conditions as recommended in ISO 17025:2015, copyright of this certificate is owned by the issuing laboratory and may not be replaced other than in full except with the prior written approval of the Head of the issuing laboratory. * Next Calibration Due Date as recommended by original equipment manufacturer. The customer should be aware that any number of factors may causes the instrument to drift out of calibration before the specified calibration interval has expired

Figure A. 3 – Certification of Calibration for Vane Probe

Table A. 4 - Specifications on Solarimeter KIMO-SL 200 Instrument

	Descriptions
Instrument 3	Solarimeter KIMO-SL 200 Instrument
Figure	
Features	<ol style="list-style-type: none"> 1. Provide analysis of sunshine on site, on short and long-term period. 2. Provide automatic data saving and compilation at the end of experimental measurements. 3. Provide storage and saving of average values of power 4. Provide update of energetic exposure calculation every minute. 5. Provide reading and graphical approximation of data by 24 hours via transfer data software. 6. Absorb solar radiation through diffuser and correction filter.
Specifications	<p>Instrument SL 200</p> <ol style="list-style-type: none"> 1. Solar intensity measuring range: 1 Wh/m^2 to 1300 Wh/m^2 2. Energetic exposure measuring range: 1 Wh/m^2 to 500 Wh/m^2 3. Frequency of measurements: 2/s 4. Accuracy: 5% of measurements 5. Calculation frequency (Wh/m^2): 1/min (Average on 60 sec) 6. Operating temperature: -10°C to $+50^\circ\text{C}$ 7. Storage temperature: -10°C to $+55^\circ\text{C}$ <p>Solar Cell</p> <ol style="list-style-type: none"> 8. Operating temperature: -30°C to $+60^\circ\text{C}$ 9. Humidity dependence: 100%RH 10. Effective area: 1cm^2 11. Nominal Sensitivity: 100mv for 1000W/m^2 12. Material: Polycrystalline silicon
Applications	<p>Solarimeter KIMO-SL 200 provide the measurement for the global solar radiation. Global solar radiation is the sum of direct solar radiation and diffused solar radiation.</p> <p>Applied to measure solar intensity / radiation available and provide output voltage for analysis to make direct recording on average temperature.</p>

Table A. 5 – Specifications on Extech 3-in-1 Humidity, Temperature and Airflow Meter

	Descriptions
Instrument 4	Extech 3-in-1 Humidity, Temperature and Airflow Meter
Figure	 <p>The image shows a handheld, black and grey Extech 3-in-1 meter. At the top, there is a circular fan for airflow measurement. Below the fan is a small LCD display showing '32.3' and '24.2'. The main display in the center shows '32.3' and '24.2'. At the bottom, there is a yellow and black logo with the text '3 in 1'.</p>
Features	<ol style="list-style-type: none"> 1. Allow the measurement of 3 parameters at once (Velocity, Temperature, and Humidity). 2. Captures maximum and minimum value simultaneously. 3. Allow value holding for recording. 4. Can be connected with Thermocouple but in limited amount.
Range Specifications	<ol style="list-style-type: none"> 1. Velocity range: 0.4 to 30m/s. 2. Temperature range: -0 to 50°C. 3. Relative humidity range: 10.0 to 95.0%
Applications	Applied to record on ambient and airflow relative humidity.

Appendix B – Mesh Independency Test

B.1 Mesh Independency Test at 0.5m/s Inlet Velocity

Table B. 1 – Mesh Independency Test Statistical Values

No. trials	Relevance Center	Smoothing	Min Size $\times 10^{-4}$	Max Face Size $\times 10^{-2}$	Max Size $\times 10^{-2}$	Iterations	Min AR	Max AR	Aspect ratio	Nodes	Elements	Max Velocity (m/s)	Max Pressure (pascal)	Percentage Difference
1	Coarse	Medium	9.3	9.3	18.6	758	1.17	90.33	77.02	4,073	19,474	2.20	4.97	0.00
2	Medium	Medium	4.6	4.6	9.3	371	1.17	41.83	35.79	12,866	63,426	1.94	2.69	0.12
3	Fine	Medium	2.7	2.7	5.4	299	1.16	16.39	14.15	41,546	211,895	2.13	2.68	0.10
4	Fine	High	2.7	2.7	5.4	300	1.16	13.94	12.04	41,535	211,833	2.13	2.67	0.00
5	Fine	High	2.7	2.6	5.4	286	1.16	16.51	14.26	45,797	234,255	2.05	2.84	0.04
6	Fine	High	2.7	2.5	5.4	291	1.16	23.74	20.48	49,759	255,797	2.15	2.79	0.05
7	Fine	High	2.7	2.4	5.4	295	1.16	22.05	19.05	55,613	286,526	2.17	2.88	0.01
8	Fine	High	2.7	2.3	5.4	300	1.16	24.72	21.34	61,661	319,085	2.26	2.76	0.04
9	Fine	High	2.7	2.2	5.4	295	1.16	21.62	18.64	68,615	356,364	2.16	2.77	0.04
10	Fine	High	2.7	2.1	5.4	295	1.16	10.43	9.01	77,127	402,355	2.20	2.78	0.02
11	Fine	High	2.7	2.0	5.4	297	1.16	23.05	19.89	88,016	459,863	2.33	2.82	0.06
SUM												23.72	32.65	
AVERAGE												2.16	2.97	

B.2 Mesh Independency Test at 0.7m/s Inlet Velocity

Table B. 2 – Mesh Independency Test Statistical Values

No. trials	Relevance Center	Smoothing	Min Size $\times 10^{-4}$	Max Face Size $\times 10^{-2}$	Max Size $\times 10^{-2}$	Iterations	Min AR	Max AR	Aspect ratio	Nodes	Elements	Max Velocity (m/s)	Max Pressure (pascal)	Percentage Difference
1	Coarse	Medium	9.3	9.3	18.6	762	1.17	90.33	77.02	4,073	19,474	3.097	9.71	2.41
2	Medium	Medium	4.6	4.6	9.3	379	1.17	41.83	35.79	12,866	63,426	2.728	5.29	-9.79
3	Fine	Medium	2.7	2.7	5.4	306	1.16	16.39	14.15	41,546	211,895	2.968	5.24	-1.85
4	Fine	High	2.7	2.7	5.4	307	1.16	13.94	12.04	41,535	211,833	2.979	5.21	1.49
5	Fine	High	2.7	2.6	5.4	295	1.16	16.51	14.26	45,797	234,255	2.873	5.54	4.99
6	Fine	High	2.7	2.5	5.4	300	1.16	23.74	20.48	49,759	255,797	3.020	5.46	0.13
7	Fine	High	2.7	2.4	5.4	302	1.16	22.05	19.05	55,613	286,526	3.040	5.63	-0.53
8	Fine	High	2.7	2.3	5.4	307	1.16	24.72	21.34	61,661	319,085	3.169	5.41	-4.79
9	Fine	High	2.7	2.2	5.4	304	1.16	21.62	18.64	68,615	356,364	3.030	5.42	-0.20
10	Fine	High	2.7	2.1	5.4	303	1.16	10.43	9.01	77,127	402,355	3.090	5.45	-2.18
11	Fine	High	2.7	2.0	5.4	305	1.16	23.05	19.89	88,016	459,863	3.270	5.54	-8.13
SUM												33.26	63.92	
AVERAGE												3.02	5.81	